Supplementary Materials

FKBP10 promotes M2 polarization of macrophage via MEK/ERK/CXCL8 axis and facilitates tumor progression in clear cell renal cell carcinoma

Supplementary Materials Checklist

Supplementary Methods

Supplementary Tables

Table S1 Key resources table

Table S2 Gene list of published immune-related signatures for the TIME classification.

Table S3 Gene lists of published 12 renal cell signatures for the Jaccard analysis.

Table S4 Clinical phenotype data of seven single-cell sequencing datasets utilized in the study.

Table S5 List of signature genes expressed in 74 defined cell clusters in ccRCC.

Table S6a Gene list of four TIME subtypes related signatures.

Table S6b Total results of GO and KEGG enrichment analysis of TIME related signatures.

Table S7 TIME subtypes of ccRCC patients.

Table S8a List of gene loadings within each gene expression programs that involved in meta-program 1.

Table S8b List of gene loadings within each gene expression programs that involved in meta-program 2.

Table S8c List of gene loadings within each gene expression programs that involved in meta-program 3.

Table S8d List of gene loadings within each gene expression programs that involved in meta-program 4.

Table S8e List of gene loadings within each gene expression programs that involved in meta-program 5.

Table S8f List of gene loadings within each gene expression programs that involved in meta-program 6.

Table S9 List of signature genes for ecosystem subtypes.

Table S10 Detail information of 15 genes involved in the optimal prognostic model.

Supplementary Figures

Figure S1 Flowchart summarizing the entire study design.

Figure S2 Quality control metrics of single-cell RNA sequencing data across all samples prior to filtering.

Figure S3 Quality control metrics for single-cell RNA sequencing data after filtering.

Figure S4 Comparative analysis of immune and stromal cell proportions between TLS-high and TLS-low groups.

Figure S5 Distinct characteristics of TIME subtypes.

Figure S6-S16 Gene expression within each gene expression program in each sample.

Figure S17 Hallmark pathways enrichment of six malignant meta-programs.

Figure S18 Distributions and clinical associations of six program tumor cells.

Figure S19 Analysis of ligand-receptor interactions in tumor ecosystems using CellphoneDB.

Figure S20 Ligand-receptor interactions, distribution, and signaling pathways across tumor ecosystems.

Figure S21 GSEA ridge plot analysis of tumor ecosystem signatures across GO, KEGG, and Hallmark gene sets.
Figure S22 Spatial co-localization analysis between EMT-high tumor cells and specific immune cell types.
Figure S23 NicheNet analysis and functional enrichment of the ecosystem 2 signature.
Figure S24. Assessment of prognostic model performance through forest plot and 10-fold cross-validation.
Figure S25 Forest plots of univariable and multivariable Cox regression analyses for the prognostic model across multiple cohorts.
Figure S26 Validation and evaluation of ISM-EMTRS prognostic potentials.
Figure S27 Validation of the role of FKBP10, DPEP1 and DNASE1L3 in ccRCC across 6 cohorts.
Figure S28 Association of FKBP10, DPEP1, and DNASE1L3 expression with survival outcomes in immunotherapy cohorts.
Figure S29 FKBP10 is an independent prognostic factor and remodels the tumor immune microenvironment in ccRCC.
Figure S30 Analysis of immune cell infiltration stratified by FKBP10 expression levels in E-MTAB-1980 and Checkmate cohorts.
Figure S31 Analysis of immune cell infiltration stratified by FKBP10 expression levels in TCGA-KIRC and JAVELIN cohorts.
Figure S32 Analysis of transcription factor binding and prioritization of a key regulator at the CXCL8 locus.

Supplementary Method

scRNA-seq Data Processing

The initial step involved the exclusion of peripheral blood mononuclear cell data to emphasize the tumor-infiltrating immune cells. Low quality cells (<300 or >5,000 genes detected; <500 UMIs; >20% (for tumor samples) or >80% (for benign samples) mitochondrial reads; >1% hemoglobin gene content) were also excluded before being merged together. The mitochondrial gene content restrictions were based on the observed mitochondrial read disparities in prior kidney scRNA-seq and bulk RNA-seq studies [1-4]. Subsequently, DoubletFinder was employed for potential doublet cell filtration [5]. Normalization was achieved using NormalizeData function, with 3,000 highly variable genes (HVGs) identified using the FindVariableFeatures function, and gene scaling to unit variance. Cell clusters were delineated through principal component analysis (PCA) of the top 20 principal components (PCs), integrating batch effect rectification via the harmony package. The Louvain method was employed for clustering, and dimensionality reduction was performed using Uniform Manifold Approximation and Projection (UMAP).

We annotated the six major cell types identified in our dataset on the basis of well-known marker genes, including CD3D, CD3E, CD8A, CD4, NKG7 for T lymphoid cells; CD79A, CD79B, CD19, MS4A1 for B lymphoid cells; C1QA, C1QB, C1QC, CD68, ITGAX for myeloid lineage; PECAM1, KDR, AQP1, PLVAP for endothelial cells; COL1AL, COL3A1, ACTA2, PDGFRB for fibroblast; EPCAM, PAX8, KRT18, KRT8, NNMT for epithelial cells. Among these epithelial cells, malignant cells were further distinguished from non-malignant cells by inferring large-scale CNVs using inferCNV. Non-malignant epithelial cells derived from normal samples were used as references for CNV estimation.

We conducted a second round of clustering to further characterize the subpopulations of major cell types. Owing to the variable amount and properties of cells in each major cell type, different parameters for clustering were used. For the clustering of NK or T cells, the top 20 PCs were selected based on 3,000 HVGs (resolution=0.8). For clustering of B cells, the top 15 PCs were selected on the basis of 2,000 HVGs (resolution=0.6). For myeloid cells, the top 20 PCs were selected on based on 3,000 HVGs (resolution=0.5). For endothelial cells, the top 15 PCs were selected based on 2,000 HVGs (resolution=0.4). For fibroblasts, the top 15 PCs were selected based on 1,000 HVGs (resolution=0.4).

As a result, 75 cell clusters were identified. Annotation relied on the most highly expressed immune-related genes in each cluster, with the gene list curated according to previous findings [6]. To facilitate data visualization, cells were re-clustered into five embeddings using Seurat, including (1) NK and T cells, (2) myeloid cells, (3) B cells, (4) endothelial cells, (5) fibroblast. Next, we used the FindAllMarkers function to identify differentially expressed genes (DEGs) with adjusted $P<0.05$ using the Bonferroni correction.

CytoTRACE Stemness Analysis

CytoTRACE was utilized to assess cellular stemness within the epithelial cluster, with higher gene counts in single cells indicating lesser differentiation and elevated stemness [7]. This algorithm aids in identifying genes

that significantly correlate with cellular gene counts and stemness, thereby enabling precise stemness scoring.

Immune Infiltration Analysis

To comprehensively characterize the immune cell composition in the tumor microenvironment, we applied multiple computational algorithms, including ESTIMATE, Cibersort, MCP-counter, EPIC, and xCell. These methods leverage distinct principles to infer immune cell abundances from bulk transcriptomic data, providing complementary insights into stromal, immune, and malignant cell proportions.

The ESTIMATE algorithm employs single-sample gene set enrichment analysis (ssGSEA) to generate stromal, immune, and combined ESTIMATE scores, reflecting the presence of stromal and immune cells in tumor tissues. Tumor purity was derived from the ESTIMATE score using the formula: Tumor Purity = cos (0.6049872018 + 0.0001467884 × ESTIMATE score) [8]. Cibersort utilizes support vector regression to deconvolute expression data against the LM22 leukocyte signature matrix, quantifying 22 immune cell subtypes [9]. MCP-counter calculates the geometric mean of marker gene expressions to estimate absolute abundances of 8 immune and 2 stromal cell types [10]. EPIC employs constrained least squares regression to infer proportions of immune and cancer cells [11], while xCell applies ssGSEA-based enrichment to score 64 immune and stromal cell types [12]. The integration of these methods ensures robust and complementary evaluation of immune infiltration.

Sample Collection and Cell Culture

ccRCC and corresponding para-carcinoma tissues were collected directly from the operating room during nephrectomy. At the time of specimen extraction, samples of around 1-1.5 cm were obtained by the treating surgeon from tumor regions and para-tumor regions (at least 1 cm apart). Once in the operating room, small tissue aliquots (of around 5 mm^3) were separated from each sample for subsequent experiments. One aliquot was placed in 10% formalin for immunohistochemistry (IHC). The remainder of the tissue was placed in liquid nitrogen and transported on regular ice to the laboratory for subsequent quantitative real-time polymerase chain reaction (qPCR) and western blotting analysis.

The human renal cell carcinoma cell lines 769-P, 786-O and OS-RC-2 were used for experimental validation. All cell lines were cultured in RPMI1640 Medium, supplemented with 10% Fetal Bovine Serum (FBS) and 1% penicillin/streptomycin, and were maintained in an incubator at 37℃ and 5% CO2. Cell lines were sub-cultured by detaching cells using 0.25% trypsin EDTA, quenching, washing, and resuspension of the cell pellet in fresh media.

Quantitative Real-time Polymerase Chain Reaction

Tissues were homogenized and incubated for the indicated times with either compound or vehicle, and RNA was isolated using a universal RNA purification kit. cDNA was generated using a reverse transcription kit. qPCR was executed in triplicate using SYBR Green Master Mix on Quant-Studio 5 System. Gene expression

levels were quantitatively assessed with the method of $2^{-\Delta\Delta Ct}$.

Protein Extraction and Western Blot Analysis

For proteins extraction, tissues or cells were homogenized in RIPA lysis buffer containing 150 mM NaCl, 1.0% IGEPAL CA-630, 0.5% sodium deoxycholate, 0.1% SDS, and 50 mM Tris (pH 8.0), supplemented with protease and phosphatase inhibitors, and incubated on ice for 30 minutes to ensure complete lysis. The homogenates were then centrifuged to remove the cellular debris. The protein concentration in the supernatants was quantified using a BCA Protein Assay Kit. For electrophoresis, lysates were prepared by mixing 2× sample buffer (0.125 M Tris-HCl, pH 6.8, 4% SDS, 20% glycerol) enriched with 4% β-mercaptoethanol, followed by denaturation at 100℃ for 10 minutes. Denatured proteins were resolved on SDS-PAGE gels and subsequently transferred onto PVDF membranes. Non-specific binding sites on the membranes were blocked with 5% skim milk at room temperature. Primary antibodies against FKBP10 (1:5000), DNASE1L3 (1:1000), DPEP1 (1:2000), MEK (1:10000), ERK (1:3000), p-MEK (1:1000), p-ERK (1:2000), ELF3 (1:200), Vinculin (1:20000), and CXCL8 (1:1000) were applied to the blocked membranes and incubated overnight at 4℃. After incubating with horseradish peroxidase-conjugated secondary antibodies, the protein bands were visualized using the Amersham ImageQuant 800 imaging system.

Immunohistochemical Staining

Formalin-fixed, paraffin-embedded (FFPE) sections of ccRCC tissues (4 μm thickness) were subjected to IHC staining using standard protocols. Briefly, sections were deparaffinized in xylene and rehydrated through a graded ethanol series. Antigen retrieval was performed by incubating slides in citrate buffer (pH 6.0) at 95℃ using a microwave heating system. Endogenous peroxidase activity was quenched with 3% hydrogen peroxide, followed by blocking with 5% BSA.

Primary antibodies against FKBP10 (1:200), DNASE1L3 (1:200), DPEP1 (1:1000), N-cadherin (1:4000), Vimentin (1:5000), and E-cadherin (1:5000) were applied to tissue sections and incubated overnight at 4℃. After washing with PBS, slides were incubated with HRP-conjugated secondary antibodies. Diaminobenzidine (DAB) was used as the chromogen, and hematoxylin was applied for nuclear counterstaining.

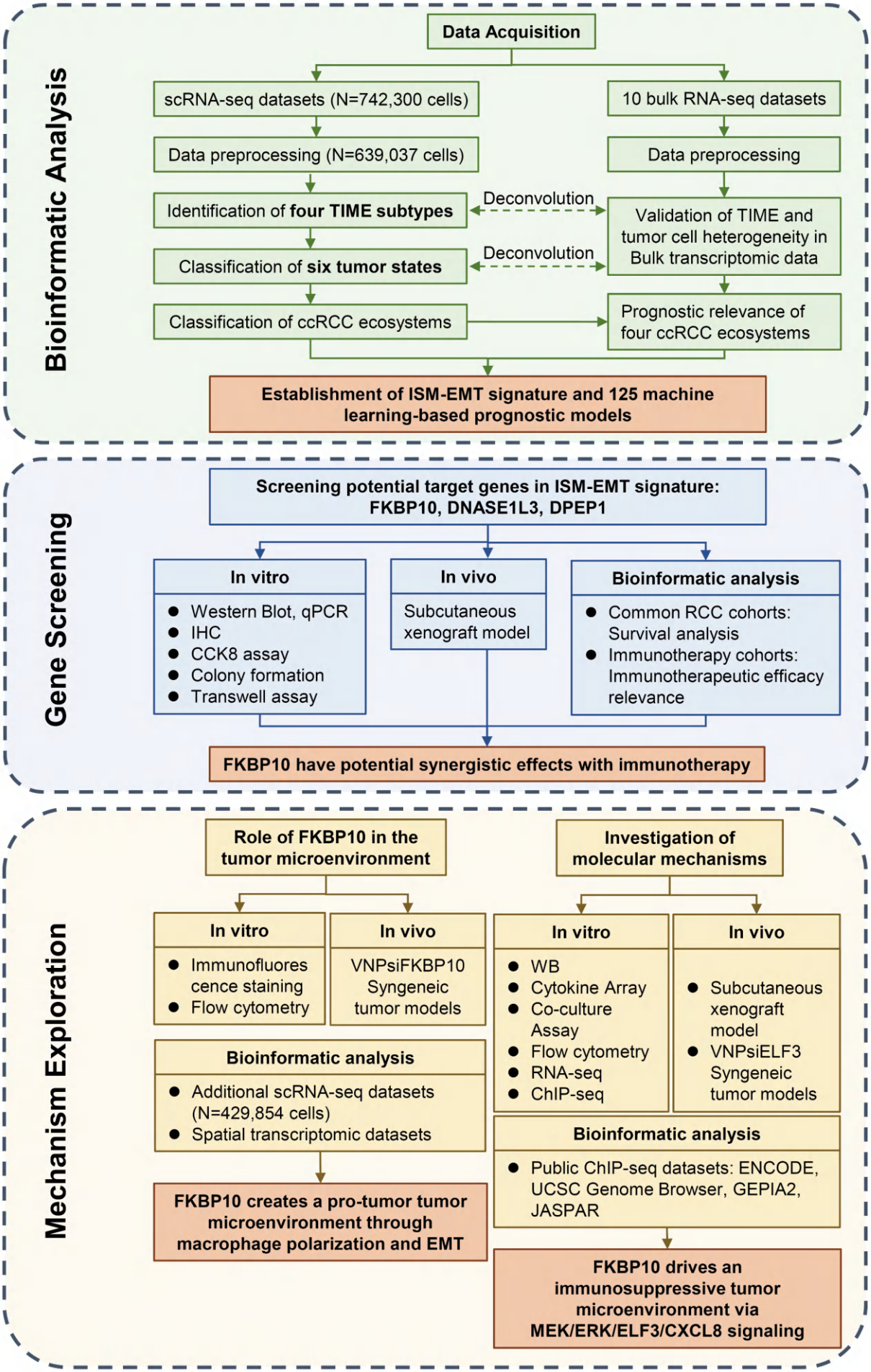

Figure S1 Flowchart summarizing the entire study design.

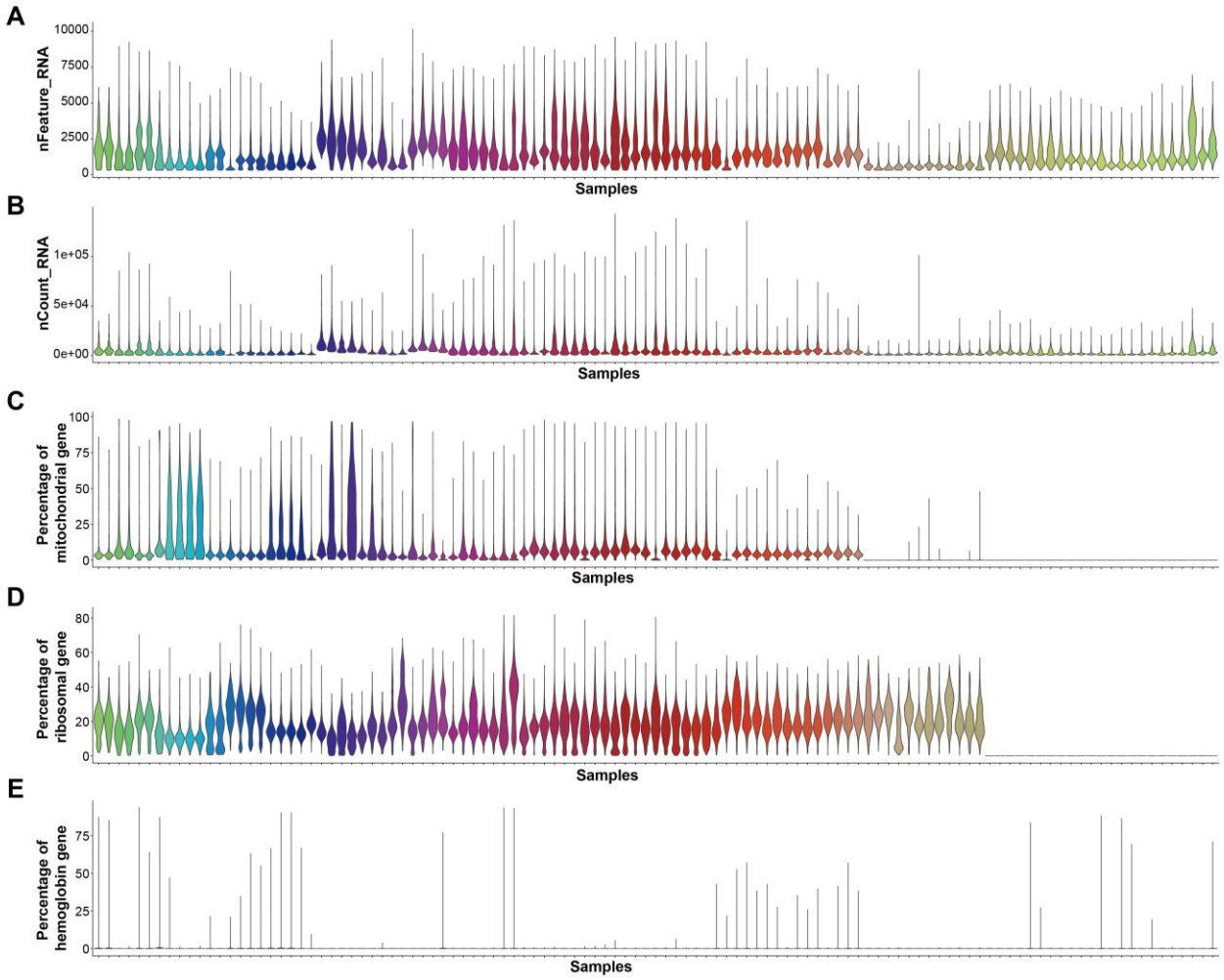

Figure S2 Quality control metrics of single-cell RNA sequencing data across all samples prior to filtering. Violin plots display the distribution of five key QC metrics for each sample: (A) nFeature_RNA: the number of unique genes detected per cell. A low count may indicate a damaged or low-quality cell. (B) nCount_RNA: the total number of molecules (UMIs) detected per cell. Extreme values (very low or very high) can suggest poor cell quality or the presence of multiple cells (doublets), respectively. (C) Percentage of mitochondrial gene: the percentage of cellular transcripts mapping to the mitochondrial genome. A high percentage is indicative of cellular stress or apoptosis. (D) Percentage of ribosomal gene: the percentage of transcripts mapping to ribosomal protein genes. (E) Percentage of hemoglobin gene: the percentage of transcripts mapping to hemoglobin genes. The shape of each violin represents the kernel density estimation of the data distribution. These metrics are crucial for identifying and removing low-quality cells to prevent technical artifacts from influencing downstream analyses.

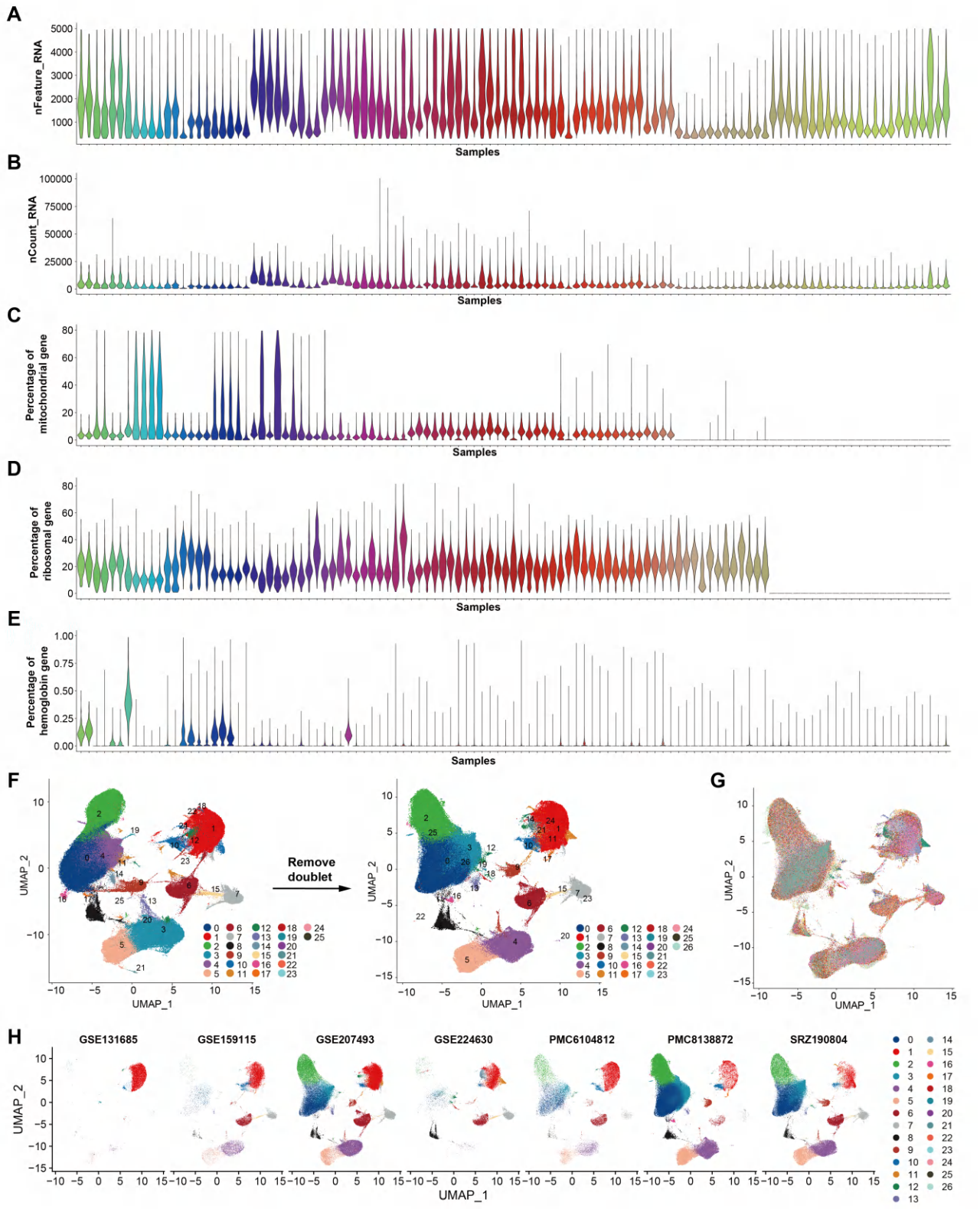

Figure S3 Quality control metrics for single-cell RNA sequencing data after filtering.

(A-E) Violin plots display the distribution of key QC metrics across all samples after quality filtering. Violin plots show number of detected genes per cell (nFeature_RNA), total UMI counts per cell (nCount_RNA), and the percentage of reads mapping to mitochondrial, ribosomal, and hemoglobin genes. Cells falling outside defined thresholds for these parameters were filtered to ensure data quality for downstream analysis. (F) UMAP plot showing clusters of all cells from seven public datasets before doublet cell filtration (left), and after doublet cell filtration (right). Dots represent individual cells, and colors represent different clusters. (G)

UMAP plot showing clusters of all cells, with color coded by samples. It can be seen that the Harmony algorithm effectively eliminates the batch effect of different samples. (H) UMAP visualization after Harmony integration, with cells split by dataset. Harmony effectively aligns datasets by removing technical variations while preserving biological structures, as evidenced by the overlapping distribution of analogous cell populations across samples.

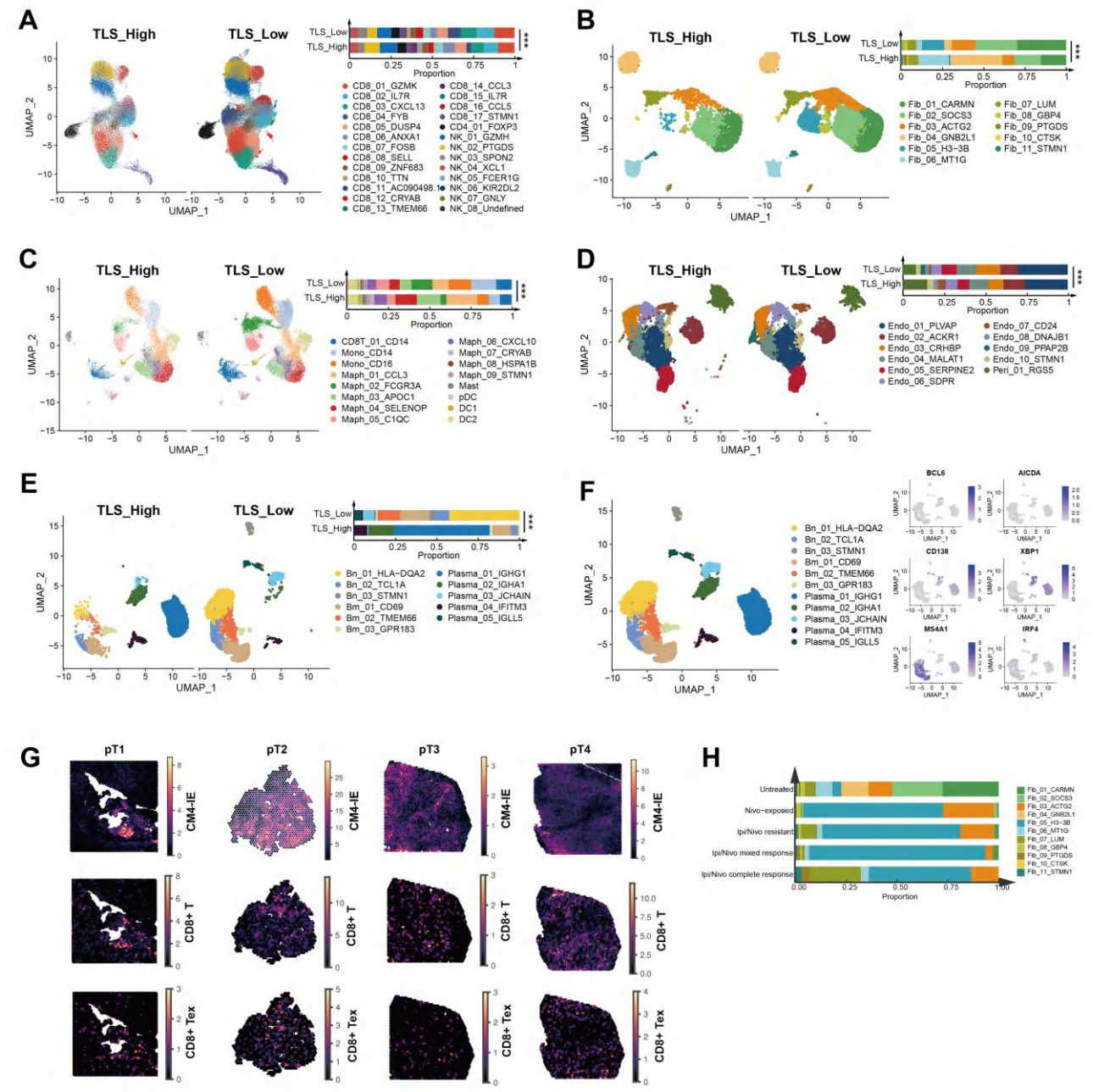

Figure S4 Comparative analysis of immune and stromal cell proportions between TLS-high and TLS-low groups.

(A-E) DimPlot illustrating the distribution of NK/T cells (A), fibroblasts (B), myeloid cells (C), endothelial cells (D), and B cells (E) across TLS-high and TLS-low groups. Cells are colored by cell type, and groups are segregated based on TLS signature scores. Stacked bar plot quantifying the relative proportions of each cell type within TLS-high and TLS-low groups. The B-cell compartment demonstrates the most notable shift, with

altered subset composition in TLS-high samples. Statistical significance was assessed using Chi-square test. TLS, tertiary lymphoid structure. (F) FeaturePlot visualization of germinal center (GC) gene expression levels for BCL6, AICDA, MS4A1, CD138, XBP1, and IRF4 across the B-cell subsets. Expression gradients are depicted from low (gray) to high (blue). (G) Spatial co-localization analysis between CM4-IE cells cells and specific T cell types. Representative spatial transcriptomics map showing the distribution of CM4-IE-high cells, CD8+ T cells, and exhausted CD8+ T cells within the tumor microenvironment. Color gradient indicates signature score intensity. CM4-IE-high cells exhibit spatial proximity to CD8+ T cells and exhausted CD8+ T cells. (H) Immunotherapeutic relevance of fibroblast clusters. Stacked histogram showing the fibroblast clusters proportion in ICB-treated and ICB-untreated cohort. Fib_05_H3-3B was found to significantly enriched in ICB-treated samples. Chi-square test was used for statistical analysis. Nivo, Nivolumab (anti-PD-1 monotherapy); Ipi, Ipilimumab (anti-CTLA-4 monotherapy).

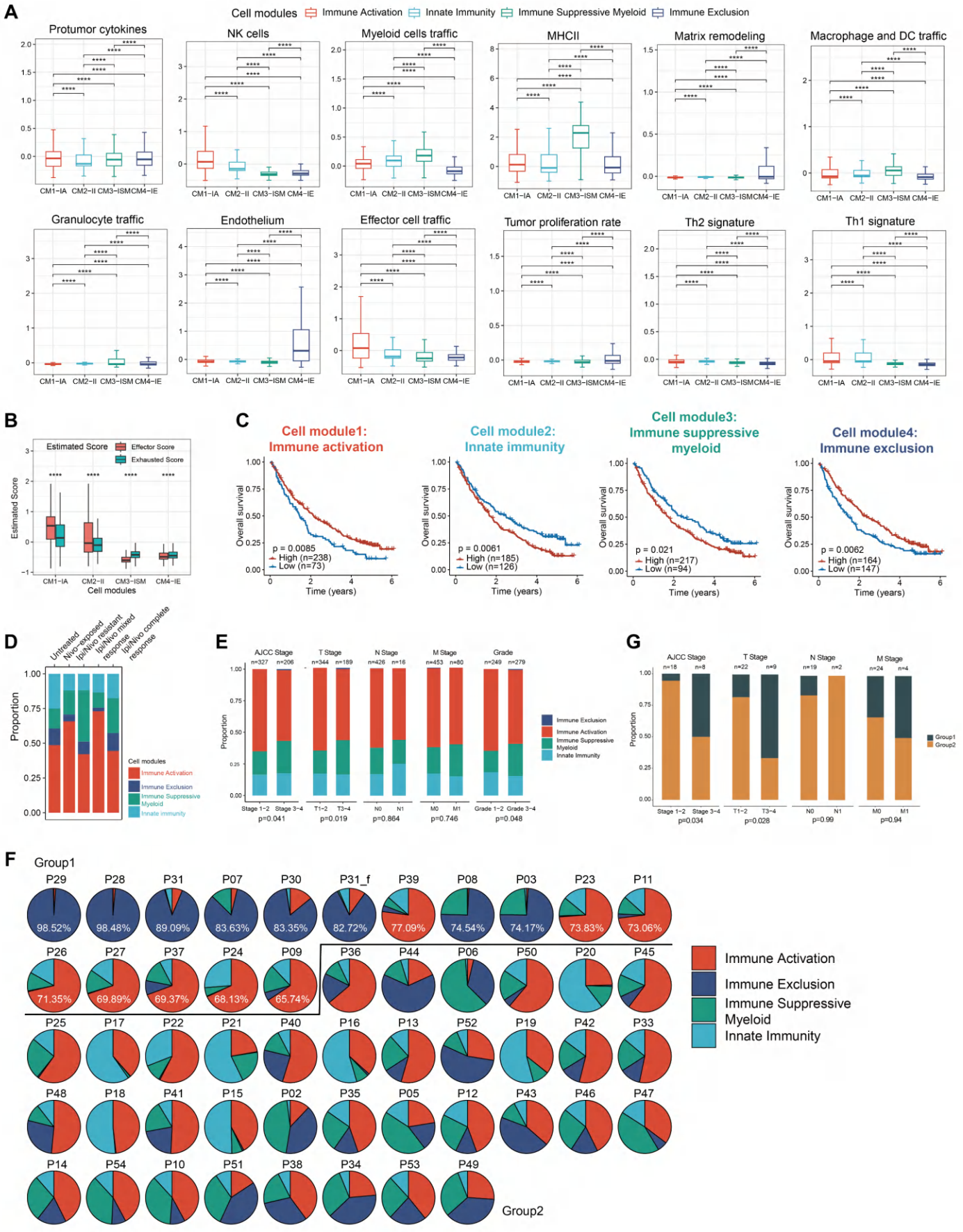

Figure S5 Distinct characteristics of TIME subtypes.

(A) Boxplots showing the expression of supplementary immune-related signatures in different TIME subtypes. Wilcoxon rank-sum test (two-sided) was applied for significance test. *, $P < 0.05$; **, $P < 0.01$; ***, $P < 0.001$.

IA, immune activation; II, innate immunity; ISM, immune suppressive myeloid; IE, immune exclusion. (B) Boxplots showing the expression of exhausted and effector signatures in different TIME subtypes. Wilcoxon rank-sum test (two-sided) was applied for significance test. *, $P < 0.05$; **, $P < 0.01$; ***, $P < 0.001$. (C) Overall survival (OS) of cases stratified by BisqueRNA predicted TIME-specific cell types proportion in Checkmate cohort (including all samples). Log-rank test was used for statistical analysis. (D) Stacked histogram showing the TIME proportion in ICB-treated cohort. (E) Stacked histograms showing TIME-specific cell types proportion across different tumor stages and pathological grades. Cell types proportion were predicted by BisqueRNA in TCGA-KIRC cohort. Chi-square test was used for statistical analysis. (F) Pie charts showing the proportion of TIME specific cell types across 52 patients. Patients with cells (≥65%) from sole individual TIME subtype were classified as group 1 (monotypic TIME dominance) (n = 16), while patients with cellular composition shared by multiple TIME subtypes were classified as group 2 (heterotypic TIME integration) (n = 36). (G) Stacked histograms showing group cluster proportion across different tumor stages in our integrated scRNA-seq datasets. Chi-square test was used for statistical analysis.

T01: 829 cells; 9 programs

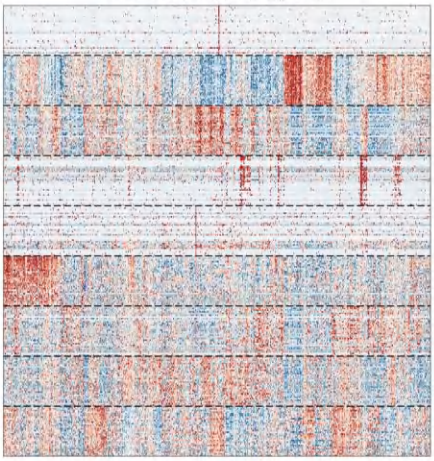

T01_1; T01_2; T01_3; T01_4; T01_5; T01_6; T01_7; T01_8; T01_9

RNASE1	PECAM1	GIMAP7	CCL14	FN1	SPARCL1
VWF	FAM167B	ECSCR.1	HYAL2	ENG	CHN1
RP11.486I11.2	SESN3	PLVAP	C2CD4B	SPARC	STAB1
ADGRL4	MEF2C	APOLD1	SH3BP5	TGFBR2	MIR22HG
FLIP1L	GSN	CDH5	THBD	IGFBP7	PODXL
RPL10	RPL13	RPL7	RPL9	RPS3	RPS14
RPL18A	RPL5	RPL10A	RPS18	RPS3A	RPS27
RPL23A	RPL11	RPL13A	RPL7A	RPS6	RPL21
RPL8	RPL41	RPL18	CIRBP	RPL12	RPS15A
RPS27A	RPL36	RPL19	EPB41L4A.AS1	RPS8	NPM1
CD74	LAP3	RARRES3	GBP4	HLA.DQA1	CXCL11
PSMB9	CST3	TNFSF10	C1S	CTSS	S100A11
HLA.DRA	HLA.DOB	APOL1	WARS	PSME2	PSMB8
GBP5	TAP1	TAPBP	C3	B2M	IFI44L
VAMP5	IFI27	SAMD9L	UBE2L6	HLA.DPA1	STAT1
KIAA0101	STMN1	TK1	SPC25	CDK1	TOP2A
ZWINT	TYMS	DUT	TUBA1B	CENPU	DHFR
PCNA	PTTG1	H2AFZ	GINS2	UBE2T	MND1
UBE2C	RAD51	CENPK	CDC45	RAD51AP1	CDT1
PKMYT1	BIRC5	TCF19	POC1A	E2F1	RNASEH2A
IL3RA	CD37	LSP1	CLEC2D	S100A4	S1PR4
TYROBP	MS4A7	EREG	FAM26F	FCER1G	TSPAN1
KCNAB2	TIMP2	AIF1	RP11.295G20.2	CD48	TIMP1
SLC2A6	RASAL3	LYPD3	GPX4	KRT7	PFN1
TMSB4X	CLDN7	FCGR3A	PILRA	GMFG	OLR1
JUN	ATF3	IER2	EGR1	SOCS3	FOS
ZFP36	PPP1R15A	HSPA5	IRF1	KLF10	TSC22D3
RHOB	FOSB	JUNB	DUSP1	DDIT3	GADD45B
BTG2	HERPUD1	CEBPD	CDK2AP2	IFIT2	CISH
SRSF3	DDIT4	EGOT	DNAJB11	ATF4	EFNA1
CUBN	CYB5A	MT.CO1	FTL	AQP1	GPX3
SLC5A12	SERF2	SLC16A9	DNPH1	PDZK1IP1	GSTA1
ADIRF	APOM	PEBP1	DAB2	GLYATL1	OCIAD2
LRP2	NAT8	HMGN3	MT.CO2	FABP7	PCSK1N
SMIM24	CXCL14	ERBB3	CAMT	TMEM174	UQCRQ
PHLDA1	MT2A	ELL2	CEBPB	DUSP6	MIDN
HBEGF	TGIF1	KDM6B	ARID5B	TNFRSF12A	MCL1
YBX3	SPSB1	MT.ND1	CHD1	LRRFIP1	TRIB1
NFIL3	PFKFB3	IER3	CSNK1A1	EPHA2	MT.CYB
ETS2	GCH1	YWHAZ	KLF4	FOSL1	MT1E
NNMT	UBC	SLC3A1	PKM	HSPA1A	HSPA1B
PGK1	HLA.A	PFKP	HSP90AB1	ENO1	ALDH1A1
ITM2B	ATP5B	ACAA2	HLA.B	TUBA1C	HSPA8
DNAJA1	TMEM176B	HLA.C	BBOX1	CNDP2	HLA.DRB1
ACAT1	MAGED2	LGALS3BP	TCP1	HSPA9	PDZK1

T02: 156 cells; 5 programs

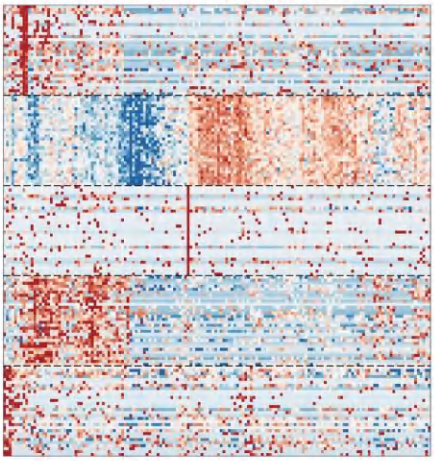

T02_1; T02_2; T02_3; T02_4; T02_5

PTER	ATP5G3	COX7B	CAPN6	B4GALT2	SLC2A2
PRKCDBP	CHST13	GPD1	SPNS2	CES2	ST20
NDUFS6	TIMM8B	GAMT	ATP5A1	PRELID1	MRPL35
ATP5G1	GTF3A	TMEM141	PPIA	MYO1B	NME1
PCSK1N	COX7A2	ICMT	PEPD	TRIB3	COX4I1
RPS8	RPL10	RPL8	RPS14	CCNI	RPL21
RPS27	RPS6	RPL13A	RPS20	RPL12	FTH1
RPL41	RPL36	RPS24	RPL27A	RPL11	RPL35
RPL19	RPL13	RPL30	EIF1	RPLP2	RPL18A
RPS27A	RPS4X	RPL32	RPS3A	RPS3	RPL23A
FLT1	PLVAP	RGCC	INSR	PLPP1	HSPG2
PDGFD	IGFBP7	GSN	A2M	RASSF1	SDPR
IPO11	CLEC2B	SPRY1	GNAI2	NRP2	EVA1B
RND1	APOLD1	SPARC	CYP2U1	PGM2L1	AIF1L
RAB5A	TACC1	VWA1	BAZ2B	GRB10	FRMD8
HSPD1	BBOX1	AMN	HSPE1	TMEM176B	CFI
SLC17A3	LGALS2	TMEM27	SLC13A1	ZFAND2A	KHK
TCN2	SLC3A1	TMEM176A	PRODH2	HSPH1	AQP1
CXCL14	TINAG	CLDN2	HSP90AB1	NAT8	CUBN
MT.CYB	ACSM2A	MIOX	CTSH	AOC1	MT.CO3
UBD	S100A11	IL32	PFN1	WARS	INHBA
ANXA2	PSME2	S100A1	ANXA3	PSMB10	YKT6
CDK7	RP11.283G6.4	CAV2	TRAF1	LAP3	S100A10
FAM129A	RAC1	RASGRP3	SOD2	SESN2	CX3CL1
IGFBP3	PSMB9	TYMP	GARS	ATP2B1	APOL1

T03: 1334 cells; 6 programs

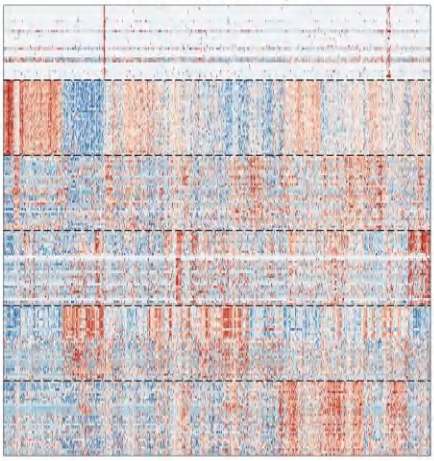

T03_1; T03_2; T03_3; T03_4; T03_5; T03_6

TOP2A	CDK1	MKI67	CENPF	TPX2	UBE2C
PTTG1	BIRC5	BUB1	CDC20	STMN1	RACGAP1
ANLN	UBE2T	FAM83D	CCNB2	S100A2	TUBA1B
PBK	SPC25	RRM2	TUBB	H2AFZ	GTSE1
SHCBP1	HMMR	NUSAP1	PRC1	ZWINT	CENPE
RPS18	RPL9	RPS4X	RPL23A	RPL13A	RPS3A
RPL10	RPL13	RPL11	RPL21	RPS14	RPS3
RPS27A	RPS8	RPS6	RPS2	RPS23	RPL18
RPL7	RPL18A	RPL8	RPS27	RPL24	RPL5
RPS5	RPL30	RPL34	RPS24	JUNB	RPL37A
S100A10	ITM2B	FHL1	KRT8	IGFBP6	CLDN4
KRT18	S100A11	TSPAN1	CLDN7	HSPB1	NAPSA
TMEM176B	AHNAK2	DEFB1	CKB	SMIM24	LINC01320
TMEM176A	ANXA1	REG1A	AOC1	GUCA2B	FAM134B
ANXA2	CRIP1	TNFRSF12A	HSP90AA1	S100A6	LDHA
CD74	RARRES3	B2M	HLA.B	PSMB9	HLA.A
HLA.C	HLA.DRA	HLA.DRB1	IL32	IFIT2	GBP4
HLA.DMA	SERPINA1	GBP1	HLA.F	PSMB10	HLA.DQA1
TAP1	APOL1	TAP2	WARS	TAPBP	LAP3
IGFBP3	PSMB8	STAT1	UBD	HLA.DQB1	HLA.DRB5
NEAT1	MT.ND4	MT.ND3	MT.CO2	MT.ATP6	XIST
MT.ND1	MT.ND2	MT.CO3	MALAT1	MT.CYB	MT.CO1
MT.ND5	YBX3	VEGFA	KDM6B	JUND	FLNA
SLC5A3	ITGA3	AHNAK	PLEC	GLS	AGRN
SYNPO	HIPK2	CCNL1	TJP2	AC058791.1	VMP1
GSTA2	GSTA1	KHK	NAT8	APOM	CYB5A
PDZK1IP1	BBOX1	MGST1	PRAP1	AQP1	CUBN
ACSM2B	HRSP12	UQCRQ	TXN	OCIAD2	AGXT2
ATPIF1	AGT	ECH1	MSRA	DNPH1	CXCL14
ATP5G3	CMBL	SSR4	FBP1	COX6C	GAL3ST1

T04: 695 cells; 4 programs

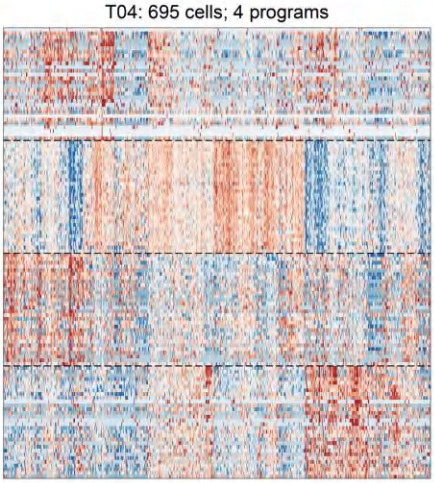

T04_1; T04_2; T04_3; T04_4

CDHR1	DNAJB1	HSPE1	BAG3	ZFAND2A	HSPA6
HSPA1B	HSPA1A	SERPINH1	SMIM24	CACYBP	HSPD1
SLC17A3	HSP90AA1	NR4A1	NMB	CRYAB	HSPB1
HSPH1	DNAJB4	SCGN	COX6A1	CHCHD10	AC004012.1
UBB	ATP5B	DRAIC	GBP1	RP11.63A11.1	CYR61
RPL13A	RPL10A	RPS2	RPL18A	RPS5	RPL21
RPS3	RPS3A	RPL41	RPL3	RPL7	EEF1A1
RPLP0	RPL10	RPL11	RPL8	RPL23A	RPL5
RPS6	RPL19	RPS4X	GNB2L1	RPS27A	RPS17
RPS14	RPL15	RPS12	RPS18	RPS10	RPS9
FOSB	MALAT1	JUN	NEAT1	JUND	EGR1
FOS	BRD2	KLF6	FUS	RHOB	ATF3
SLC38A2	ZFP36L1	INTS6	ATF4	MT.ND2	DDX5
H3F3B	JUNB	VEGFA	IER2	UBC	BTG1
HIST1H4C	DUSP1	VMP1	MIDN	CTD.3252C9.4	MT.ND1
HLA.A	HLA.C	HLA.B	IGFBP3	B2M	S100A11
S100A6	PFN1	LGALS1	HLA.F	ARPC1B	IGFBP7
CD70	PSME2	IFI27	C15orf48	IGFBP2	GAPDH
ACTB	CYBA	IFI6	P4HB	TIMP1	LGALS3BP
ANXA2	IGFBP6	SH3BGRL3	CST3	CD63	CD59

T05: 1051 cells; 5 programs

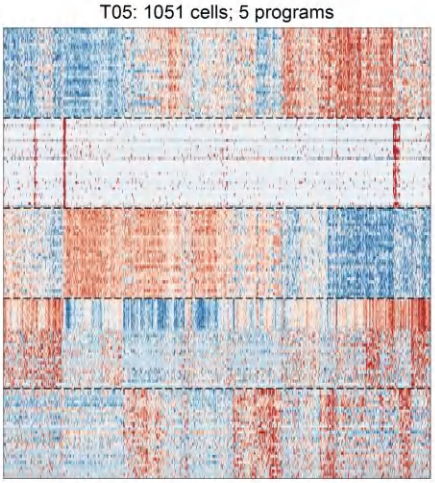

T05_1; T05_2; T05_3; T05_4; T05_5

BAG3	HSPH1	HSPD1	HSP90AB1	XBP1	HSPB1
CRYAB	ZFAND2A	DNAJB4	DDX5	DNAJA1	SELK
HSPE1	DNAJB1	CLK1	HSP90AA1	HSPA5	MCL1
CCNL1	SERPINH1	DDIT3	HSPA1B	PPP1R15A	HSPA8
ATF3	EGR1	HSPA4	UBC	DEDD2	H3F3B
UBE2C	CCNB2	CCNB1	CENPF	NEK2	PLK1
TOP2A	PTTG1	NUF2	HMMR	STMN1	UBE2T
CDK1	H2AFZ	CDCA8	CEP55	MKI67	HJURP
PRC1	AURKB	ASPM	NMU	CDC20	CKAP2
KIF20A	CDCA3	TPX2	FAM64A	CENPW	ARL6IP1
ALDOA	EEF1A1	PKM	RPL10A	BST2	RPL3
PGAM1	TMEM59	TPI1	HINT1	RPS3A	RPL4
RPL7	GAPDH	RPL5	SKP1	LAPTM4A	RPL21
RPL13A	PGK1	HLA.C	RPS5	GNB2L1	LDHB
FGG	RPS3	RPS27A	EIF3E	RPS2	RPS4Y1
MT.ND5	MT.ATP6	MT.ND4	MT.ND1	MT.CO2	MT.ND2
MT.CO1	MT.CYB	MT.ND3	MT.CO3	MT.ND4L	ST5
KCNQ1OT1	RRBP1	POLR2J3	INTS6	PLCG2	C1orf186
AGRN	RGS16	RP11.467L13.7	CSAD	RP11.412D9.4	LINC01320
RPL22L1	PAX2	CH17.189H20.1	HILPDA	RP11.796E2.4	HOOK2
MT2A	MT1E	PHLDA2	PHLDA1	LRRFIP1	CEBPB
MT1X	S100A16	PIM3	YWHAQ	CFLAR	TM4SF1
SERPINE1	FAM110C	FTH1	MAP1B	SMIM3	ODC1
S100A10	G0S2	FOXC2	FKBP5	SOD2	TXNRD1
BIRC3	DUSP5	TUBB2A	MSC	BHLHE40	PTPN1

T07: 1161 cells; 7 programs

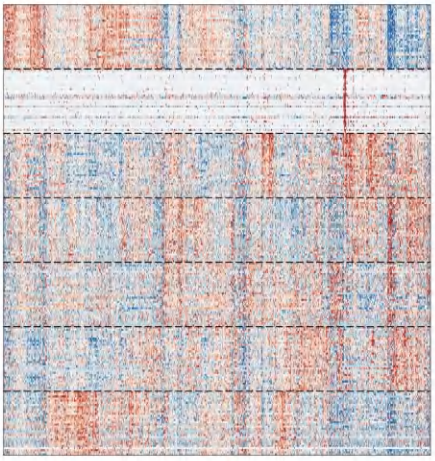

T07_1; T07_2; T07_3; T07_4; T07_5; T07_6; T07_7

RPS4X	RPS6	RPL10A	RPS14	RPL18A	RPS3
RPL10	NPM1	RPS2	GNB2L1	RPS15A	RPL23A
RPL11	RPL41	RPS18	RPL7A	RPS3A	RPL14
RPL35A	RPL6	RPL13	RPS23	RPL3	RPL5
RPL31	RPS13	BTF3	RPS7	RPL18	RPL12
PTTG1	MKI67	NEK2	UBE2C	TOP2A	HJURP
TROAP	KIF14	SPC25	CDKN3	RP11.844P9.2	ASPM
CCNB1	HIST1H4C	CENPF	UBE2T	CENPA	STMN1
PBK	HMMR	CDC20	NUF2	TUBA1B	CDCA3
CENPW	BIRC5	CDK1	KIF20A	NUSAP1	PLK1
S100A11	MT2A	S100A10	TIMP1	ANXA2	FTH1
MT1X	EMP3	S100A6	TMSB10	LGALS1	CD63
CYBA	SPP1	PKM	GAPDH	S100A16	CRYAB
IL32	SERPINA1	CLIC1	ACTB	MT1E	IGFBP3
PLP2	HLA.A	CD44	SERPINE2	PFN1	ENO1
NFKBIA	EGR1	CXCL2	SDC4	IER3	PPP1R15A
FOSB	ATF3	IRF1	NFKBIZ	MCL1	NFKBID
TNFAIP3	MAFF	JUNB	BTG2	C11orf96	JUND
PNRC1	CYLD	FSTL3	TNFAIP2	CXCL8	MIDN
ICAM1	SOD2	CXCL3	XBP1	ABL2	GEM
CP	UQCRB	MALAT1	FGB	AC159540.1	VCAN
VEGFA	ABCC3	IRS2	PNISR	ANKRD12	N4BP2L2
NEAT1	SON	APOB	NPTX2	RPL39	PDK4
NAP1L1	HSP90B1	HSPE1	RPS24	TXNIP	KLF6
SPINK13	DDX17	ADM	KCNQ1OT1	GOLGA4	RP5.1021I20.2
KHK	CYB5A	CD74	LGALS2	HLA.DRA	NNMT
HLA.A.1	HLA.DPA1	B2M	TMEM176B	RBP4	TMEM176A
HLA.DRB1	CXCL14	MYH8	SEPP1	HLA.C	TMEM37
REG1A	NDUFA4L2	NAT8	HMGN3	TPI1	HLA.B
CLU	GPX3	ECH1	PGK1	CD24	ACMSD
TCEA1	CHCHD10	SPINK1	RNF187	TSLP	NUPR1
RPLP1	SLC3A2	FTL	BEX2	RPS16	EIF1
HSPA9	EIF2S2	RPL13A	LARP6	RPS27	REXO2
GFPT1	CEBPG	RPL30	CLGN	CCPG1	SARS
MTHFD2	SEC11C	CTC.573N18.1	RPL37A	NACA	SHMT2

T10: 146 cells; 7 programs

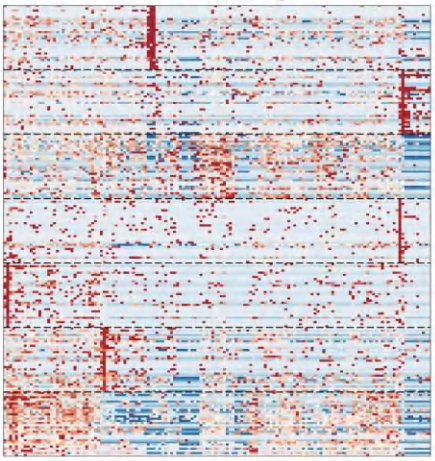

T10_1; T10_2; T10_3; T10_4; T10_5; T10_6; T10_7

MARCKSL1	BCL2A1	EBI3	LAMP3	CD40	TUBB6
TRAF1	SRGN	BIRC3	RASSF4	EPSTI1	CCR7
LITAF	NUB1	PLEK	NFKBIA	POGLUT1	SAMSN1
CD83	N4BP2L1	CKB	GSN	IRF8	MGLL
IRF1	TXN	RASSF2	CD86	MIR23AHG	SLC5A6
H4C3	SPAG4	NDUFA4L2	MT2A	PBK	PIMREG
CKS2	TUBA1C	IGFBP7	CRYAB	VIM	TUBA1B
CAV1	ANGPTL4	CDCA3	ANXA2	EGLN3	FHL2
ATP8B3	KRT8	RARRES2	FOS	CALD1	RHEB
ATF3	GAPDH	PPFIBP1	PHLDA2	ENPEP	MIF
CORO1A	ARHGDIB	SGMS1	EVL	YWHAZ	TRAF3IP3
GNAI2	CNN2	SELPLG	BIN2	RAC2	LCK
ITGAL	CXCR6	SYNE1	RCSD1	ZC3HAV1	ITGB2
VAMP4	ARL4C	THEMIS	IQGAP1	RFX7	ARFGAP1
TMSB4X	ZFP36L2	TRMT2B	TAGAP	GIMAP4	GIMAP7
FGL2	SAMHD1	FAM13A	FUBP3	SMIM14	HPS5
SLC22A5	GCLC	SCD	APBB3	KLHL24	SKIL
EFR3A	SLC39A10	MS4A6A	NUDT16	MYOF	ZBTB4
ABL2	VCL	SGK1	HLA.DRA	GRN	FAM91A1
PRKD2	RBBP9	ZNF852	WARS1	TNKS1BP1	DDX60L
CASZ1	RAMP1	MAVS	LARP1B	FLAD1	NDUFAF7
CTTN	COQ2	DDIT3	TOPORS	TMEM97	RASGEF1A
PSMA8	STAMBPL1	STX11	PRPF18	CNNM2	RIPK2
CGAS	BAG3	PRTFDC1	NFE2L3	BCAT1	SCNN1B
CCDC150	PMAIP1	USP25	SCPEP1	EAF2	ZNF689
IL2RA	LTA	FOXP3	C1QBP	TNFRSF4	CORO1B
EIF5A	TTLL12	MCRIP2	SOCAR	NPM1	NOP16
MYC	RAB33A	LTB	UTP11	CEP72	ZBTB32
RRP9	WDR77	LAIR2	HMGA1	PAFAH1B3	ATP5MC3
APRT	SLIRP	WDR43	IMPDH2	HACD1	SNRPG
PON2	HLA.DQA2	RAMP1.1	CTHRC1	CST7	XCL1
CMC1	PON3	HLA.DQA1	HLA.DMA	FAM174B	HLA.DRB1
CD27	HLA.DRB5	SYNGR2	PMCH	DCTPP1	ITM2A
SEC11C	DBI	NMNAT3	TAF13	VCAM1	CTSW
PPIA	XCL2	ARF5	COCH	TYMS	NAA60

T06: 3301 cells; 6 programs

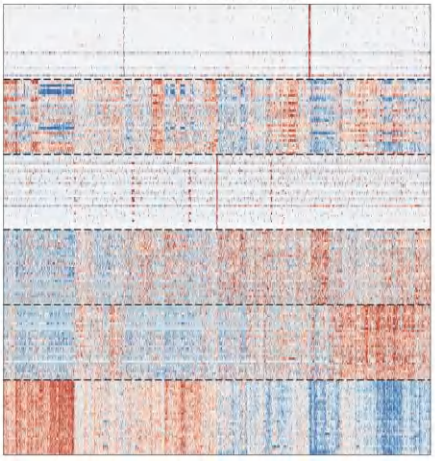

T06_1; T06_2; T06_3; T06_4; T06_5; T06_6

TOP2A	PTTG1	UBE2C	CCNB2	TPX2	CDKN3
CDCA3	CDK1	HJURP	CDC20	BIRC5	MKI67
PBK	CENPF	HMMR	GTSE1	ASPM	DLGAP5
NUF2	STMN1	HMGB3	TROAP	ANLN	SPC25
AURKB	NUSAP1	CEP55	UBE2T	TUBA1B	CENPA
RPL8	RPL7	MT.ND2	UQCRB	MT.ND5	MT.ND3
CD74	RPL12	RPL30	HLA.DQA1	FXYD2	EEF1D
HLA.DPA1	PABPC1	RARRES3	EIF3E	GNB2L1	RARRES2
B2M	MT.CO2	HLA.DRA	RPL10	HLA.A	HINT1
HLA.DPB1	RPS2	RPS20	RPLP0	RPL7A	HLA.B
TYROBP	C1QB	C1QA	SRGN	EREG	C1QC
CCL4	GPR183	MS4A6A	TNFAIP3	IL1B	CCL4L2
APOC1	NLRP3	LAPTM5	REL	PLEK	RGS1
DUSP2	FAM26F	TMSB4X	LST1	MS4A7	DUSP4
FCER1G	AIF1	PTPRC	CCR7	TCHH	CSF1R
CCL2	KDM6B	IER3	CDKN1A	PLEKHA1	YBX3
H3F3B	MIDN	PFKFB3	IGFBP3	SOD2	MIR22HG
ZFP36L1	TNFRSF12A	ODC1	MCL1	NEAT1	NAMPT
LMNA	ETS1	HMGN3	PTRF	FOSL2	CITED4
ITGA3	ANGPTL4	AHNAK	TNFRSF21	NFIL3	MAP2K3
TSPAN1	CDHR5	CES2	PDZK1IP1	CYB5A	NAT8
AMN	KRT18	SMIM24	AOC1	PCSK1N	TMEM176A
LGALS2	ECH1	TMEM176B	CXCL14	AKR7A3	BSG
KHK	SLC2A5	ACSM2B	HLA.DRB1	TM4SF5	SLC6A13
ITM2B	ACAT1	MGST1	ADIRF	HSPE1	PEBP1
RPL18	RPL13A	RPL36	RPS27	RPLP2	RPL21
RPL9	RPS16	RPL13	RPS3	RPL19	RPS18
RPS25	RPS13	RPL27A	RPL18A	RPL5	RPS5
RPL15	RPL38	RPL23A	NPM1	RPL3	RPS27A
RPS6	RPL35	RPL11	RPS3A	RPS14	RPS23

T11: 845 cells; 5 programs

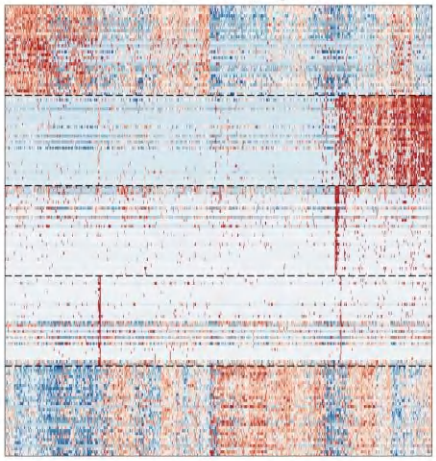

T11_1; T11_2; T11_3; T11_4; T11_5

PDZK1IP1	CYB5A	ATP5MC3	CXCL14	PCSK1N	CLTRN
KHK	UQCRQ	SMIM24	HINT1	DEFB1	TRIM54
GPD1	GAL3ST1	AZGP1	COX6A1	SLC23A3	ADIRF
SLC5A12	SLC39A5	TNFRSF12A	TSPAN1	NAT8	GPX3
GSTK1	UQCR10	SLC37A4	COX5B	CUBN	CYB5R3
CD3E	TMSB4X	SRGN	ARHGDIB	ZFP36L2	HCST
CORO1A	PTPRCAP	IL2RG	CD52	HLA.C	CD37
CD3D	HLA.E	CD69	JUNB	LSP1	BTG1
CYTIP	LCP1	LCK	CD2	PTPRC	CD53
ALOX5AP	EVL	CD7	TNFAIP3	CD8B	CD96
HLA.DRA	HLA.DPB1	HLA.DPA1	HLA.DQA1	LYZ	TYROBP
FN1	HLA.DRB1	C1QA	VSIG4	HLA.DRB5	FCER1G
MS4A6A	HLA.DQB1	S100A9	HLA.DQA2	C1QB	CD86
FCGR3A	C1QC	HLA.DMB	RNASE6	AIF1	C1orf162
SPI1	FGR	FCGR2B	CTSS	SIGLEC10	SLAMF8
ASPM	CENPF	PTTG1	CDCA3	MKI67	UBE2T
CENPE	TACC3	CDKN3	STMN1	NMU	RRM2
PHF19	CCNB1	FAM83D	H2AZ1	TUBB4B	PRC1
ARL6IP1	ANLN	MYH9	PRR11	TUBA1B	APOBEC3B
INCENP	UBE2C	CCNB2	PCLAF	LGALS1	LMNA
SQSTM1	ENO2	SARS1	PLIN2	EIF1	NPM1
VIM	CCNI	EEF1D	CNBP	EIF4A2	S100A6
PTGES3	UCHL1	RACK1	ALDOA	FTL	TCEA3
TCEA1	BEX2	PCBP2	NOP53	RBCK1	TAGLN2
U2AF1	PSAP	EPRS1	EEF2	NUPR1	TNIP1

T13: 958 cells; 4 programs

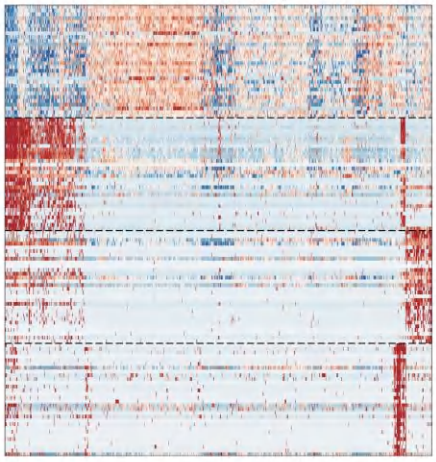

T13_1; T13_2; T13_3; T13_4

PDZK1IP1	HINT1	COX7C	ANGPTL4	PPIB	GAPDH
ATP5MC3	TRABD2B	ALDOA	MIF	DEFB1	COX5B
CD151	MGST1	PRELID1	TNFRSF12A	S100A1	COX6A1
NNMT	ALKAL2	CXCL14	TPI1	RBP5	S100A10
CA12	ADIRF	MLEC	AQP1	TMEM176B	HSPB1
C1QA	C1QB	APOE	C1QC	TYROBP	HLA.DPA1
HLA.DPB1	RNASE1	HLA.DRB1	HLA.DRA	HLA.DRB5	CST3
S100A8	GPX1	FTL	CD74	FCER1G	AIF1
TMSB4X	HLA.DQB1	GRN	MS4A6A	HLA.DQA1	LAPTM5
C1orf162	PLTP	APOC1	TREM2	LYZ	S100A4
PTPRCAP	CD3E	BTG1	TMSB4X.1	SIRPG	CD69
CST7	JUNB	SLAMF1	P2RY10	CD52	SRGN
HLA.C	LCK	ZFP36L2	DUSP2	CD2	MEI1
CD3D	ARHGDIB	KLRB1	GZMA	CD7	CYTIP
NKG7	TMIGD2	CD8A	SPNS3	CORO1A	CD27
HMMR	PTTG1	CCNB1	BUB1B	CENPF	CDC20
H2AZ1	PIMREG	UBE2S	CKS2	CDC25C	MKI67
PCLAF	BUB1	CCNB2	TRIP13	TUBB4B	ARL6IP1
ASPM	STMN1	CDCA8	TPX2	OIP5	CDCA3
TROAP	KIF20A	PRR11	FOXM1	PLK1	HMGN2

T15: 247 cells; 5 programs

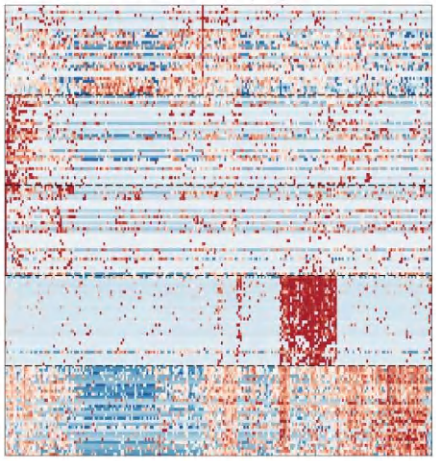

T15_1; T15_2; T15_3; T15_4; T15_5

TM4SF1	AKR1C1	AKR1B1	SERPINE2	HMOX1	AKR1C3
PRSS23	PYGL	NQO1	ATP5MC3	ATP5F1C	MAL2
TXN	ANXA2	ANXA5	WLS	SLC25A5	AHCY
G6PD	ACTG1	TUBB	COX5A	CHD1L	DERL3
NDUFA4	PRDX5	PPIA	FTL	FTH1	ATP5MF
SLC3A1	MSLN	LINC01320	NAT8	BAIAP2L2	RDH5
RNF186	METAP1D	CDHR5	PDZK1	NBPF1	FCGRT
EFNA1	TMEM176B	BBOX1	KCNQ1OT1	PCK1	ZNF639
ATP1B1	SLC23A1	RTN4	TMEM176A	CNTNAP5	CCN1
UGT2B7	STX16	APLN	KHK	SLC5A1	FAM13A
CA12	VEGFA	NDRG1	MT1X	DEPP1	TGFBR2
SERPINB9	MYEOV	PLOD2	SEMA4B	SOX4	SYCE1L
LGALS1	FCAMR	MT2A	ANGPTL4	KLF13	ITK
TNFRSF1B	GMEB1	MDC1	MGLL	TNS1	ARRDC2
TMSB10	CMTM3	SREBF2	C16orf74	F2R	IGFBP3
TMSB4X	CD3E	PTPRCAP	NKG7	PTPRC	RAC2
CST7	CD8A	CD27	CORO1A	CD3D	GZMK
HCST	GZMA	CD2	CXCR3	LAPTM5	GPSM3
LSP1	ARHGDIB	CTSW	SIT1	TRAF3IP3	RGS1
PRF1	SH3BGRL3	LCP2	LCP1	ITM2A	ITGA4
HLA.DRB1	HLA.DRB5	CD74	VCAM1	HLA.DQA1	C1S
HLA.A	SYNGR2	CD151	HLA.C	PDIA6	MAL
CFB	HLA.B	HLA.DRA	TAP1	SERPING1	CLU
IL18BP	HLA.DQA2	SERPINA1	CTSS	HLA.DQB1	C3
WARS1	SPINT2	FN1	TNFSF10	HLA.DPA1	PSAP

T12: 1318 cells; 5 programs

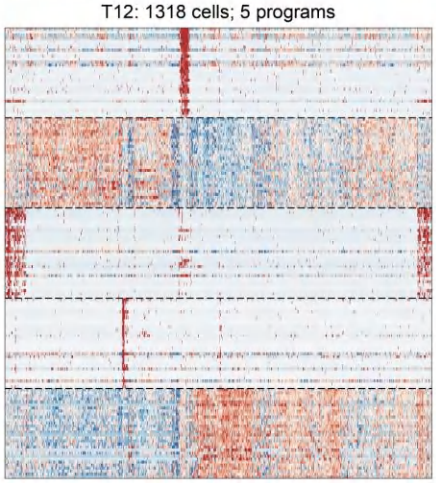

T12_1; T12_2; T12_3; T12_4; T12_5

HLA.DPA1	TYROBP	HLA.DRA	HLA.DPB1	MS4A6A	AIF1
HLA.DQA1	HLA.DRB5	FCGR2B	C1QC	HLA.DQA2	HLA.DQB1
HLA.DRB1	C1orf162	FCER1G	RNASE6	MS4A7	C1QB
IGSF6	FGL2	CTSS	LYZ	FCER1A	PLD4
LAPTM5	CLEC7A	CALHM6	C1QA	DOK2	CD1E
VIM	NPM1	DUSP1	TNIP1	CCNI	ENO2
PCBP2	TAGLN2	CNBP	EEF1A1	EEF1D	EEF2
SQSTM1	RHOB	NOL3	S100A6	UBC	CAV1
HSP90AB1	RACK1	EIF4A2	TGFBI	GLUL	EFEMP1
TCEA3	EIF3L	CPE	ANXA4	NOP53	PKM
CD69	PTPRCAP	CD3E	CD3D	CD96	XCL1
CD2	ARHGDIB	CD8B	CD52	IL2RG	CD8A
XCL2	LCK	BTG1	KLRD1	CD7	RGS1
CORO1A	EVL	SPOCK2	KLRB1	TMSB4X	CD160
HOPX	TBC1D10C	SLAMF6	CD3G	LTB	TMIGD2
PTTG1	PIMREG	CENPA	KIF20A	CENPF	CDKN3
BIRC5	DEPDC1	PLK1	CDC20	MKI67	CCNB2
CCNB1	CDCA3	CDC25C	CEP55	TOP2A	HMMR
H2AZ1	UBE2S	ASPM	TPX2	HMGB3	STMN1
KIF14	SHCBP1	NEK2	TUBA1B	SGO1	UBE2C
ATP5MC3	PRELID1	UQCRQ	PDZK1IP1	GCHFR	GPD1
CXCL14	PEBP1	CYB5A	NAT8	COX4I1	GSTK1
PEPD	COX6A1	SLC39A5	SLC5A12	COX5B	GSTA2
KHK	ANPEP	ASPDH	UQCR10	AQP1	TMEM174
GPX3	DDT	AKR1A1	ATP5PF	CLTRN	TRIM54

T16: 108 cells; 4 programs

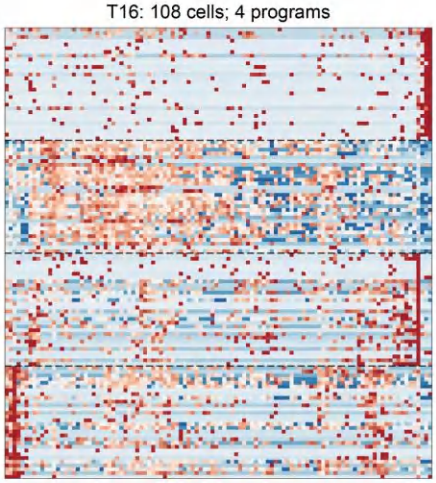

T16_1; T16_2; T16_3; T16_4

FUS	KLF6	SULT1C2	SLC25A16	PUM2	NFIB
RHPN2	BHMT2	YPEL2	ACSM2B	ADAMTS9.AS1	EXOC4
FNDC3B	CCNL1	SORBS2	LIFR	PKN2	TIPARP
RBM6	RALGAPB	DST	ACSM2A	IFRD1	TTC14
PTPRK	SRSF1	NUMB	BLNK	SEL1L3	LINC00937
FXYD2	ATP5MC3	COA3	UQCRQ	NDUFS3	NCBP2AS2
TMEM14B	ATP5MC1	COX5A	ATP5PB	COX7B	ATP5F1C
NIPSNAP2	MRPS26	C4orf3	UQCR11	UQCRB	FABP3
LDHB	CRYAB	NDUFB5	DLD	FAM162A	PRDX2
CYB5A	TMEM256	RBP5	CYC1	ALDOC	COX4I1
APOC1	APOE	C1QA	TYROBP	C1QC	C1QB
FCER1G	HLA.DPA1	SAT1	HLA.DPB1	HLA.DRA	MS4A6A
CD74	LYZ	RGS1	HLA.DRB5	CXCL13	TMSB4X
HLA.DMA	HLA.DRB1	GBP5	ZFP36L1	HLA.DQB1	SRGN
FXYD5	NPC2	PDK4	CELF2	HLA.DQA1	CTSW
UCHL1	LGALS1	ANXA2	SQSTM1	YWHAQ	S100A10
MYEOV	MCUB	S100A11	PHLDA2	CAP1	STIP1
PSMB10	CAV1	BID	PKM	S100A6	ISG20
GBP1	PSMD13	TALDO1	LMNA	SLC35A4	IDO1
WARS1	PFN1	VAMP5	VIM	S100A16	BCAP29

T27: 262 cells; 6 programs

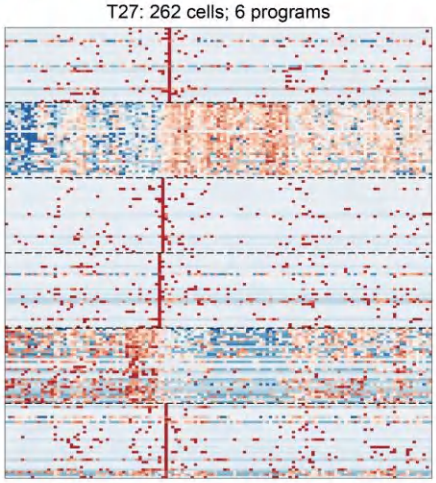

T27_1; T27_2; T27_3; T27_4; T27_5; T27_6

FBXO30	TMEM79	RP11.354K1.1	DNAJC18	C6orf203	UGT2B7
KIAA1586	BATF3	KDM1B	ALS2	BNIP1	PVRL3
ASAP3	FAM43A	RP11.359P5.1	FGA	CD55	IL1RL1
ZBTB49	LPIN1	CUL9	RP11.1C1.4	RP11.326I11.3	RP3.395M20.12
LEPROT	RP1.232P20.1	DNAJB11	CCBL2	CTC.338M12.5	ZC3H8
RPS3A	EEF1A1	RPS8	RPL11	GNB2L1	HINT1
RPS18	RPL5	RPS12	RPS23	RPL15	MARCKSL1
BTF3	RPL10A	NPM1	EEF1B2	RPL9	RPL34
RPL14	RPL32	HMGN2	RPL37	RPS27A	SRP9
RPS14	RPS7	NDUFS5	HIST1H4C	RPL24	CCDC148
LGALSL	PCDP1	MAEL	CNOT10	LRRN2	RP11.545I5.3
DIRC3	CCDC30	KCTD18	RP11.488L18.10	RP5.864K19.4	ISY1
SNX18	SPRED2	CISH	MRPS9	HOXD.AS2	ZBTB49.1
RARRES1	E2F6	C3orf58	ATAD3A	ATAD3B	LRP11
ACY1	ENAH	KDM5B	CTB.178M22.2	HS2ST1	RP11.490M8.1
SST	TRAF3IP1	RP11.145A3.1	CNOT10.1	CDK7	IL1RL1.1
CCDC138	IKZF2	CDKN1A	E2F6.1	RP11.488L18.10.1	IGIP
TMEM17	C2orf74	TUBA4A	PCYT1A	STT3B	HOXD1
TAF9	SPINK1	RND3	MAP7D1	NBPF12	MAP4K3
UBE2E2	ACOX2	EGR1	HHATL	RP11.417J8.3	AHI1
ENPEP	ATP1B1	CHPF	SLC6A3	CP	DPP4
F5	AC074289.1	LPCAT1	KCNK3	QSOX1	KIAA1244
SLC36A1	TGFA	ELK4	ADAMTSL4	CXCR4	NRP2
NBL1	MICAL1	LRRC41	NIPAL3	VEGFA	ECE1
SLC12A7	MST1	CERS2	AGRN	C6orf106	TNS1
IDH1.AS1	CAPG	KALRN	SCLY	AC079354.2	LAPTM4A
FBXO30.1	FHL2	ANKRD31	RIOK2	ABRACL	C4orf6
ZKSCAN4	WWC2.AS2	GCA	NMNAT1	DBT	ANP32E
PSORS1C1	PEX13	CYB5R4	OSGEPL1	PPP1R7	B3GALT4
EFNA4	CEP57L1	FDPS	TSPAN1	DNPH1	NAT8

T32: 1683 cells; 6 programs

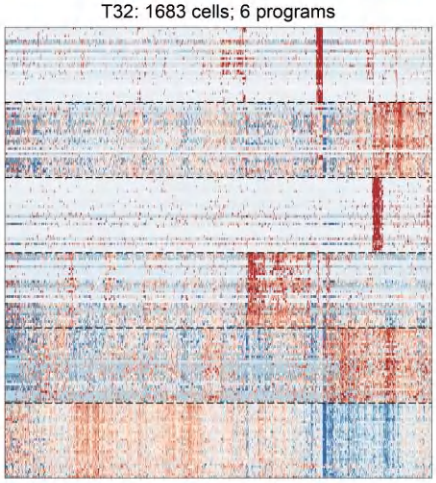

T32_1; T32_2; T32_3; T32_4; T32_5; T32_6

LAPTM5	FCER1G	C1QC	C1QA	C1QB	CD74
HLA.DPB1	LST1	STAB1	HLA.DPA1	HLA.DQA1	IL1B
HLA.DRB1	TREM2	HLA.DRA	HLA.DQB1	CD84	HLA.DQA2
HLA.DRB5	AIF1	S100A4	MNDA	C1orf162	FCGR1B
FAM198B	HLA.DMB	RGS1	FCGR3A	HCLS1	CD53
S100A11	ANXA3	SH3BGRL3	LAMC2	HMGA1	S100A16
CLIC1	WDR1	PSMD2	TAGLN2	ANXA5	ACTR3
YWHAQ	HBEGF	S100A10	UCHL1	S100A6	SFN
PRDX1	PNPLA1	PLK2	IL8	ARPC2	MAL
SSR3	CALM2	TPM3	PRELID1	HNRNPAB	YBX1
CENPA	NUF2	HJURP	CDC20	CCNA2	CENPF
KIF14	CKAP2L	SPC25	CENPE	ASPM	PTTG1
TACC3	CDCA8	SGOL2	STMN1	CCNB1	DEPDC1
H2AFZ	TRIP13	HMMR	KIF20A	NEK2	BUB1
SMC4	NCAPH	HIST1H4C	NCAPG	KIF2C	HIST1H1B
GSTA1	NAT8	LRP2	CYP4A11	CTXN3	GSTA2
C1orf210	HAO2	AGMAT	GC	FMO1	MPC2
PDZK1	KHK	APOM	ALPL	AC009014.3	DNPH1
SLC23A3	PLCH2	DAB2	AKR1A1	ACMSD	ACOT7
SMPDL3A	LAMTOR5	HMGN3	BHMT2	HSPE1	SLC3A1
AGRN	IGFBP7	FAT1	FSTL1	ITGAV	SPTBN1
CDH6	DST	VEGFA	TNFSF10	MACF1	CP
ATP13A3	PXDN	MUC1	LAMA4	CLDN1	KCNK3
LOX	SLC2A1	CRIM1	HLA.A	HSPG2	TAPBP
GOLGB1	LPCAT1	LAMC1	SLC34A2	TRABD2B	EIF4G1
RPS3A	RPS27	RPL9	RPL10A	RPS8	RPL5
EEF1A1	BTF3	RPS23	RPS14	RPS27A	RPL14
RPL32	RPL35A	CCNI	RPS18	RPL24	RPL15
RPL29	NPM1	RPL11	RPL34	GNB2L1	RPL22
CNBP	DUSP1	RPL37	RPL37A	EEF1B2	EPB41L4A.AS1

T24: 2718 cells; 7 programs

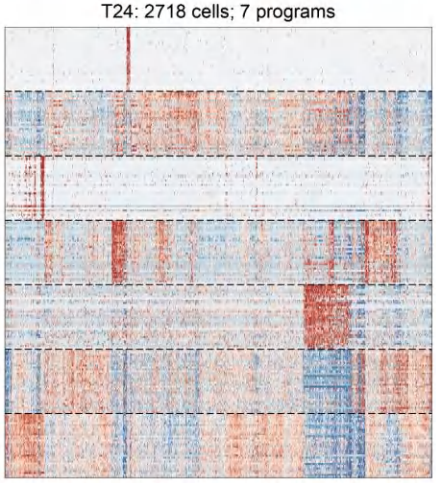

T24_1; T24_2; T24_3; T24_4; T24_5; T24_6; T24_7

CD8A	NKG7	CD3E	GZMK	GZMA	CD3D
PTPRCAP	IL2RG	FYB1	CD27	CST7	HCST
LTB	CD53	CTSW	CD2	GMFG	CORO1A
PTPRC	CD8B	CD37	ARHGDIB	TRAF3IP3	CD3G
LCP1	HAVCR2	CD52	GZMH	DOK2	CD7
EIF1	FTL	FTH1	GABARAP	PPP1R15A	PCBP2
RGS2	KDELR1	CCNI	EPB41L4A.AS1	BTG1	ZFAS1
PNM1	RHOB	VDAC2	ZFP36	NR4A2	PFDN5
IGBP1	BTG2	ATP5MC2	C1orf43	SQSTM1	EIF4A2
CCDC28A	BAG3	EIF4EBP3	ATF3	ALDOA	UBC
PTTG1	CENPF	ASPM	KIF20A	MKI67	BIRC5
HMMR	TPX2	CCNB2	CCNB1	CDC20	PLK1
NUF2	NUSAP1	PIMREG	NEK2	GTSE1	TK1
CDCA3	PBK	CDKN3	KIF14	TOP2A	STMN1
CKAP2L	H2AZ1	HJURP	UBE2T	CENPE	TROAP
OAS1	MX1	OASL	IFI35	ISG15	RSAD2
MX2	LY6E	IFITM3	IFI6	IFIT1	IFITM2
SAMD9L	UBE2L6	ISG20	PSMB9	IRF7	IFI27
IFIT3	TRIM22	TNFSF10	DDX58	PLSCR1	ETV7
XAF1	SAMD9	IFIT2	VAMP5	OAS2	GBP4
EEF1A1	TPT1	CRYL1	C3	PTMA	PLCB4
RBP5	CLU	COMMD6	P3H2	HNMT	HSP90AB1
BGN	EEF1D	SLC38A1	GLUL	RARRES2	PELO
CD74	EEF1B2	ARID5B	ITM2B	CRYAB	NOP53
NNMT	MAP3K7CL	MID1	VIM	IGFBP7	EFEMP1
DCBLD2	VCAN	CDK6	MYLK	MET	TRIO
LRP1	MACF1	NAV1	SLIT3	DCDC2	FAT1
COL21A1	MYOF	AHNAK2	DST	CD81	EPHA7
DDX17	AHNAK	GLS	PLOD2	WWTR1	MTRNR2L8
ATP2B4	ANO6	MTRNR2L12	ITGA3	MRTFA	AKT3
ACTB	CFL1	PFN1	RAN	PKM	TNFRSF12A
S100A16	EIF5A	HINT1	SLC25A5	ANXA2	ARPC2
ACTG1	PGAM1	MYL12A	CSRP1	ATP5MC3	SLC25A3
COX5A	CNN2	SYNGR2	VDAC1	RHOA	S100A11
MYL12B	SLC9A3R1	YIF1A	TUBA1B	SH3BGRL3	MYDGF

T33: 435 cells; 4 programs

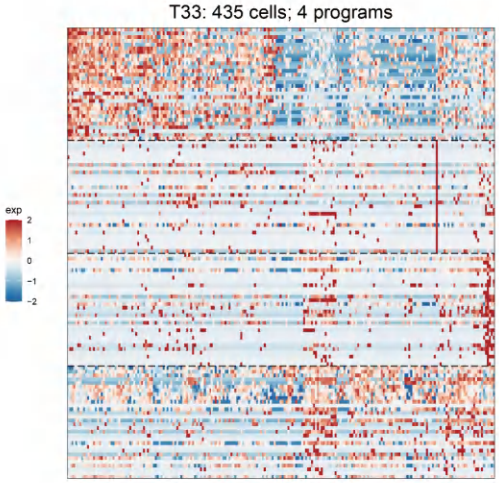

T33_1; T33_2; T33_3; T33_4

HLA.DPB1	CXCL2	CD74	DUSP1	NFKBIZ	HLA.DPA1
HLA.DRA	EGR1	SPON2	FNIP2	HLA.DRB5	FN1
HLA.DRB1	IER3	CCNL1	JUN	PTMA	EBF1
SLC29A1	HLA.DQA1	CTSK	ATF3	BTG2	PPAP2B
TFPI	HLA.E	IRF1	HLA.DOA	FOSL2	GLUL
S100A9	UCHL1	MYO1B	SV2A	MAST2	KNG1
ATP1A1	AC123886.2	MXRA8	RP11.782C8.2	TTC4	PTH2R
SQSTM1	GALNT5	KLHDC3	PIGR	CDKN1A	TPD52L1
CLDN19	PAPPA2	RP1.223E5.4	HCN3	CLIC1	SHROOM3
WHSC1	RP11.624M8.1	RP11.367N14.2	APLF	RP1.151F17.1	X15.Sep
SEMA3F	GPX3	STK39	RP4.543J13.1	PDZK1IP1	PLCD4
RP11.10L7.1	CYTL1	GALNT14	RP5.1092A3.4	DAB1	RHOU
PAPPA2.1	MTRNR2L12	YOD1	LRP2	PRLR	TNNT2
VCAN	ZBED6	F2RL1	SENP5	USP46.AS1	CPOX
MFAP3L	OSBPL11	CCSAP	KCNAB2	SPDYA	PLCL2
S100A10	PRDX6	RPL14	SEMA4A	AC073218.2	RPL5
RPL24	NPM1	EIF4A2	ATPIF1	PPP1R3G	HIGD1A
PTGER3	BRINP2	SST	VEPH1	SPAG17	TMEM171
RP1.60O19.1	NGEF	PDZK1IP1.1	SH3D21	KIF6	KLHL20
RPS8	FYB	RPL9	OVGP1	SLC15A2	RPL11

T42: 391 cells; 3 programs

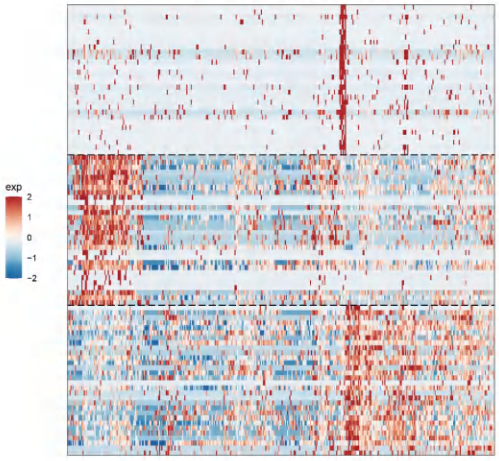

T42_1; T42_2; T42_3

LDB2	SLCO2A1	SLC9A3R2	FCN3	TP53I11	CYYR1
GFOD1	SH3PXD2A	FLT1	SPARC	PLVAP	RBP7
THBD	RAMP3	NOTCH4	MMRN2	RAMP2	ESM1
VWF	TMEM88	RNASE1	TIMP3	RGCC	CASP10
KDR	FAM167B	RAPGEF5	CD93	EGFL7	GIMAP7
NAT8	MIOX	GPX3	GSTA2	AMN	SMIM24
PEBP1	BBOX1	SLC5A12	PPP1R14D	PDZK1	SLC16A9
PDZK1IP1	KHK	GSTA1	APOM	ACSM2B	AQP1
FTL	C1orf210	CYP4A11	MPC2	ANXA4	TMEM174
AL139246.5	ALDOB	AGMAT	GAMT	CYB5A	CDHR5
CXCL11	SOD2	RRAD	VIM	HLA.C	MT2A
IRF1	RPS2	ICAM1	TAP1	HLA.B	NFKBIA
GBP2	LMNA	BIRC3	FAM107A	HLA.A	TM4SF1
ETV7	UBE2L6	TAGLN2	CAV1	MT1E	CD74
TYMP	TAPBP	HLA.DRA	PNRC1	C1S	FSTL3

T43: 3036 cells; 5 programs

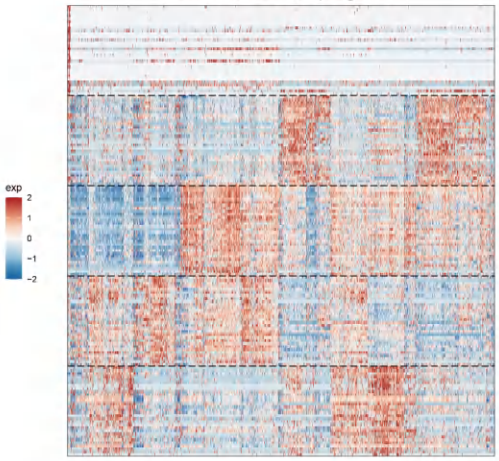

T43_1; T43_2; T43_3; T43_4; T43_5

EPO	PTN	PTGIS	SCNN1B	PART1	FAM180A
CLDN11	ARG2	PGF	IGF2.1	TNNT3	FABP5
NID2	IL6	IGFBP5	GRM8	CFH	SCNN1G
FRZB	MIAT	EDIL3	PAX5	AC091946.1	NPPC
BMPR1B	GNAS	WFDC2	COL6A3	FABP7	EGFL7
EEF1A1	RNF5	LINC02532	SNX3	CLIC1	EZR
RPL35A	CD24	IMPA2	LGALS2	CUTA	SMIM24
GLUD1	DNPH1	TNFSF10	RCAN2	TXN	TINAG
NAT8	CLDN4	MYL6	PEBP1	SLC22A2	PLEKHA1
SERP1	AMD1	SARAF	RPS18	ADIRF	PNRC1
ZFP36	JUNB	ATF3	IER2	EGR1	SERTAD1
BTG2	CRYAB	SOCS3	FOSB	IRF1	LMNA
JUN	UBC	MAFF	RHOB	DNAJB1	MCL1
DUSP1	CEBPD	PPP1R15A	HSPA8	FOS	KLF6
XBP1	HSPB1	GADD45B	FAM53C	UBE2S	HSPA5
ANXA2	MMP7	TIMP1	LGALS1	GAPDH	C1R
IGFBP7	C1S	CD44	EMP3	TUBA1B	VIM
IFITM3	S100A13	SELENOM	CAV1	FTH1	CST3
PKM	TGFBI	S100A11	SERPINE2	RPLP1	TAGLN2
S100A6	C3	TMSB10	RAB13	CTHRC1	CD151
AMN	CES2	PDZK1IP1	SLC5A12	AGT	KHK
SLC7A7	AKR7A3	SLC25A5	CALM1	MT.CO1	MT.CO3
MT3	GPX3	CTSH	PRELID1	HLA.G	SERPINA1
PEPD	GPD1	ATP5MC3	HSP90AA1	DDC	MRPL41
PLIN2	PTGR1	MT.ND4	SLC2A5	AOC1	TMEM174

T35: 594 cells; 10 programs

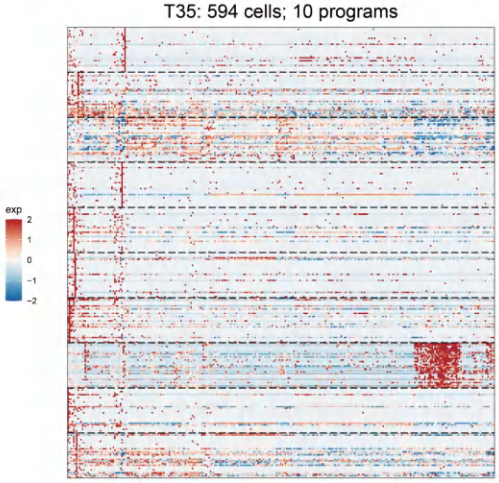

T35_1; T35_10; T35_2; T35_3; T35_4; T35_5; T35_6; T35_7; T35_8; T35_9

ZNF438	TNF	NOMO2	GPATCH3	EIF2AK3	MAD2L1BP
IGHMBP2	NR4A2	AC115618.1	DUSP4	NFKBIE	JUN
ZNF266	SLA	CDH1	SMARCA2	CNTRL	KLHDC8B
APPL2	CDB4	GZMK	SMARCA2	HSPA1B	HMGCS1
RP11.27N19.2	HSPA1A	USP43	PER01A	PRPAP1	CTD.2574L9.4
STK11IP	NR0B2	HSPB1	PTPRK	RP11.473M20.16	RSRP1
PTK6	ENDOG	RND3	NGFR	AZI1	CKB
HSPD1AA1	IRF7	DNAJB1	COL4A2	XKR8	APLF
ZNF227	EIF4EBP1	ACBD4	RPL41	MTPAP	ZP1
RPL36	UBB	RPL13	RPS14	EIF1	C19orf13
TOB1.1	CACYS1	GAPDH	TNFSF13B	VIM	NDUFAB1.2
CYP4F3	IFI27	C2CD5	IPO13	ACTG1	TUBE1
MT.ND4	MDK	SH3BGRL3	NAT14	PPDPF	RBM3
AKAP13	S100A10	ANXA2	ACTB	IQCE	RPS4A
RPS18	PTTG1	CDC20	THBS2	SPC24	P4HB
PYRL4	BBC3	TAF1A	CDKN1A	AC018464.3	XKR6.1
JADE1	GDF15	LIF	LIG1	ZBTB48	AEN
PIDD	COL1A1	RP11.967K21.1	DNAJC27	MCC	CLIC3
PAXBP1	SLC37A3	ZBTB7B	MALAT1	RCOR2	TRIM11
TOR4A	PDP1	FAM120A1	CDA1	TUFT1	HSD17B7
TMEM132A	AMOTL1	WDR35	TIPARP.AS1	TAF1D	LYPD4
GABPB2	PET112	MYO1B	ETFDH	GABPB1	RP11.430H10.1
PHACTR1	RPS25	TRIM29	IRS1	ZFAS1	RCOR2.1
ZNF529	WSB1	ARAP3	ARHGEF25	RPS21	CCDC9
AC093323.4	TUBGCP4	AC018464.3.1	CTDSP1	CENPP	PPIL3
SLC37A3.1	PTK6.1	MRC2	ANGPTL4	FTH1	TMEM132A.1
ARHGEF25.1	VSIG10	PHKA1	TAF1A.1	PLEKHG4	VPS18
LANCL2	WDR25	CCDC85B	CORO2B	KLHL21	PTPDC1
ICAM1	GABPB2.1	TAMM41	HLX	TBC1D25	EDC3
SRGAP1	MIIP	ADM	MALT1	SLC30A4	CXCL5
ZFAS1.1	SNHG12	ETFDH.1	LTBP4.1	WDR85.1	EPB41.4A.AS1
GOLT1A	HSP90AB1	PET112.1	AACS	TAF1D.1	XKR6.2
EIF1.1	RP11.967K21.1.1	CTD.2314B22.3	RABGGTB	ZNF277.1	RPL26
MPV17L2	NPM1	IL1RL2	KLHL21.1	TUBGCP4.1	WDR31
UBIAD1	SNRNP48	RPL41.1	CENPQ.1	DDX19B	HNRNPDL
CYB5A	CXCL14	USP28	PXDC1	CCDC146	SPINT2
CMBL	CRYAB	RARRES2	TXN	GSTA1	NQO1
TMEM176A	TMEM27	VAMP8	COX4I1	OCIAD2	TMEM176B
ANXA4	HRSP12	ATP5G3	RAB17	AC015177.1	MT1M2
PDZK1IP1	TMEM171	DAB2	NAT8	CYSTM1	COX5B
DNAJC27.1	STK11IP.1	LIF.1	CTD.2314B22.3.1	SNRG12.1	ZNF599
RHOE.1	RP11.967K21.1.2	ZNF529.1	RP3.510D11.2	PPARA	TTLL6
ZFAS1.2	TUBB2B	RCOR2.2	C19orf38	MFAP4	ZNF227.2
PHKA1.1	WDR31.1	APLF.1	UAP1L1	GNB1L	MT.ND2
RPS27	SPINK1	RP11.558F24.4	LINC00926	TIPARP.AS1.1	KLHL21.2
MT1X	MT2A	RP11.430H10.1.1	ETFDH.2	RCOR2.3	TIPARP.AS1.2
CENPQ.2	NHLRC1	ENTHD1	RGS9	FTL	ZNF668
NPM1.1	ACTG1.1	FTH1.1	ENTPD1.AS1	CMTM7	RPS6
MRPS6	EEF1A1	C15orf48	HNRNPA1	SLC35B3	COA7
IQCB1	EDC3.1	GAPDH.1	SCCPDH	PABPC1	SMIM10

T45: 1902 cells; 5 programs

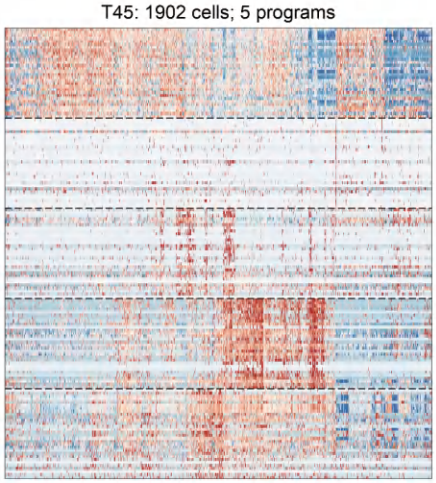

T45_1; T45_2; T45_3; T45_4; T45_5

CRYAB	ZFP36	FOSB	JUNB	DDX5	SERTAD1
UBC	MYC	CYR61	SOCS3	DNAJA1	EIF1
HSPA8	NNMT	EGR1	MAFF	ATF3	HSP90AB1
HSPB1	ACTG1	HSPA1B	GADD45B	DNAJB4	RPS27
FOS	CDKN1A	RPL21	RPL9	HSPA1A	RPS3
SFRP2	COL3A1	COL1A2	DKK3	TIMP1	CD44
COL1A1	CPE	F2R	CTGF	SERPINE1	COL6A2
TSPAN2	COL6A3	SPARC	COL8A1	TSHZ2	CFH
BGN	EFEMP1	SEMA3C	C1R	MFSD2A	IGFBP7
MT1G	LOXL2	JMY	CTHRC1	CYP1B1	CHST7
EEF1A1	GPR137B	GNG11	VIM	RPS12	IFI27L2
ANK2	HAVCR2	PTGS1	KMO	ALDH8A1	UGT3A1
ZFAND2A	CA2	LIPC	PAH	TEX41	NPTX2
GPM6A	RPL12	QPRT	S100A13	GPX3	IRF8
MOXD1	EIF4EBP1	B2M	HPGD	SERPING1	TUBA3D
CES2	AMN	KHK	ACSM2B	CYP4A11	AGT
CDHR5	PEPD	BBOX1	SLC22A6	SMIM24	TXN
GPX4	GPD1	SLC6A13	PEBP1	PDZK1IP1	APOM
CYB5A	GSTA2	SLC16A9	SLC5A12	G6PC	ASPDH
RAB11FIP3	AZGP1	MIOX	MT.CYB	ACSM2A	FBP1
AC022509.2	BIRC3	MT.CO3	MT.CO1	IGFBP3	MT.ND4
MT.CO2	MT.ND3	SDC4	ZFP36L1	IL32	WTAP
SOX9	MT.ATP6	FSTL3	SOD2	MT.CYB.1	CFLAR
TPM1	PFN1	NBL1	TYMP	ATP1B1	THBS1
IFFO2	KDM6B	SET	VXN	SLC5A3	FLNA

T47: 3197 cells; 7 programs

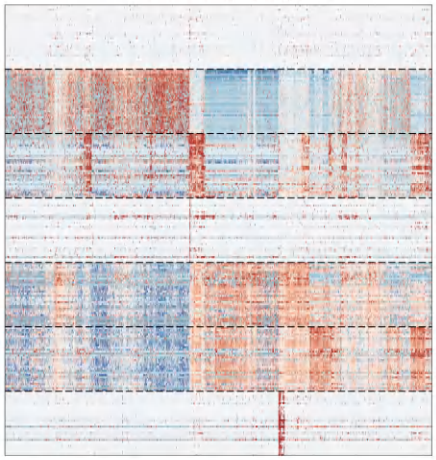

T47_1; T47_2; T47_3; T47_4; T47_5; T47_6; T47_7

DCN	MEG3	COL1A1	ITGBL1	INHBA	LUM
COL1A2	SFRP4	MXRA5	SFRP2	COL8A1	THBS2
PHACTR2	ID3	FERMT1	BGN	PRRX1	COL12A1
COL11A1	TIMP3	COLEC12	RGS16	AL356512.1	SPARC
MFAP5	COMP	RAB31	OLFML2B	LINC01521	MFAP2
NEAT1	MALAT1	N4BP2L2	VMP1	P3H2	XIST
ZBTB38	ABCC3	RHEX	BHMT2	PAG1	AL713998.1
ZBTB20	SLC25A37	SPINK13	MUC20.OT1	KLF6	DDX17
CFLAR	PDK4	DNAH11	CPD	CES4A	MBNL1
PAX2	PPP2R3A	QTRT1	VEGFA	PNISR	MAST4
JUNB	FOS	JUN	EGR1	DNAJB1	TPT1
PPP1R15A	SERTAD1	ATF3	FOSB	GADD45B	IER2
RHOB	DUSP1	AC020916.1	HSPA1B	HSPA1A	RPL6
KLF4	ZFP36	BTG2	CRYAB	INTS6	HSPA8
DNAJB4	DNAJA1	HSP90AA1	RPL21	UBC	SERPINA1
PIGR	CLIC6	LTF	MMP7	LINC00284	TMEM98
LCN2	CCL2	SERPINA1.1	SAA2	ZNF667.AS1	CXCL3
KCNJ15	CXCL2	CXCL1	RIPOR3	CLDN7	PHACTR2.1
IGFBP7	PROM1	VCAM1	PCSK1N	PACSIN3	IER3
CYR61	SFRP2.1	BGN.1	SAA1	MAP7	ANK3
GSTA1	GAPDH	SPP1	RPS2	LGALS3	HP
CRABP1	GSTA2	APCS	ARG2	LDHB	RPL10A
RPL7A	CD24	RACK1	PRDX1	RPS4X	RPS14
AGT	RPL3	HINT1	AKR1B1	NNMT	RPS3
CLU	ATP6V0E1	HNRNPA1	BTF3	FGG	SLC25A6
FTH1	EIF1	ZFAS1	VIM	RPS27	PNRC1
RPS21	RPS13	RPS12	RPL18A	HLA.C	HLA.DQA1
BTG1	CCNI	FTL	CD74	RPL30	RPL19
RPL41	RPS27A	RPL27	PSMA7	RPL9	SQSTM1
RPS29	RPL10	HLA.B	RPLP1	HLA.DRA	RPS26
NUF2	DEPDC1	CDKN3	CCNB1	NEK2	PTTG1
CKAP2L	NDC80	NCAPH	PIMREG	SPC25	HMMR
AURKA	STMN1	BIRC5	TOP2A	H2AFZ	CCNB2
SGO1	CKS2	HJURP	UBE2C	TUBA1B	PBK
CENPA	GTSE1	ASPM	BUB1B	CDCA8	ASF1B

T44: 1562 cells; 5 programs

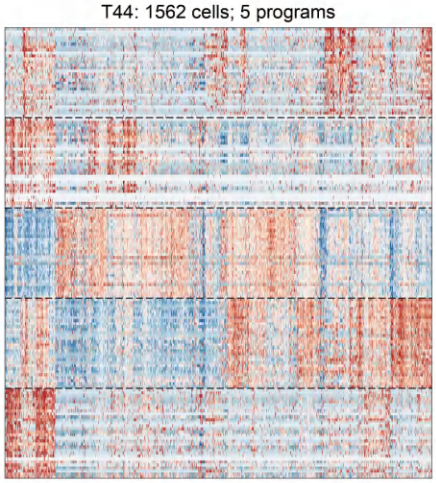

T44_1; T44_2; T44_3; T44_4; T44_5

MT2A	C11orf96	CP	MT1X	CEBPB	PNRC1
PGF	SOD2	TGFBI	NPTX2	RPS12	CDKN1A
DUSP1	IGFBP7	CTHRC1	TMSB10	RHOB	MT1F
YBX3	CXCR4	RARRES2	ELL2	STC1	NAMPT
C1R	ZFP36L1	TMEM173	BACE2	KLF4	MT1E
UBD	RARRES3	CD74	IL32	PSME2	HLA.DRB1
HLA.B	PFN1	B2M	HLA.DQA1	CXCL11	LAP3
HLA.A	GBP4	HLA.C	HLA.DRA	TAP1	PSMB9
TYMP	G0S2	LTB	ISG20	HLA.DPA1	PSME1
HLA.DPB1	SLC26A9	CTSS	GC	S100A11	AC022509.2
VIM	RPL13A	MSLN	RPS27A	RPL10	RPS3
RPL9	RPS18	RPL37A	RPL13	RPSA	RPS5
RPL11	RPL23A	RPS15	RPS24	FAM120AOS	RPL7A
PNCK	RPL41	RPL35	RPL27A	RPL18	RPS2
RPL14	BST2	RPS8	RPL18A	FAU	RPS28
HSPA8	DNAJB1	BAG3	DNAJA1	HSPA1B	HSP90AA1
SERPINH1	HSPA1A	HSPB1	FOSB	HSPD1	HSPH1
ZFAND2A	CRYAB	EGR1	HSPE1	HSPA5	PPP1R15A
DNAJB4	ATF3	ZFP36	MAFF	UBB	FOS
JUNB	BTG2	ACTG1	HSP90AB1	ACTB	MCL1
NAT8	ACSM2B	LGALS2	KHK	HMGN3	BBOX1
AMN	CYB5A	APOM	UQCRQ	FABP7	SMIM24
AQP1	GSTA1	BSG	MT.CO2	AGXT2	SLC22A2
MT.CO1	OCIAD2	SLC6A13	GSTA2	CUBN	RDH12
COX7C	MIOX	CXCL14	GSTP1	DAB2	PDZK1IP1

T46: 1244 cells; 5 programs

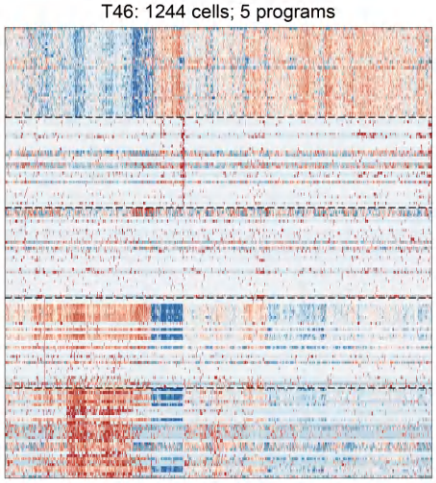

T46_1; T46_2; T46_3; T46_4; T46_5

SERTAD1	RPS3A	RPS3	FTH1	RPL7	RPL21
RPL11	RPS27A	RPL9	RPL8	ZFP36	CRYAB
EIF1	MYC	RPS4X	RPL23A	RPS5	RPL18
RPL13A	RPL41	RPL18A	RPL10	RPL5	JUNB
RPS27	RPS14	RPL3	RPS6	RPL13	RPL30
SFRP2	MMP7	COL1A1	COL6A3	COL1A2	TGFBI
PHLDA1	COL6A2	DKK3	TMEM100	CTHRC1	MT2A
ANXA2	LOXL2	BACE2	IGFBP7	MT1E	LBH
MYL9	PHLDA3	PPIC	LGALS1	FHL3	TPST2
LOXL1	PDLIM7	BGN	FSCN1	SPARC	ARHGEF2
IGLC3	IGHG1	IGHG3	SH3BP5	MZB1	CELF2
ZP1	ITGB7	IGHGP	DERL3	CCND2	CYBA
ARHGEF3	SPP1	SRGN	GJB2	FKBP11	CCL20
P2RX5	PNOC	RECQL	BIRC3	CST6	SMAP2
MEI1	IGHG2	QPCT	IGF1	TSPAN15	FSTL3
PTGS1	AC133644.2	MT.ND4	MT.ATP6	MT.ND1	MT.CO3
MT.CO2	MT.CO1	C3	RILPL1	MT.ND3	PCLAF
MT.CYB	MT.ND2	PCSK1N	CUL9	MT.ND5	NKX3.1
LRRC8D	SLC6A3	C1QL1	VEGFA	LDLRAD3	ADGRG6
C16orf74	ZNF516	PHKA2	ALKAL2	MT.ND4L	SCD
MT.CYB.1	AMN	MT.CO1.1	MT.CO3.1	KHK	MT.CO2.1
CYP4A11	CDHR5	AQP1	SLC22A6	MT.ND4.1	APOM
SMIM24	TXN	NAT8	CES2	ACSM2B	AZGP1
CYB5A	GPX4	PDZK1IP1	TM4SF5	CUBN	MT.ND5.1
MIOX	SLC6A13	MT.ND2.1	MT.ND3.1	TSPAN1	KRT18

T48: 2815 cells; 7 programs

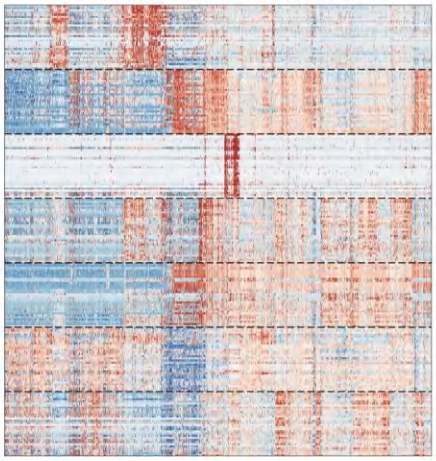

T48_1; T48_2; T48_3; T48_4; T48_5; T48_6; T48_7

CD74	HLA.C	PSMB9	B2M	ZFAS1	HLA.B
EIF1	MDK	PNRC1	HLA.DQA1	NUPR1	SELENOM
HLA.DRA	HLA.DQB1	HLA.A	IL15RA	TAP1	HLA.DPA1
HLA.DPB1	IL32	ATF4	OPTN	S100A6	CD44
HLA.DRB1	FTH1	RARRES3	RPS27	CEBPG	UBE2L6
CP	C1R	CLU	AGT	LBP	SPP1
SERPINF2	MT.ATP6	CTSD	HSP90B1	AQP3	MT.ND4
CALR	LGALS3BP	PLOD2	PDIA3	ANGPTL4	MT.ND2
FGG	APCS	P4HB	MT.CYB	CYBA	APP
MT.CO3	SLC16A3	QSOX1	MT.ND3	MT.CO1	MT.CO2
PTTG1	CENPA	CCNB1	CDC20	HMMR	DEPDC1
H2AFZ	BIRC5	DLGAP5	PIMREG	CDKN3	STMN1
NUF2	GTSE1	TOP2A	UBE2C	TPX2	ASPM
MXD3	PLK1	PBK	CDCA3	CCNB2	UBE2S
ECT2	HMGB2	MKI67	TUBA1B	HMGN2	NEK2
DNAJB1	BAG3	HSP90AA1	HSPA1B	DNAJA1	HSPB1
ZFAND2A	HSPA1A	PPP1R15A	HSPA8	HSPE1	EGR1
DNAJB4	DEDD2	JUN	MRPL18	FOS	HSPA6
HSPH1	CRYAB	ID2	DDIT3	SOCS1	BTG2
SERTAD1	SERPINH1	PLK2	GADD45B	ATF3	UBB
MT.CO3.1	MT.CO2.1	MIDN	MT.ATP6.1	MT.ND4.1	MT.CO1.1
MT.CYB.1	CXCL2	NFKBIZ	MT.ND2.1	MT.ND3.1	MT.ND1
HIPK2	CPD	TNFAIP3	C11orf96	CXCL8	IER3
MT.ND4L	SDC4	LPP	NETO2	ERRFI1	MT.ND5
EGR1.1	FOSB	KLF6	MAFF	VMP1	RYBP
GAPDH	S100A10	ACTG1	LGALS1	CAV1	VIM
TMSB10	S100A11	RPS14	RPL7	LDHA	ANXA2
PPIA	RPL10A	ENO1	RPL10	C10orf99	RPS3A
RPS27A	BTF3	TUBB	TGFBI	RPL19	RPS18
HNRNPA1	NDUFA4L2	MYL6	RPL5	YBX1	CLIC1
GSTA2	TRIM54	LGALS3	GSTA1	GAMT	LGALS2
HINT1	FXYD2	CYB5A	ARG2	RBP5	GAPDH.1
AGXT2	CALM1	PDZK1	ASGR1	TXN	RACK1
SMIM24	ACMSD	MPC2	USH1C	CMBL	ANXA4
APOM	UQCRB	FBXO25	TMEM176A	LDHB	KHK

T59: 866 cells; 9 programs

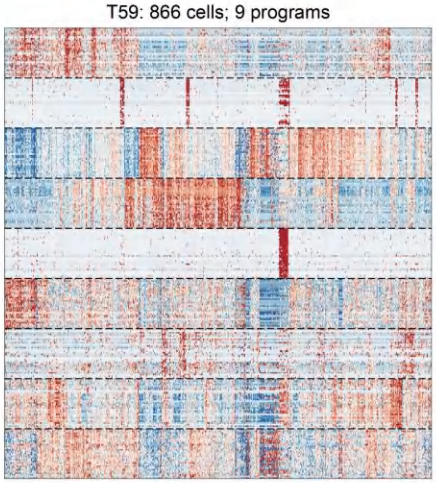

T59_1; T59_2; T59_3; T59_4; T59_5; T59_6; T59_7; T59_8; T59_9

CYP4A11	TMEM174	PLG	PCK1	APOM	SLC22A6
ALDOB	AZGP1	SMIM24	SLC5A12	PEPD	BBOX1
AGXT2	CES2	GSTA2	GPD1	AGT	ACSM2B
HMGCS2	AMN	ASPDH	KHK	CDHR5	MIOX
AKR7A3	ALDH6A1	SUSD2	GPX3	TMEM86	CBR3
CD3G	PTPRC	HCST	CD2	CCL5	CD3D
FYB1	GZMA	GZMH	AC243960.1	CD52	RAC2
THEMIS	PRF1	S100A4	NKG7	GZMM	ARHGAP30
PYHIN1	AKNA	EMB	CD84	CD48	TRG.AS1
CYTH4	TRC1D10C	GNLY	CD37	GPR171	LINC00861
RPL10	RPL41	RPS14	EPB41L4A.AS1	RPS9	RPS27
RPL11	RPL30	RPS5	FAU	RPS2	ZFAS1
RPS3	RPL18A	RACK1	RPL18	RPS23	RPS4X
RPL13	NPM1	RPL7A	RPS28	RPL8	RPS18
RPL19	RPS21	RPL38	RPL39	RPL28	RPL35A
HSP90AA1	DNAJB1	FOSB	DNAJA1	ATF3	JUN
HSPA1B	FOS	HSPA1A	EGR1	JUNB	DNAJB4
HSPH1	HSPB1	HSP90AB1	ZFP36	PPP1R15A	HSPE1
BTG2	HSPA8	IER2	MAFF	SERPINH1	BAG3
SERTAD1	MRPL18	CRYAB	NFKBIZ	SOCS3	MCL1
MGP	RAMP2	SLC9A3R2	RAMP3	RNASE1	FCER1G
TYROBP	ACKR1	PECAM1	ENG	XCL2	ECSCR
EGFL7	FN1	HSPG2	RGCC	GSN	TPSB2
PTGDS	VWF	RGS5	SRGN	SOX18	RBP7
PLPP1	C1QB	MMRN2	CTSG	C1QA	NPDC1
NEAT1	LRP2	LRRK2	GOLGB1	HIPK2	TAST
ZBTB20	MALAT1	SYNE2	N4BP2L2	VEGFA	ATP11A
APLP2	SLC4A4	ARHGEF28	MYO9A	DDX17	VPS13A
TNS1	SERINC1	MT.ND3	CANX	KCNQ1OT1	GTF2I
MT.CYB	CMYA5	ENPEP	VMP1	HNRNPU	MAML2
CAV1	TGFBI	IER3	IGFBP3	PHLDA1	SLC8A1
CYR61	CLDN1	EMP3	MMP7	RRAD	VIM
VCAN	C11orf96	PIM1	PLP2	ITGA3	EFNA5
PHLDA2	FSTL3	LMNA	TPM1	CRIM1	TNFRSF12A
ACTN1	SYTL2	ANXA2	LUCAT1	COL6A2	LOX
TYMP	RARRES3	LAP3	HLA.DQA1	CTSS	S100A11
IL32	CXCL11	ISG20	HLA.DRA	HLA.DRB1	PSMB9
CD74	WARS	HLA.G	PSME2	UBE2L6	IFI27
HLA.C	HLA.DPA1	B2M	HLA.DOB	HLA.B	HLA.DQA2
HLA.A	HLA.DRB5	GBP1	GBP5	PSMB8	SECTM1
NAT8	SLC17A3	PGAM1	TPI1	PDZK1IP1	PSAT1
LDHB	HINT1	POLR2L	TNFAIP6	GSTA1	ALDH1A1
PRDX4	GSTP1	PRDX2	MIF	MPC2	ATP5MC3
COX7B	CST4	LEPROT	UQCRQ	CLTRN	LDHA
ATP5MC1	ATP5F1E	NDUFS6	TPM1.1	TM4SF18	DNPH1

T60: 3365 cells; 5 programs

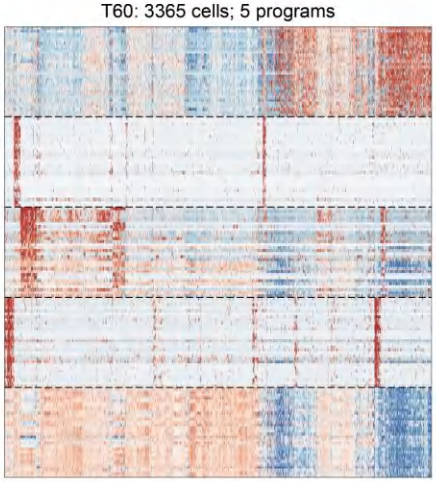

T60_1; T60_2; T60_3; T60_4; T60_5

MALAT1	MME	DDX17	KCNQ1OT1	N4BP2L2	HNRNPU
PNISR	NEAT1	POLR2J3.1	VEGFA	SLC7A2	CADM1
RBM39	PRRC2C	WSB1	FTX	PAX8	VMP1
GLS	PLEKHA1	FNDC3B	FAM13A	ZBTB20	MUC20.OT1
LINC01320	SLC5A3	BICD1	CA12	LPP	MTR
PTPRC	PDCD1	NKG7	CD2	TRAC	CD3E
CORO1A	CD27	TRBC2	EOMES	SPOCK2	CD3D
S100A4	CCL5	CD96	GZMK	CCL4L2	CCL4
SRGN	RAC2	PRF1	TNIP3	GIMAP6	SH2D1A
FYB1	SIT1	CD6	RGS2	CD8A	DOK2
TFF3	IER2	ATF3	JUNB	FOS	NRN1
SERPINA1	CXCL6	DUSP1	EGR1	IGFBP2	BTG2
SMIM10	RPS8	JUN	IGF2.1	FRZB	JUND
RPS24	RPS23	CXCL2	RPL7	TNXB	TFF1
RPS26	RPL3	CLDN11	PPP1R15A	RPL23A	RHOB
CCNB1	TPX2	NUSAP1	HMMR	PTTG1	CENPA
TOP2A	AURKA	CCNB2	MKI67	CENPF	KIF20A
PIMREG	BIRC5	UBE2S	GTSE1	CEP55	ASPM
KIF14	CKAP2	UBE2C	TUBA1B	KIF23	NEK2
NUF2	BUB1B	TROAP	CDK1	CDCA3	KIF20B
GAPDH	RPS13	RPS3	FTH1	LDHA	RPL35A
RPL21	TPT1	PFN1	TPI1	RPS12	GPX4
GSTP1	RPL18A	RPLP1	RPL10A	LGALS3	FAU
S100A10	RPS25	RPL10	RPL15	RPL41	EEF1B2
RPS5	RPS27A	EIF3K	ACTG1	RPL8	UBA52

T61: 2244 cells; 6 programs

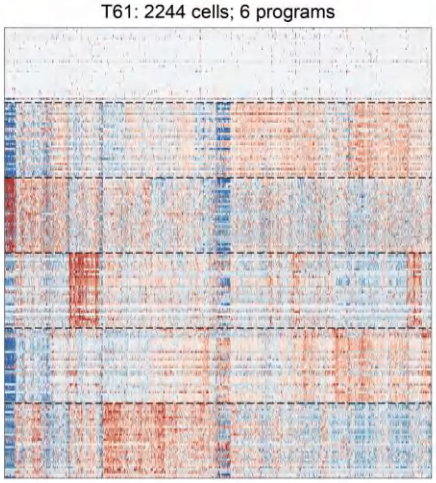

T61_1; T61_2; T61_3; T61_4; T61_5; T61_6

PTPRC	TNFRSF1B	LST1	AIF1	FGL2	HCK
MS4A7	LILRB1	LIMD2	SPN	SAMSN1	LCP1
MX2	S100A4	DOCK10	CD48	OSCAR	TYROBP
ITGA4	ITGAL	MYO1G	IKZF1	PLEKHO1	C19orf38
FCGR3A	FCER1G	GMFG	AC004687.1	TMSB4X	BCL2A1
JUNB	EIF1	DUSP1	RPL30	KLF2	RPS14
JUND	RHOB	RPL41	RPS27	JUN	IER2
RPL23A	HSPA1A	FOS	RPL9	CIRBP	RPL10
ATF3	RPL21	RPS3	UBC	EPB41L4A.AS1	RPL11
HSP90AB1	RPS5	HSPA1B	RPS27A	SNHG8	NOP53
MALAT1	NEAT1	HNRNPU	HNRNPA2B1	KCNQ1OT1	VMP1
SYNE2	ZBTB20	SFPQ	GOLGB1	POLR2J3.1	N4BP2L2
MUC20.OT1	AHNAK	MACC1	WSB1	MCL1	PPP1R10
PPP1R15B	PNISR	INTS6	DDX17	ZNF292	CNKSR3
MACF1	ENOSF1	CCNL1	FAM133B	FOSB	AFF4
CD74	HLA.DRA	GBP4	PSMB9	RARRES3	HLA.DRB1
IL32	HLA.DQA1	WARS	HLA.DPA1	B2M	HLA.C
HLA.B	LAP3	ISG20	HLA.E	STAT1	ISG15
APOL1	TAP1	HLA.A	CXCL11	IFIT3	HLA.DPB1
CXCL10	PSME2	HLA.DMA	CTSS	HLA.DQB1	APOL2
IGFBP7	VIM	IER3	RRAD	RPL3	RPS6
RPL12	RPL18A	RPS2	TM4SF18	RPS4X	RPL4
TIMP1	RPS8	RPL6	TPM1	RPL28	EMP3
ANXA2	RPL7A	RPS18	RPL8	C1R	TMSB10
RPLP0	PRSS23	RPS16	RPL15	RPL10A	PPP1R14B
NAT8	GPX3	PDZK1IP1	SLC6A18	LY6E	TSPAN1
AQP1	AGT	GAL3ST1	CYB5A	NAPSA	AMN
APOM	SLC22A2	CUBN	ANXA4	GAPDH	GSTA1
ATP5MC3	SMIM24	HMGN3	NIT2	CES2	BBOX1
ITM2B	HMOX1	SLC34A1	PCSK1N	MT.CO1	ECH1

T62: 508 cells; 4 programs

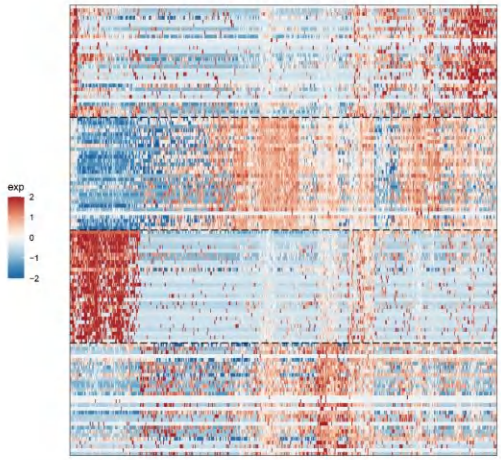

T62_1; T62_2; T62_3; T62_4

SELPLG	HSPA1B	JUNB	B2M	CD69	PTPRC
HLA.C	CD52	HSPA1A	SYNGR1	IL7R	CXCR4
DUSP2	DNAJB1	HSP90AA1	NFKBIA	HLA.B	GZMA
S100A4	CCL5	CD247	TMSB4X	BTG1	NKG7
ZFP36L2	GATA3	RPS29	HSPA8	JUN	HSPA6
FTH1	RPL41	HINT1	TPI1	RPL10	CD63
RPS12	CRYAB	GSTP1	RPL26	RPS14	RPL23A
RPS5	RACK1	NACA	BRI3	RPL35A	CYB5A
MGST1	TMEM176B	ATP5MC2	TOMM7	TMEM176A	RPS15
ZFAS1	AC078883.3	NNMT	RPS15A	RPS7	RPL13
MALAT1	NEAT1	POLR2J3.1	VMP1	FUS	PLAGL1
HNRNPA2B1	KLF6	WSB1	FRMD4A	PDK4	MUC20.OT1
KHDC4	FTX	LRRC41	NUTM2B.AS1	KCNQ1OT1	ABCC3
NOTCH2NL	SLC16A12	MCL1	SPG7	SLC25A37	LINC01320
ZNF83	ACADL	ERRFI1	PREX2	RHEX	ARHGEF10
MT.CO2	C3	LGALS3BP	ZNF490	MT.CO1	IGFBP5
HSP90B1	C1QL1	MT.CYB	COL1A2	CXCL14	IGFBP3
PTTG1IP	P4HB	ZNF497	C17orf51	SERPING1	AC010331.1
S100A11	GAL3ST1	AOC1	RPTOR	PKM	SLC6A8
APLP2	MT.ND4	CHPF	TGM2	ZNF362	FGB

T63: 1352 cells; 8 programs

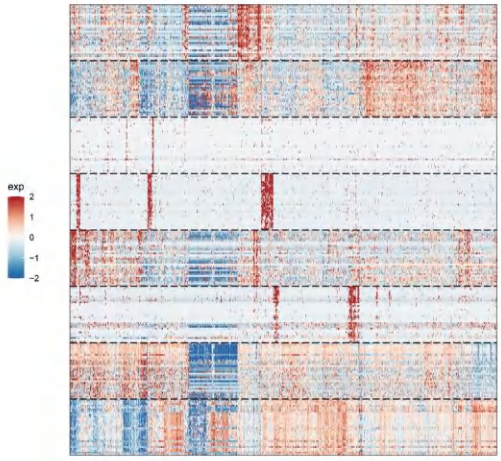

T63_1; T63_2; T63_3; T63_4; T63_5; T63_6; T63_7; T63_8

RARRES3	HLA.DRA	PSMB9	HLA.C	CD74	CXCL10
B2M	HLA.DRB1	LAP3	HLA.E	HLA.B	CXCL11
ISG20	PSME2	GBP4	TAP1	ISG15	IL32
HLA.F	HLA.DRB5	PSMB8	UBE2L6	WARS	HLA.DQA1
HLA.A	HAPLN3	VAMP5	PSME1	CXCL9	IFI27
NAT8	GAL3ST1	SLC6A18	SLC17A3	AMN	PDZK1IP1
GSTP1	GAPDH	FOLR1	SLC22A18	PRDX4	SMIM24
BSG	CYB5A	PGAM1	THY1	TPI1	AKR1B1
ATP5MC3	DNPH1	GPX4	PRELID1	COX6A1	CYC1
FCGRT	ANXA4	NAPSA	PRDX2	ATP5F1B	APOM
KDR	RGCC	TMEM204	ESM1	CLEC14A	ADGRF5
TP53I11	PDGFD	PLVAP	CDH5	CDH13	UNC5B
RFLNB	FLT1	ADGRL4	AZM	LRRC32	RHOJ
PODXL	FLT4	RAMP2	S1PR1	PLPP1	ROBO4
F2RL3	ANGPT2	LDB2	JAM3	HSPG2	APOLD1
CORO1A	CCL5	GZMA	NKG7	CD3D	CD3G
FYB1	CST7	CD3E	PTPRC	TRAC	RAC2
LCK	CD2	HCST	IKZF1	S100A4	SLA
CD37	TRBC2	SRGN	CD48	CD53	GZMK
LIMD2	CD247	CTSW	CD8A	RUNX3	CYTIP
TGFBI	ITIH5	IGFBP5	CPE	IGFBP3	PGF
MUC1	B4GALNT1	AHNAK2	C3	CAV1	NEFL
BGN	COL1A2	C5orf46	FLNA	ANGPTL4	MXRA7
COL6A3	NDUFA4L2	CST3	PMEPA1	COL23A1	DEGS1
C1R	CD151	CTSZ	SERPING1	MXRA8	EMP3
TF	INHA	FGA	FGB	FGG	EPO
S100A1	TSC22D4	BACE2	ASGR2	COLEC11	ADRA2A
VNN2	TTR	F2	LAD1	NCAM1	CLDN11
ASGR1	TFF3	WFDC2	CLU	CXCL2	AC002480.2
TPST2	TSPAN8	MAL	RPS7	SERPIND1	CFH
MALAT1	MT.ND2	MT.ND1	MT.CO3	MT.ATP6	MT.ND3
NEAT1	MT.ND4	MT.ND5	VEGFA	DDX17	SYNE2
MT.CO1	AKAP9	PNISR	HNRNPU	KCNQ1OT1	SORBS2
NCL	FAT1	MT.CYB	MT.ND6	ATP11A	POLR2J3.1
TNS1	PKHD1	ZBTB20	LINC01320	ZNF395	PRRC2C
FOS	EIF1	RPL10	JUND	DUSP1	JUNB
ZFP36	RPL41	RPS5	RPL8	RPS3	RPS14
RPL11	RPL30	RPL10A	RHOB	RPS8	RPS13
RPS3A	RPL19A	RPL18	RPS2	IER2	RPS18
RPL13	ATF3	RPL7A	RPL21	EGR1	CEBPD

T64: 322 cells; 4 programs

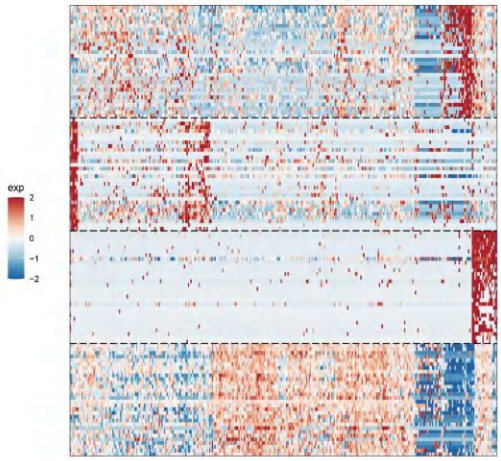

T64_1; T64_2; T64_3; T64_4

MALAT1	ZBTB20	VMP1	CCNL1	MCL1	N4BP2L2
MUC20.OT1	GOLGB1	VEGFA	DNAH11	NFKBIZ	RBM33
FKBP5	ITPRIPL2	FOSB	PNISR	RBM39	LINC01320
PLEKHH2	WDR60	TRA2A	ZBTB16	DDX3X	CHORDC1
CREBRF	WEE1	NEAT1	JMJD1C	GCC2	STAT3
CCL20	C1S	MT3	TMSB10	MT1H	LINC01638
C1R	BICDL2	CAV1	IL1R2	MT1G	EIF4EBP1
CXCL8	MT1X	GPNMB	IGFBP7	MMP7	PRSS23
C3	SYTL2	AEBP1	C2	ANXA2	LOX
CEBPB	LGALS1	CP	PHLDA1	TGFBI	EFEMP1
NKG7	CCL5	CST7	CD37	GZMA	PTPRC
CD48	TMSB4X	SRGN	GZMH	TRBC2	CD52
CYTIP	RUNX3	RAC2	TBC1D10C	CD7	SKAP1
PRF1	S100A4	TRDC	HOPX	LCK	LIMD2
KLRB1	GPSM3	CD3D	KLRD1	SLAMF6	SPN
TMEM176A	TMEM176B	TECR	LGALS2	CYB5A	PEBP1
ADIRF	FTH1	BBOX1	GAMT	IMPA2	HLA.B
ATP5F1D	TMEM37	AMN	MT.CO1	PPIA	SERPINA1
OCIAD2	PDZK1	SLC6A13	DUSP1	ACY3	CALM3
ADI1	ACO2	HPN	NDUFA2	GPX4	CLU

T65: 1899 cells; 4 programs

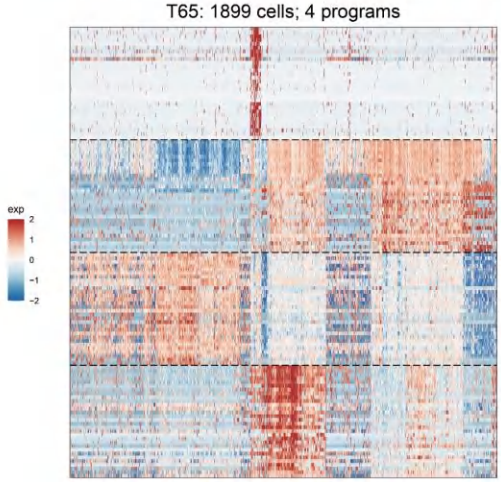

T65_1; T65_2; T65_3; T65_4

GZMA	NKG7	PTPRC	CORO1A	DOK2	CCL5
S100A4	CD52	TMSB4X	GZMM	GIMAP7	GZMH
PTPN7	GATA3	TBC1D10C	PRF1	TRBC1	SASH3
GRAP2	CCR5	HCST	CTSW	TRAC	TRBC2
CD3G	CD3E	CD2	DUSP2	CD69	SAMD3
MT.CYB	MT.ND4	MT.ATP6	MT.CO3	MT.ND1	MT.CO1
MT.ND2	MT.CO2	MT.ND3	MT.ND5	ATP1B1	VCAN
VEGFA	MALAT1	CA12	LINC01320	EDIL3	MTRNR2L12
SLC38A1	N4BP2L2	ATP11A	SPP1	TFPI	BICD1
APP	ITM2B	MT.ND4L	VCAM1	SYNE2	MYO9A
FTH1	CYB5A	GAPDH	HINT1	PEBP1	RPLP1
MYL6	RPL41	TPT1	LGALS4	SERF2	PPIA
S100A10	GSTP1	MYL12B	RPS28	VAMP8	TXN
CCDC146	CHCHD2	S100A11	TMSB10	ADIRF	BRI3
RPS15	FTL	TPI1	GPX4	RBP5	PRDX5
FOS	JUN	IER2	DNAJB1	HSPA1A	EGR1
JUNB	JUND	ATF3	PPP1R15A	UBC	CRYAB
DUSP1	HSPA1B	ZFP36	HSPA8	FOSB	HSPB1
C11orf96	SERTAD1	SERPINH1	TUBA1A	SOCS3	HSP90AA1
CYR61	HSP90AB1	BAG3	DNAJA1	BTG1	H3F3B

T66: 610 cells; 7 programs

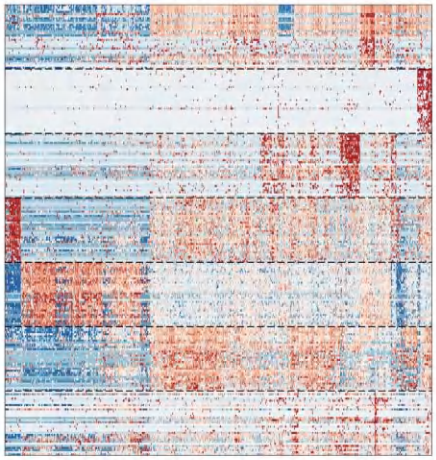

T66_1; T66_2; T66_3; T66_4; T66_5; T66_6; T66_7

MT.CO2	MT.CO1	MT.CO3	MT.ND3	NAT8	CUBN
MT.ATP6	MT.ND5	LRP2	MT.CYB	MT.ND1	MT.ND4
SLC3A1	SLC22A2	MT.ND2	SLC13A1	AMN	IL17RB
SLC22A11	THY1	TMEM37	KLHDC7A	CLDN2	CDH16
FCGRT	ITM2B	CYBA	ERBB3	CNTNAP3	TMEM176B
PTPRC	LIMD2	NKG7	CST7	CD8A	FYB1
GZMA	CD3D	DUSP2	HCST	GZMK	PYHIN1
CTSW	PRF1	LSP1	CD27	DUSP4	CORO1A
CXCR4	CD247	PTPN7	TTN	TRBC1	IL2RG
TRBC2	PTPN22	RAC2	PREX1	CD3E	IL16
VIM	TGFBI	SFRP2	ARL4C	TIMP1	CPE
COL6A2	COL1A2	MXRA8	IGFBP5	C1R	COL1A1
BGN	NTM	LINC01638	CAV1	TMSB10	SPON2
LGALS1	DDIT4	AEBP1	C3	SLC38A5	B4GALNT1
C1S	PGF	NPTX2	LOX	STEAP3	TUBA1A
NEAT1	NAMPT	PPP1R15B	KDM6B	FAM133B	KCNQ1OT1
HNRNPU	ARL5B	MALAT1	MCL1	WSB1	ZBTB10
FOSB	STAT3	UBE2D3	CCNL1	HSPH1	NFKBIZ
HNRNPA2B1	HSP90AA1	HSPD1	IRF1	VMP1	CHORDC1
YBX3	KANSL1L	PLEKHA1	AC020916.1	SLC17A4	NFKBID
FTL	GAPDH	HINT1	GPX4	PLIN2	CYB5A
EEF1A1	SERF2	COX7C	ATP5F1E	TPT1	RPL3
RPLP1	LDHA	GSTA1	ATP6V1F	ATP5MC3	ALDOB
UQCRQ	COX4I1	MIF	TPI1	NDUFB2	RPS26
DDT	POLR2L	RPL28	UQCRB	FXYD2	ATP5MG
HLA.B	HLA.C	CLU	EZR	HLA.A	B2M
HLA.E	ADIRF	TMEM176A	PERP	FOS	AHNAK2
KLF2	HLA.DRB5	CLDN4	HLA.G	COL23A1	HLA.DRB1
YWHAH	ATF3	TMEM176B.1	JUN	JUNB	DSG2
ELF3	IER2	CRIP1	DPP4	NOV	DUSP1
SAA1	MT2A	IDO1	SERPINE2	PRSS23	TRNP1
CD63	S100A3	IL32	CXCL11	CTSE	ACKR4
EMP3	C3.1	CYBA.1	CCL20	WARS	LINC01127
CXCL8	APOL1	IGFBP7	IFITM3	RARRES3	PSME2
PPP1R1A	CAV1.1	PFN1	ANXA2	CXCL9	TMSB10.1

T67: 4821 cells; 5 programs

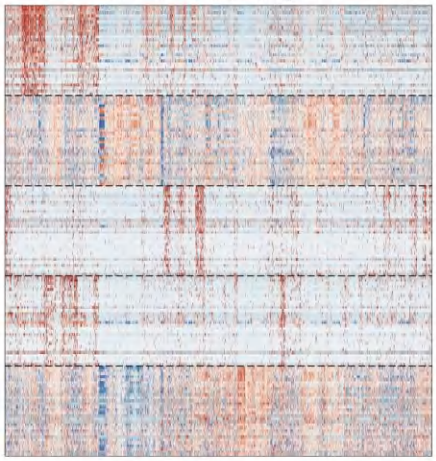

T67_1; T67_2; T67_3; T67_4; T67_5

HLA.DRA	HLA.DPA1	CD74	C1QB	HLA.DPB1	C1QA
HLA.DRB5	TYROBP	HLA.DRB1	APOE	C1QC	HLA.DQA1
FCER1G	CST3	CCL3	AIF1	FTL	LYZ
TMSB4X	CD14	MS4A6A	HLA.DQB1	MS4A7	CTSS
CXCL8	IGSF6	SRGN	CCL3L1	HLA.DMA	CD83
CXCL14	PDZK1IP1	NAT8	MT.CO2	HINT1	GAPDH
MT.ND4	RPL3	MT.ATP6	MT.CO3	MT.ND3	RARRES2
RPS8	LY6E	MT.CYB	RACK1	MT.CO1	EEF1A1
GPX3	ANGPTL4	RPL7A	SPP1	GSTA1	RPLP0
ANXA4	LDHA	RNASET2	SLC17A3	SERPINA1	RPL8
FLT1	PLVAP	TIMP3	IGFBP5	SLC9A3R2	SPARCL1
PLPP3	KDR	A2M	RAMP2	PECAM1	SPARC
COL4A1	IGFBP7	ESM1	MGP	RAMP3	HSPG2
PTPRB	PODXL	EFNB2	LDB2	EMCN	GJA1
EPAS1	SOX18	RGCC	CALCRL	PLPP1	RGS5
NKG7	CCL5	CST7	GZMA	GNLY	TRBC2
CD52	CD3D	RAC2	TRBC1	DUSP2	GZMH
S100A4	PTPRC	CD69	TMSB4X.1	CORO1A	PRF1
CD7	HCST	CD3G	TRAC	GZMB	LCK
GZMK	SH3BGRL3	KLRB1	CD2	KLRD1	CXCR4
ATF3	HSP90AA1	CRYAB	HSPA1A	HSPB1	FOS
JUN	DNAJB1	FOSB	HSPA1B	HSP90AB1	BTG2
DNAJB4	IER2	DNAJA1	EGR1	ANKRD37	BAG3
MAFF	YBX3	UBC	HSPD1	VEGFA	KLF2
JUND	RHOB	JUNB	NEAT1	ADIRF	PPP1R15A

T69: 3163 cells; 4 programs

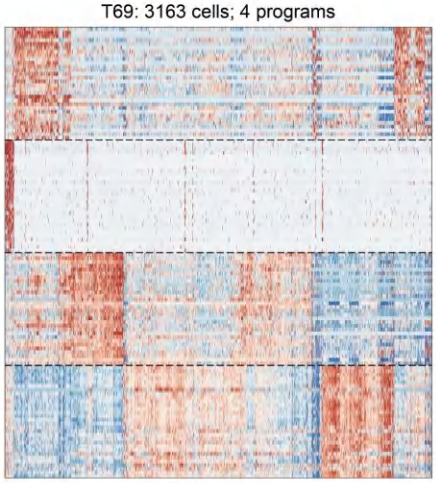

T69_1; T69_2; T69_3; T69_4

H3F3B	FABP7	F8	HSP90AB1	BEX4	F5
ACTG1	CD24	VEGFA	MDK	SNHG8	BTG2
MAFB	HSPA1B	DSP	BTG1	ATP1B1	VIM
FTCD	C14orf180	IFI27	FOS	BAZ2B	HSP90AA1
HSPA1A	SPON2	GNAS	THY1	DDX5	CYSLTR2
CORO1A	CD52	S100A4	ARHGDIB	CST7	CD3D
GZMM	LCP1	CCL5	CD3E	GZMA	DUSP2
CD3G	HCST	TRAC	TRBC2	FYB1	LIMD2
CD48	NKG7	CD69	DOK2	GMFG	GIMAP7
TRBC1	CD247	CD37	GZMH	GNLY	HCLS1
CXCL14	PCSK1N	ITM2B	GPX3	DPEP1	ISOC2
PEPD	CES2	AQP1	SLC22A18	AOC1	GSTK1
NAPSA	MT.CO3	TMEM176A	CDHR5	AGT	AZGP1
GPX4	NAT8	CTSH	GPD1	PDZK1IP1	TMEM176B
BSG	PEBP1	UQCR11	UQCRQ	MT.CO1	GAMT
RPL8	RPS19	RPLP2	RPL18A	RPL37	RPL41
MT3	RPS20	RPL7	RPS3	RPL36	RPL30
RPS21	RPS25	RPS27	RPLP0	ZFAS1	YBX3
RPL21	RPL27A	EPB41L4A.AS1	RPS16	RPS13	NNMT
TPT1	RPL11	CKB	HILPDA	RPL15	RPS14

T70: 1583 cells; 10 programs

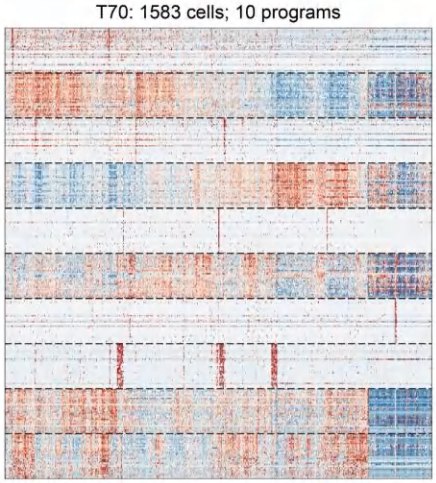

T70_1; T70_10; T70_2; T70_3; T70_4; T70_5; T70_6; T70_7; T70_8; T70_9

RSAD2	ISG15	IFIT3	IFIT2	MX1	IFIH1
IFIT1	OAS1	OASL	SAMD9	CMPK2	HERC5
TNFSF10	OAS3	IFI6	CXCL10	AL135744.1	ISG20
GMPR	GBP1	LINC02128	TNFSF13B	MAJIN	OAS2
HELZ2	CHSY3	AC115620.3	PARP14	PARP9	HERC6
AQP1	CXCL14	TMEM176A	FERD3	GPX3	LY6E
TMEM176B	KHK	CES2	AOC1	GPX4	FCGRT
NAT8	PEBP1	TMBIM6	GSTK1	TSPAN1	ANPEP
TMEM37	CDHR5	ECH1	FTL	ACSM2B	SERPINA1
FTL	CLDN7	CST3	AZGP1	CYB5A	CYB5A
MS4A6A	HLA.DPA1	AIF1	HLA.DQA1	HLA.DPB1	FCER1G
OLR1	CD14	TREM2	IL1B	HLA.DRA	LILRB4
CYBB	CFD	CD74	TLR7	C1QC	MARCH1
HLA.DRB1	IFI30	FCN1	FGL2	CXCR2	C1QA
CSTA	CD163	PLD4	SPI1	CX3CR1	LCK
VMO	RPL18	RPL10	RPL18A	APOBEC	RPS20
RPS9	RPL8	ZFAS1	RPS18	RPS5	ARL4C
EPB41L4A.AS1	BGN	RPL13	RPL10A	APOC1	RPL5
LGALS1	RPS3	CIRBP	RPS4X	TUBA1A	RPS19
RPS14	RPL24	DDIT4	IGFBP5	RPL41	RPS27
ADGRL4	PCDH17	FLT1	SOX18	KDR	ENG
EGFR	MCAM	ESM1	SPARCL1	CD93	TIE1
CLEC14A	VWF	LDB2	CALCRL	FLT4	ANGPT2
A2M	NOTCH4	EFNB2	DLL4	PCDH12	TIMP3
CDH13	HSPG2	MMRN2	PGF	PTPRB	PECAM1
TPM1	IGFBP7	C1QL1	IGFBP3	TNFRSF12A	AKR1B1
TUBA1B	ACTB	TNFAIP6	CD70	ANXA2	PDZK1IP1
ACTG1	PTGS1	RPL7A	RACK1	HMGCR	KRT19
EGFR	PFN1	GAPDH	KRT18	CD151	HINT1
RPL	RPS13	BSG	DERL1	RPN2	FLNA
CDC20	ASPM	CENPF	CDKN3	PIMREG	MKI67
NUF2	CCNB2	NMU	KIF23	CCNA2	CCNB1
CEP55	TOP2A	PTTG1	UBE2S	PLK1	NCAPH
CKS2	CDC25C	MYBL2	BIRC5	FAM83D	RTKN2
TROAP	UBE2C	HJURP	TTK	HMMR	ANLN
CORO1A	CD52	TRAC	LCK	ARHGDIB	S100A4
PTPRC	IL7R	DUSP2	KLRB1	TMSB4X	LAPTM5
CD2	GZMM	CTSW	LCP1	CCL5	GZMA
CD69	HCST	CD3G	CD7	LTB	NKG7
LIMD2	IL2RG	CXCR4	CD3D	PTPN7	GNLY
GOLGB1	NEAT1	ZBTB20	VEGFA	RNRNP1	MT.ND5
MALAT1	SYNE2	APLP2	MUC20.OT1	MT.ATP6	TGOLN2
ITGB8	AHNAK	AKAP9	AHNAK2	POLR2J3.1	DDX17
MIPOL1	HNRNPA2B1	VMP1	CANX	LMAN1	GTF2I
MT.CO3	MACF1	NORAD	MACF1	PRKCI	RNF213
JUND	JUN	FOSB	FOS	ZFP36	DNAJB1
EGR1	DUSP1	JUNB	UBC	TIPARP	KLF6
PPP1R15A	RHOB	ZFP36L1	AC020916.1	CYR61	ATF3
NFKBIZ	HSPA1A	SAT1	CXCL2	BTG2	VMP1.1
DDX3X	MCL1	CCNL1	HSPA1B	ANKRD37	KLF2

T71: 5469 cells; 8 programs

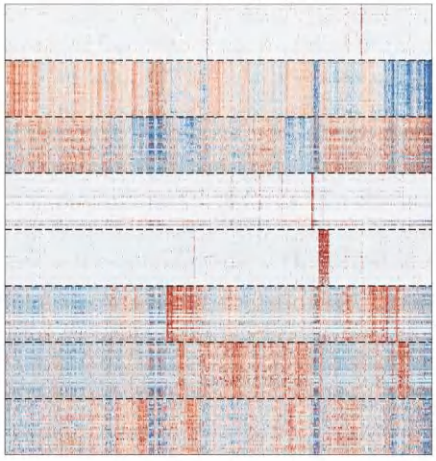

T71_1; T71_2; T71_3; T71_4; T71_5; T71_6; T71_7; T71_8

CLEC14A	IL33	A2M	FAM198B	EFNB2	MGP
CD34	PECAM1	RAMP2	ADGRL4	ENG	MMRN2
CDH5	EMCN	S1PR1	CLDN5	FLT1	GJA4
CD93	FN1	LMO2	SPARCL1	VEGFC	SLC9A3R2
RBP7	VWF	PODXL	ADGRF5	ADAMTS5	FBN1
RPS2	RPL26	RPL41	RPS18	RPL7A	RACK1
RPS12	RPL18A	RPS15	RPL29	RPL19	RPL12
RPL13	RPL10A	RPL3	RPS5	RPS23	RPS8
RPS4X	RPS7	RPS3	RPLP0	RPS14	RPS15A
RPS9	RPLP1	RPS6	RPL6	RPL32	RPL11
MALAT1	MT.ATP6	VEGFA	MT.ND1	RPL23	MT.ND2
HNRNPU	GOLGB1	VMP1	NEAT1	MT.ND3	FUS
ZBTB20	RPS11	MT.ND4	HNRNPA2B1	SRRM2	KCNQ1OT1
MT.ND5	FOSB	CCNL1	HSP90AB1	RBM39	RPS20
ZNF292	STAT3	DDX17	DDX5	SF1	PNISR
TPX2	BIRC5	MKI67	CENPF	CDKN3	CDCA3
KIF20A	ASPM	CCNB2	PTTG1	CDC20	UBE2C
CCNB1	GTSE1	CEP55	AURKB	STMN1	KIFC1
TOP2A	PBK	SAPCD2	PLK1	CENPA	HJURP
KIF23	TUBA1B	ANLN	H2AFZ	CCNA2	SPC25
CD2	CST7	CCL5	GZMA	CORO1A	CD3D
NKG7	IL2RG	PTPRC	TRBC2	LCP1	TRAC
HCST	CTSW	SRGN	LIMD2	GZMK	DUSP2
CD3G	RGS1	GMFG	CD3E	CD27	CD69
TNFRSF9	CD37	CD247	CD8A	IKZF3	SLA
HLA.DRA	CD74	HLA.DQA2	GBP4	RARRES3	HLA.C
HLA.DQA1	HLA.DRB5	B2M	PSMB9	HLA.DPA1	HLA.A
HLA.DRB1	GBP1	HLA.B	CXCL10	HLA.DQB1	IDO1
HLA.DPB1	HLA.E	LAP3	CXCL11	HLA.DMA	CXCL9
WARS	TNFSF10	CTSS	IRF1	IFI27	HLA.F
NAT8	CXCL14	CUBN	PDZK1IP1	GPX3	CES2
APOM	AMN	SLC6A13	UQCRQ	CYB5A	AGT
BBOX1	KHK	SMIM24	AQP1	COX6A1	CDHR5
SLC5A12	SLC17A3	TM4SF5	GAL3ST1	PRAP1	PEPD
AOC1	BSG	DAB2	DNPH1	TXNDC17	SLC39A5
UBC	CRYAB	DUSP1	CLDN4	NDUFA4L2	CD9
PKM	TMEM176A	JUNB	KRT7	JUND	CRIP2
TMEM176B	CLU	S100A10	TACSTD2	ZFP36	PGK1
RHOB	CLDN3	HSPA1A	KLF2	HSPB1	FOS
HSPA1B	TPI1	CLDN7	ADIRF	IER2	EIF1

T72: 2433 cells; 5 programs

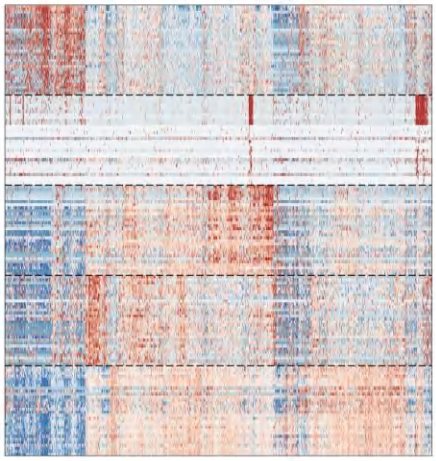

T72_1; T72_2; T72_3; T72_4; T72_5

MALAT1	NEAT1	POLR2J3.1	HNRNPA2B1	HNRNPU	VMP1
WSB1	PNISR	KCNQ1OT1	PLEKHH2	ATP13A3	DDX17
N4BP2L2	ZEB2	PLAGL1	FTX	CCNL1	MACF1
PIAS2	PAX8	VEGFA	PLEKHA1	MUC20.OT1	WDR60
ZNF83	MACC1	GLS	ABCC3	SYNE2	ARGLU1
MT.ND3	MT.ND4	MT.ATP6	MT.ND1	MT.CYB	MT.CO1
MT.ND2	MT.ND5	MT.CO3	MT.CO2	MZB1	IGHG3
IGHG4	IGHG1	IGKC	MT.ND4L	JCHAIN	CD3E
DUSP2	MT.ND6	IL7R	TMSB4X	SRGN	CD69
CD52	MTRNR2L12	CD74	PTPN22	ITGAL	RCSD1
NAT8	GPX4	KHK	BBOX1	LGALS2	ECH1
SLC6A18	CYB5A	MPC2	TMEM176B	DNPH1	GSTA1
ATP5MC3	GAL3ST1	PXMP2	LDHB	NDUFB2	AQP1
TMEM176A	HINT1	ANXA4	CXCL14	OCIAD2	IMPA2
CUBN	PTN	COX5B	RPS28	PRDX2	CHCHD10
TNFRSF12A	S100A11	TM4SF1	PFN1	ACTB	ACTG1
CTSZ	MT2A	KRT19	ANXA2	IGFBP7	CITED4
PDZK1IP1	TNFAIP6	TPM1	CLIC1	CFL1	TUBA1B
RAN	EMP3	MYL6	PHLDA1	PPP1R14B	FHL2
IL32	CAV1	TRAM1	PRSS23	CCL2	MYL12A
FOS	JUNB	EIF1	DUSP1	RPL10	RPL41
TPT1	KLF2	HSPA1A	C11orf96	RPL21	HSPA1B
ATF3	IER2	RHOB	DNAJB1	RPL23A	VIM
RPL9	RPS14	FTH1	RPL30	RPS27A	CCNI
RPS27	RPS5	UBC	RPS3	RPS2	RPL18A

T73: 309 cells; 6 programs

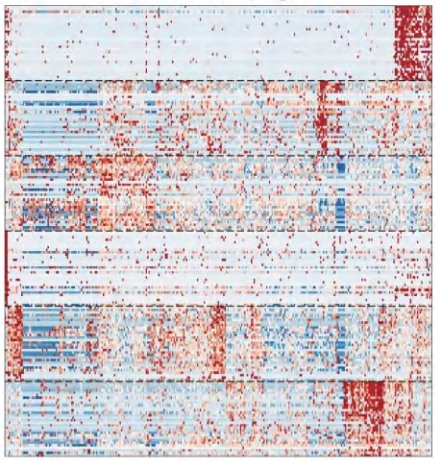

T73_1; T73_2; T73_3; T73_4; T73_5; T73_6

CD3G	TRAC	TMSB4X	IL2RG	PTPRC	TIGIT
GPSM3	LSP1	CD3D	GZMK	LAPTM5	CD27
CD2	DUSP4	ARHGDIB	ITM2A	CORO1A	EMB
HCST	TBC1D10C	UCP2	CTSW	CD52	LCP1
LCK	SPN	RAC2	GIMAP4	SRGN	TRBC2
THBS1	XIST	SYNE2	DDX17	VEGFA	SYNPO
SBNO2	LINC00472	NEAT1	MALAT1	EP400	SYNE1
MT.CO3	ZNF292	LIFR	ALPK2	LRP2	ZNF462
AHNAK	TBC1D8B	HNRNPU	LRCH1	AKAP9	SLCO3A1
IL6ST	BRAT1	SAMD4A	RRBP1	RC3H1	MKLN1
CYB5A	SLC6A13	LGALS2	NDUFC1	GAPDH	TMEM176B
CXCL14	TESC	MPC2	AC021744.1	ABCB9	BBOX1
TMEM139	TMEM176A	FBP1	GAL3ST1	DUSP28	RACK1
FTL	TPT1	PDZK1IP1	SERF2	TSTD1	CMBL
TPI1	SLC17A3	ADIRF	S100A1	MIF	HIST1H1C
IGSF6	SPI1	C1QB	FCER1G	C1QC	A2M
CD14	C1QA	HLA.DPB1	TYROBP	APOC1	CTSS
MS4A6A	ADA2	CST3	LY96	APOE	GPR65
CD4	FCGR2A	AIF1	LST1	HLA.DRA	LAPTM5.1
HLA.DQB1	RGS10	PTGER4	DSE	NRP2	HLA.DPA1
CXCL11	TNFSF10	MARCKSL1	RARRES3	C3	VAMP5
GBP1	C1R	CAV1	TYMP	IGFBP3	IL32
LY6E	IL18BP	PSMB9	NNMT	PSME1	CXCL9
SELENOM	TIMP1	CD40	S100A11	TAP1	PHLDA2
IFITM3	TMSB10	WARS	FBXL6	SPIB	EMP3
FOS	IER2	JUNB	JUND	ZFP36	SOCS3
UBC	ATF3	EGR1	JUN	FOSB	SERTAD1
DUSP1	HSPA1B	KLF2	PPP1R15A	MAFF	GDF15
BTG2	CDKN1A	CEBPD	EIF1	KLF4	NFKBIA
YBX3	MT.ND1	ST7.AS1	GADD45B	H3F3B	DNAJB1

T74: 1603 cells; 5 programs

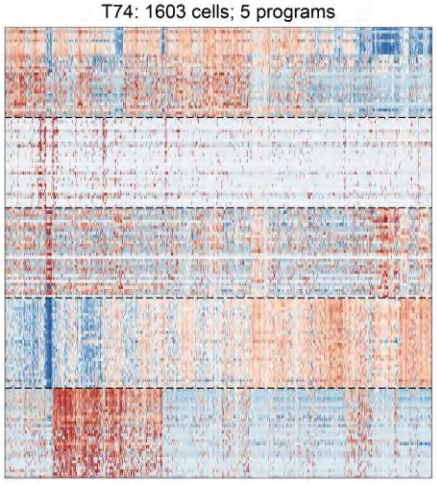

T74_1; T74_2; T74_3; T74_4; T74_5

MT.CO3	CXCL14	MT.CO2	MT.ATP6	PDZK1IP1	MT.CO1
MT.ND4	MT.ND3	MT.CYB	KRT18	CYB5A	TMEM176A
CRYAB	GPX3	HINT1	SLC17A3	CES2	GSTA2
FXYD2	SPP1	CNDP2	GSTA1	TMEM176B	SERPINA1
ANGPTL4	LGALS2	RBP5	MT.ND5	ANXA4	CKB
FLT1	ENG	SLC9A3R2	ADGRL4	COL4A1	HSPG2
VWF	CD34	SPRY1	COL4A2	PODXL	PLVAP
PECAM1	RAMP3	KDR	SULF1	CALCRL	ADGRF5
TIMP3	TM4SF1	TCF4	COL15A1	SPARCL1	EMP1
HEG1	INSR	A2M	PLXND1	CLEC14A	SH3BP5
SQSTM1	MALAT1	ATF3	TCEA1	BEX2	NEAT1
HSPA9	ZBTB20	MUC20.OT1	NUPR1	FAM13A	VEGFA
PDK4	FOSB	IGFBP5	PLCG2	AC025423.1	VMP1
CPEB4	GADD45A	N4BP2L2	ANXA1	RUFY3	PNISR
PDLIM3	ZFAND5	FTL	HSP90AA1	DDX17	MSC.AS1
RPL41	RPS14	RPL10	RPS27	RPL18	RPS11
RPS20	RPL13	RPL11	RPS8	RPL36	RPL23
RPS5	RPL24	APOE	RPL39	RPS28	RPL9
RPL35A	RPL19	VIM	RPS18	RPL37A	RPL18A
RPS3	RPL30	RPS15	LGALS1	RPL27A	RPL23A
HLA.DRA	HLA.DPB1	HLA.DPA1	CD74	HLA.DRB5	TYROBP
HLA.DRB1	SRGN	RGS1	TMSB4X	CST3	C1QA
SAT1	AIF1	HLA.DQA1	C1QB	FCER1G	CXCR4
B2M	CTSS	LYZ	HLA.DQB1	SGK1	LAPTM5
FGL2	C1QC	MS4A7	HLA.DMA	GPR183	HERPUD1

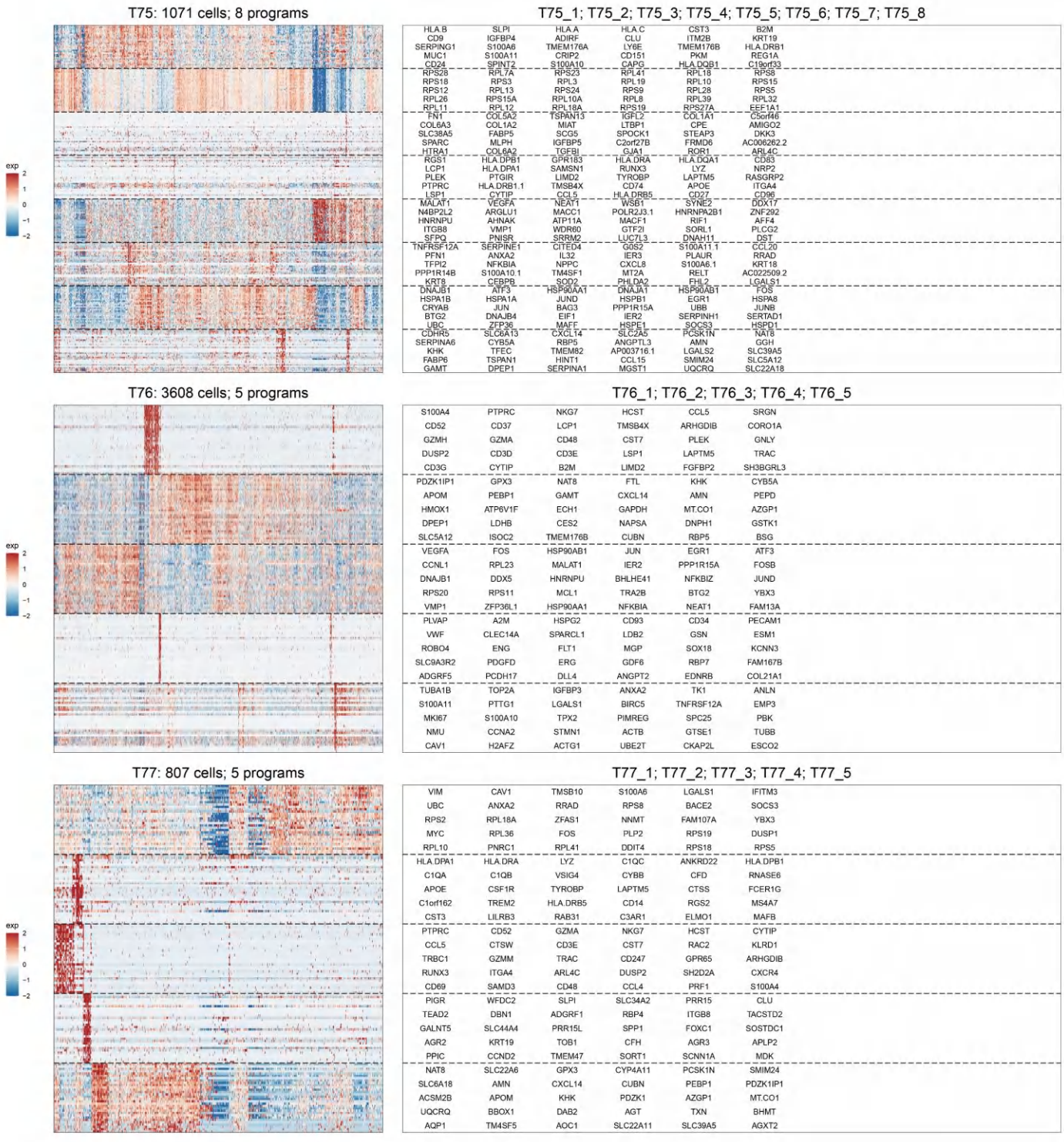

Figure S6-S16 Gene expression within each gene expression program in each sample.

Heatmap showing expression of genes within each gene expression program (GEP) across single cells in each tumor sample. Randomly selected 5% cells for each program are shown, with top 30 signature genes showed on the right. cNMF analysis was performed in 43 tumor samples separately using the optimal number of NMF components (k-value).

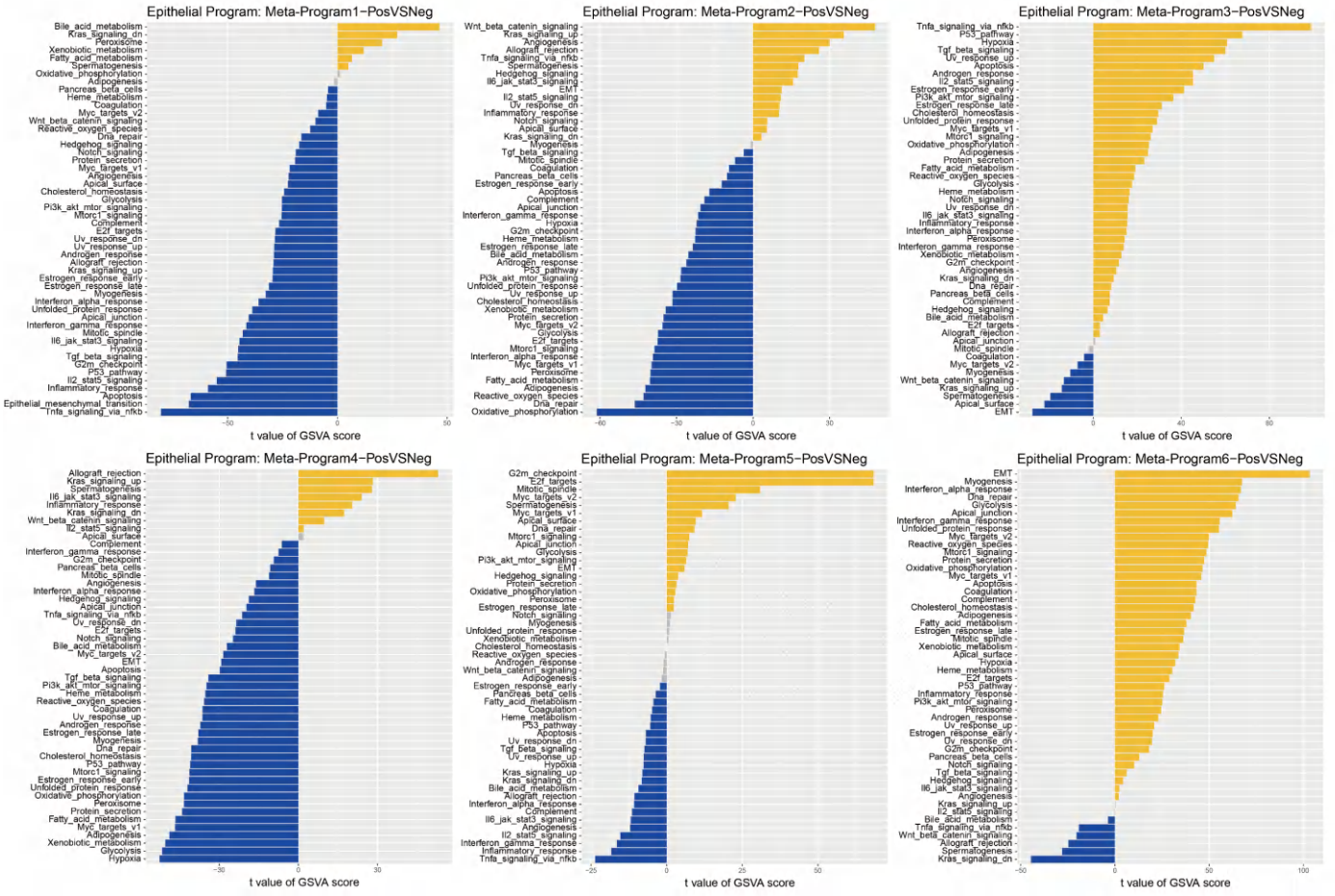

Figure S17 Hallmark pathways enrichment of six malignant meta-programs.

Diverging bar plots showing differences in pathway activities scored per cell by GSVA between program tumor cells and non-program tumor cells. t value of GSVA score was corrected for patient of origin. UV, ultraviolet; dn, down; v1, version 1; v2, version 2.

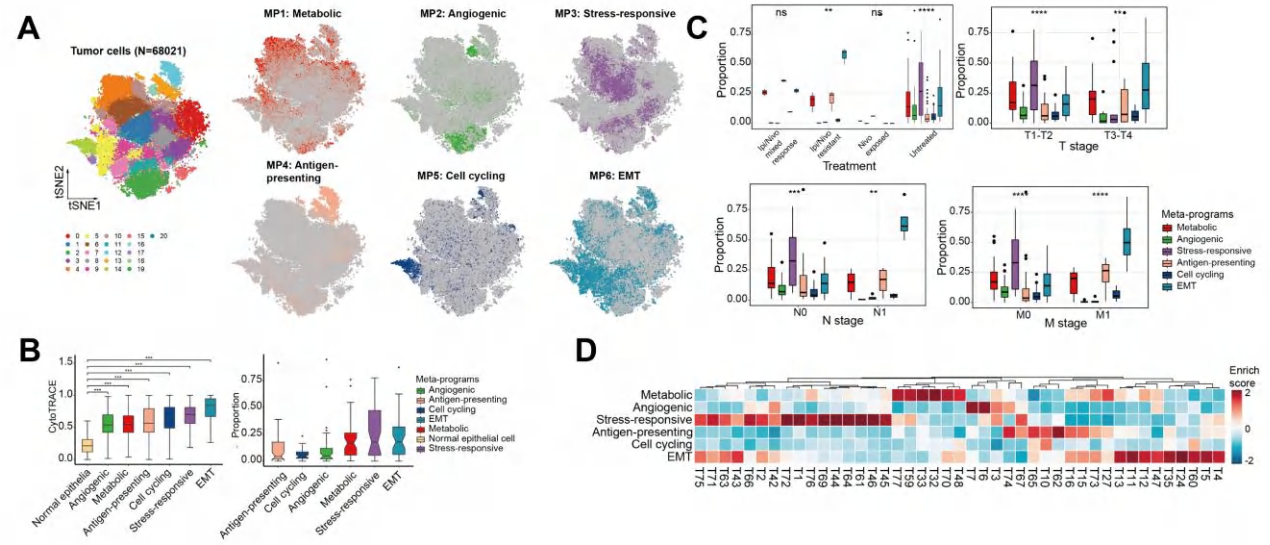

Figure S18 Distributions and clinical associations of six program tumor cells.

(A) tSNE plot showing clusters of malignant epithelial cells (left), with colored by enrichment score of each meta-program (right). (B) Boxplot showing the CytoTRACE score (left) and the proportion of program cells

for each tumor (n = 43) (right) among six MPs. (C) Boxplots showing proportion of six malignant epithelial cells in different ICB treatment, T stage, N stage, and M stage groups. (D) Heatmap showing the normalized enrichment scores for six MPs in each tumor. All samples are distinctly assigned to a specific tumor state.

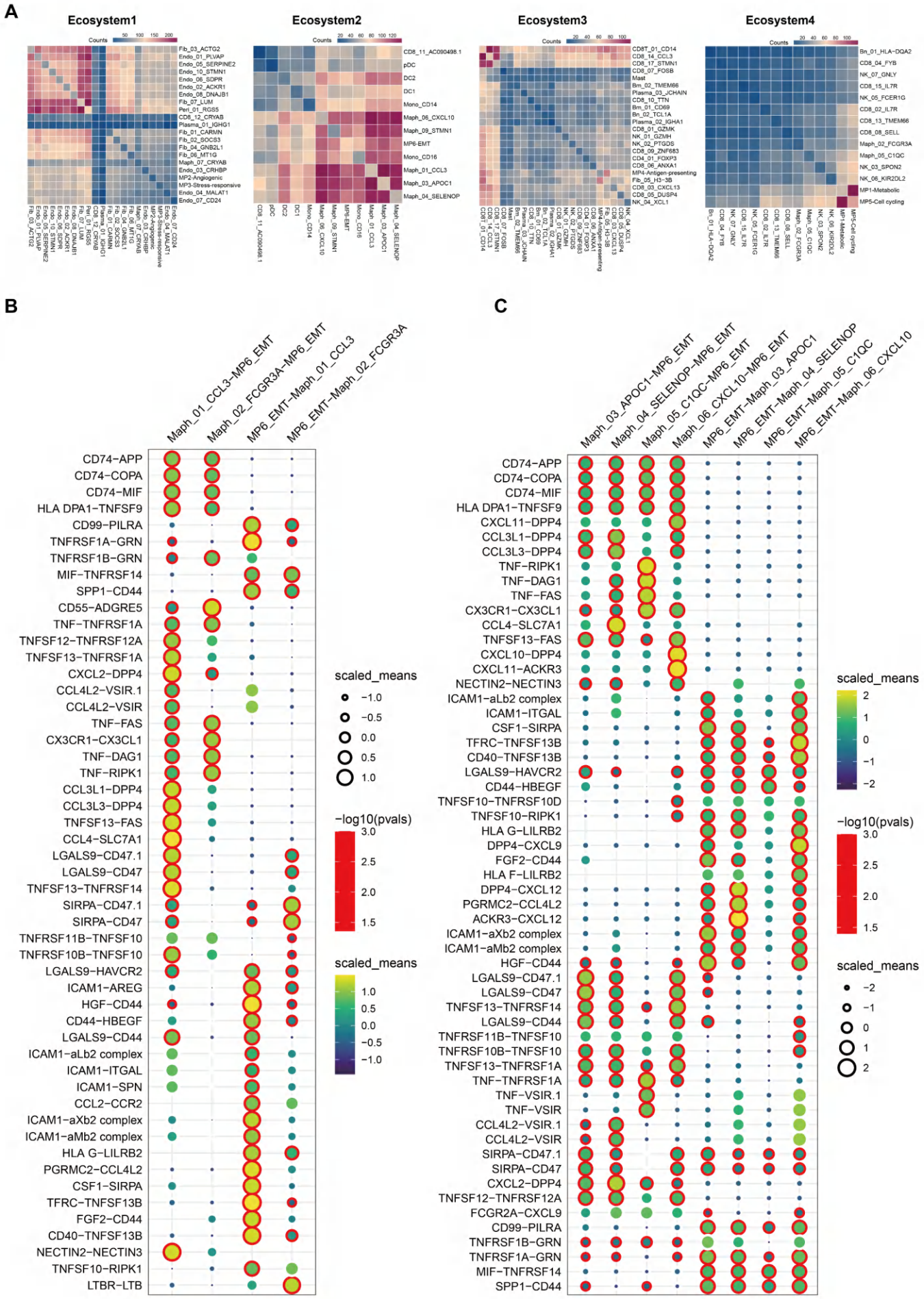
A
Ecosystem1
Ecosystem2
Ecosystem3
Ecosystem4
B
Maph_01_CCL3−MP6_EMT
Maph_02_FCGR3A−MP6_EMT
MP6_EMT−Maph_01_CCL3
MP6_EMT−Maph_02_FCGR3A
scaled_means
−log10(pvals)
C
Maph_03_APOC1−MP6_EMT
Maph_04_SELENOP−MP6_EMT
Maph_05_C1QC−MP6_EMT
Maph_06_CXCL10−MP6_EMT
MP6_EMT−Maph_03_APOC1
MP6_EMT−Maph_04_SELENOP
MP6_EMT−Maph_05_C1QC
MP6_EMT−Maph_06_CXCL10
scaled_means
−log10(pvals)
scaled_means

Figure S19 Analysis of ligand-receptor interactions in tumor ecosystems using CellphoneDB.

(A) Heatmaps of L-R interactions across four tumor ecosystems. Heatmaps display the intensity of L-R interactions within four distinct tumor ecosystems, labeled Ecosystem1 through Ecosystem4. The color scale ranges from blue (low interaction) to red (high interaction), with the counts of interactions indicated by the color intensity. These heatmaps highlight the heterogeneity and unique interaction profiles of each tumor microenvironment. (B) Dot plot of L-R interactions between EMT tumor cells and M1 macrophages in Ecosystem2. This dot plot details the interaction significance and expression levels of L-R pairs between EMT tumor cells and M1 macrophages within Ecosystem2. The dot size denotes the -log10 (p-value), reflecting the statistical significance of each interaction, with larger dots indicating more significant findings. The color of the dots varies from green to red, representing the scaled mean expression levels from low to high, respectively. Key interactions such as CD74-APP, CD74-MIF, and TNF-FAS are highlighted, showing their relevance in these ecosystems. (C) Dot plot of L-R interactions between EMT tumor cells and M2 macrophages in Ecosystem2. Mirroring the structure of (B), this dot plot shows L-R interactions between EMT tumor cells and M2 macrophages in Ecosystem2. It uses the same conventions for dot size and color coding to indicate statistical significance and expression levels. This panel focuses on illustrating the distinct interaction patterns that may influence the dynamics within the tumor microenvironment specifically involving M2 macrophages. Notable interactions include TNF-FAS, ICAM1-ITGAL, and CXCL12-CXCR4, which may play critical roles in the tumor microenvironment dynamics of these ecosystems.

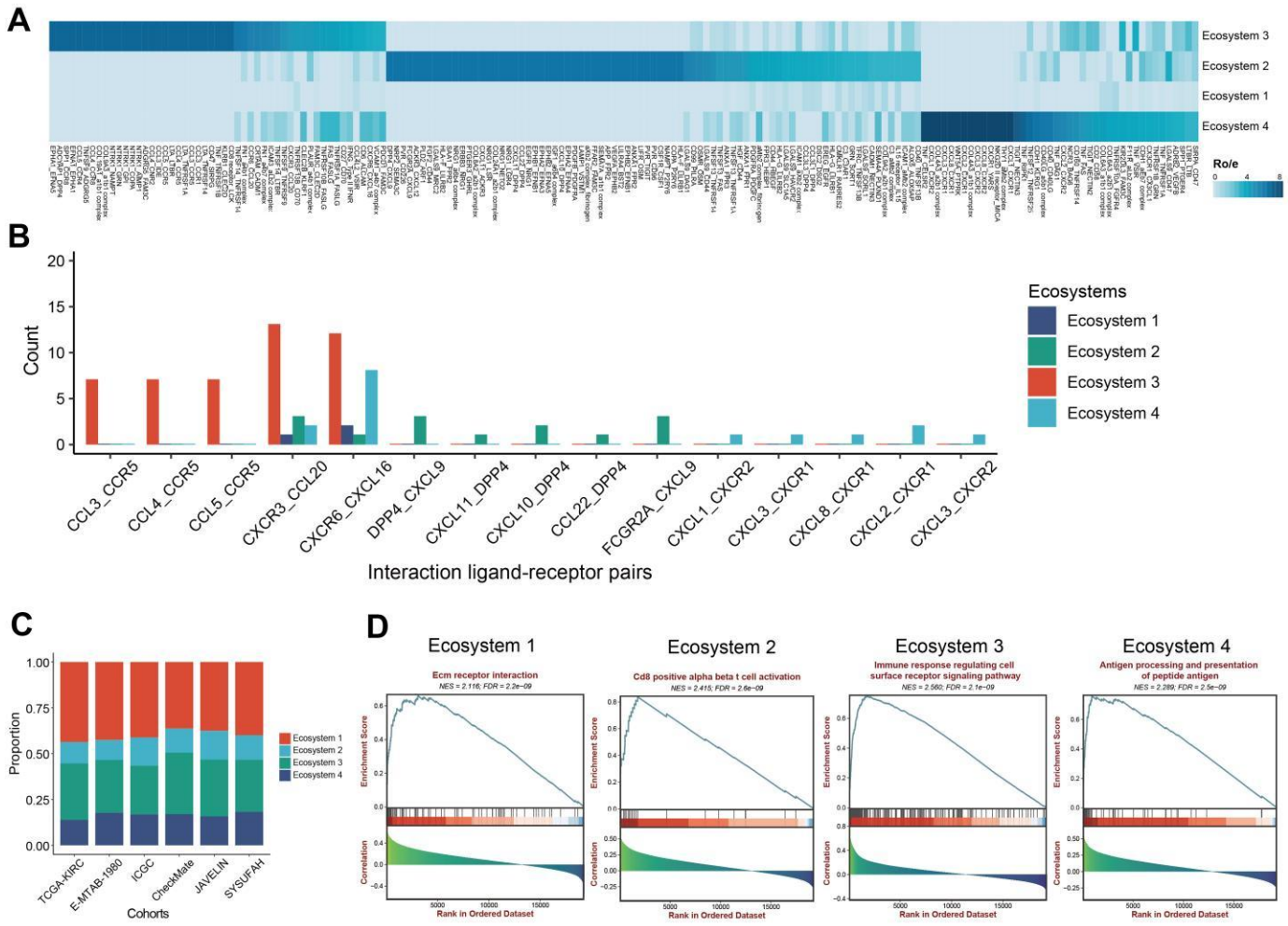

Figure S20 Ligand-receptor interactions, distribution, and signaling pathways across tumor ecosystems. (A) Heatmap showing enriched L-R pairs in four specific ecosystems, colored coded by $R_{o/e}$ enrichment values. L-R pair with $R_{o/e} > 1$ was assumed to enriched in a specific ecosystem. (B) Barplots showing the frequency of key chemokines/chemokine receptors pairs significantly enriched in four distinct ecosystems. (C) Stacked bar chart showing the proportional distribution of four tumor ecosystems in five independent cohorts (TCGA, E-MTAB-1980, ICGC, CheckMate, JAVELIN, and SYSUFAH). (D) GSEA plot visualizing significantly enriched hallmark signaling pathways of four tumor ecosystems. The normalized enrichment score (NES) and GSEA false discovery rate (FDR) are indicated for key pathways. Pathways with $|NES| > 1$ and $FDR < 0.05$ were deemed significant.

Figure S21 GSEA ridge plot analysis of tumor ecosystem signatures across GO, KEGG, and Hallmark gene sets.

(A-D) Ridge plots visualize the enrichment patterns of four tumor ecosystem signatures (Ecosystems 1-4)

against gene sets from GO, KEGG, and Hallmark databases using Gene Set Enrichment Analysis (GSEA). Each “ridge” represents the distribution of enrichment scores for a significantly enriched pathway, where the peak corresponds to the maximum enrichment score (ES) and the width reflects the density of genes contributing to the enrichment. The x-axis indicates the ES (positive/negative values denote up-/down-regulation in the signature), and the y-axis lists enriched pathways. Color intensity represents the statistical significance. Pathways with |NES| > 1 and FDR < 0.05 were deemed significant. The analysis reveals distinct biological functions associated with each ecosystem.

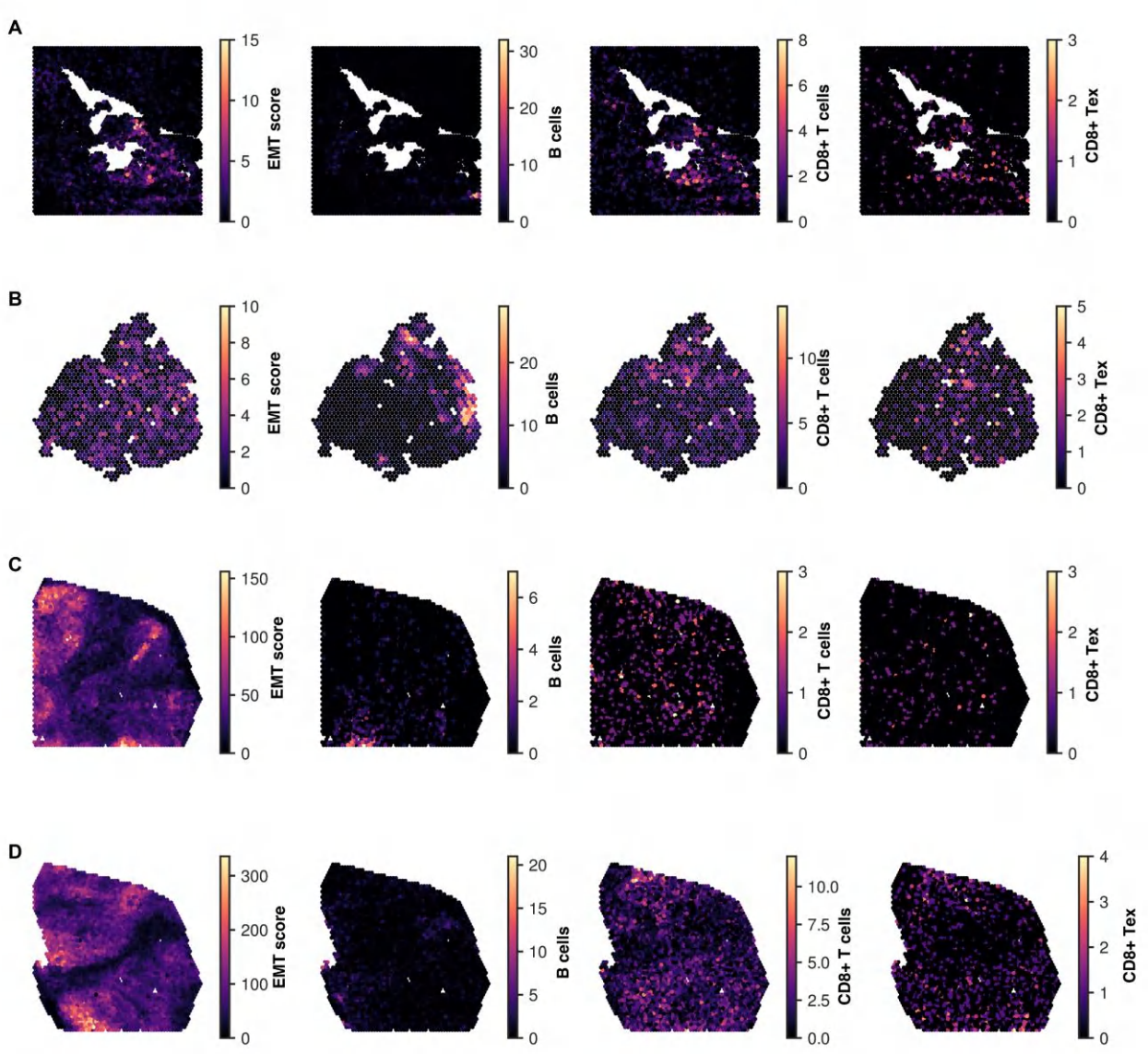

Figure S22 Spatial co-localization analysis between EMT-high tumor cells and specific immune cell types.

(A-D) Representative spatial transcriptomics map showing the distribution of EMT-high tumor cells, B cells, CD8+ T cells, and exhausted CD8+ T cells within the tumor microenvironment. Color gradient indicates signature score intensity. EMT-high tumor cells exhibit spatial proximity to CD8+ T cells and exhausted CD8+ T cells.

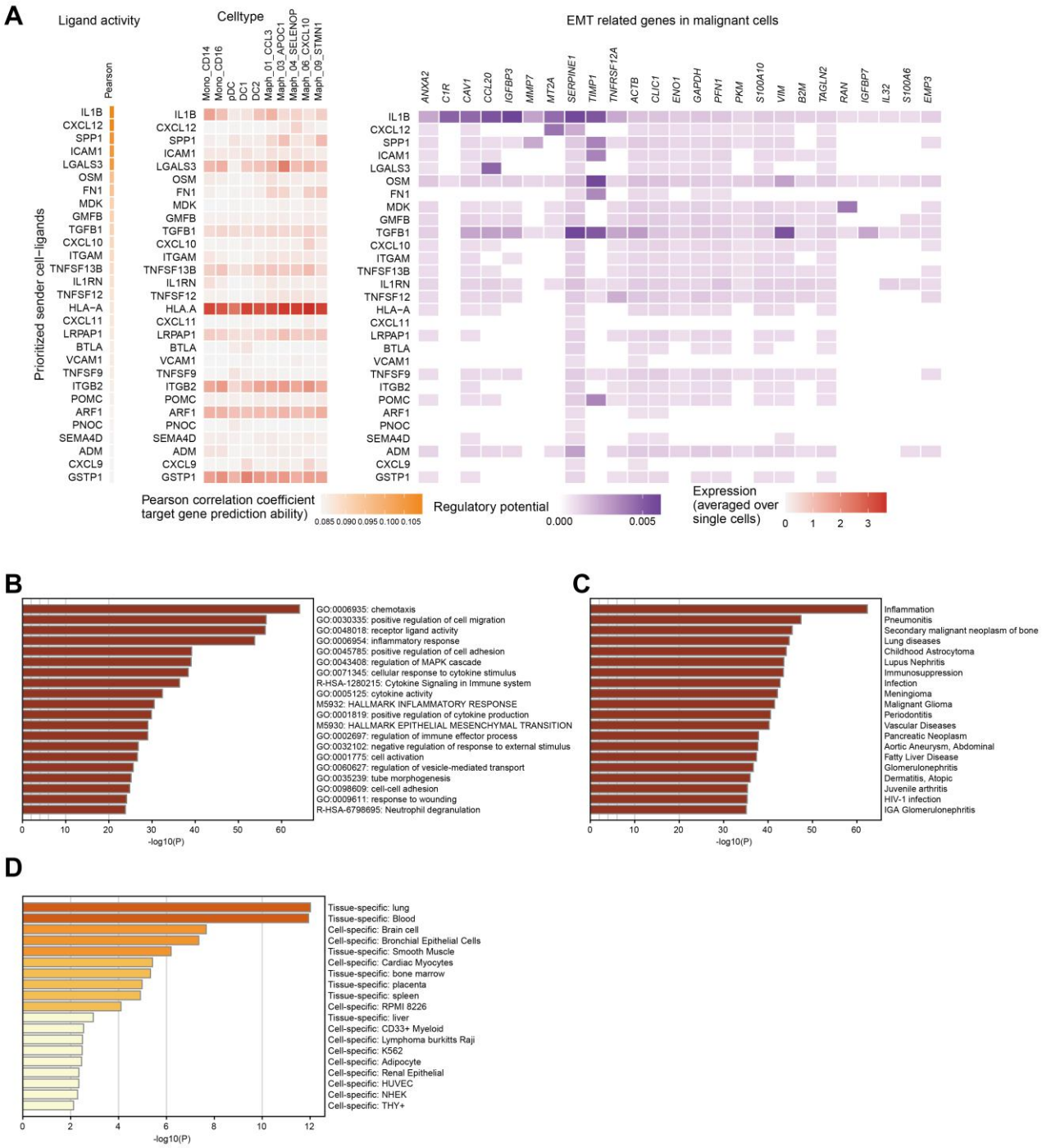

Figure S23 NicheNet analysis and functional enrichment of the ecosystem 2 signature.

(A) Outcome of predicted NicheNet's ligand activity by myeloid cells on EMT related genes. Heatmap showing the Pearson correlation indicates the target genes prediction ability of each ligand, and better predictive ligands are thus ranked higher. (B-D) Metascape enrichment analysis of the signature associated with ecosystem 2. Significant enrichments are shown for (B) epithelial-mesenchymal transition (EMT)-related pathways, (C) immunosuppression-related pathways, and (D) myeloid cell-related pathways. The consistent enrichments across categories validate the robustness of the signature. Metascape terms with adjusted $P <$ 0.05.

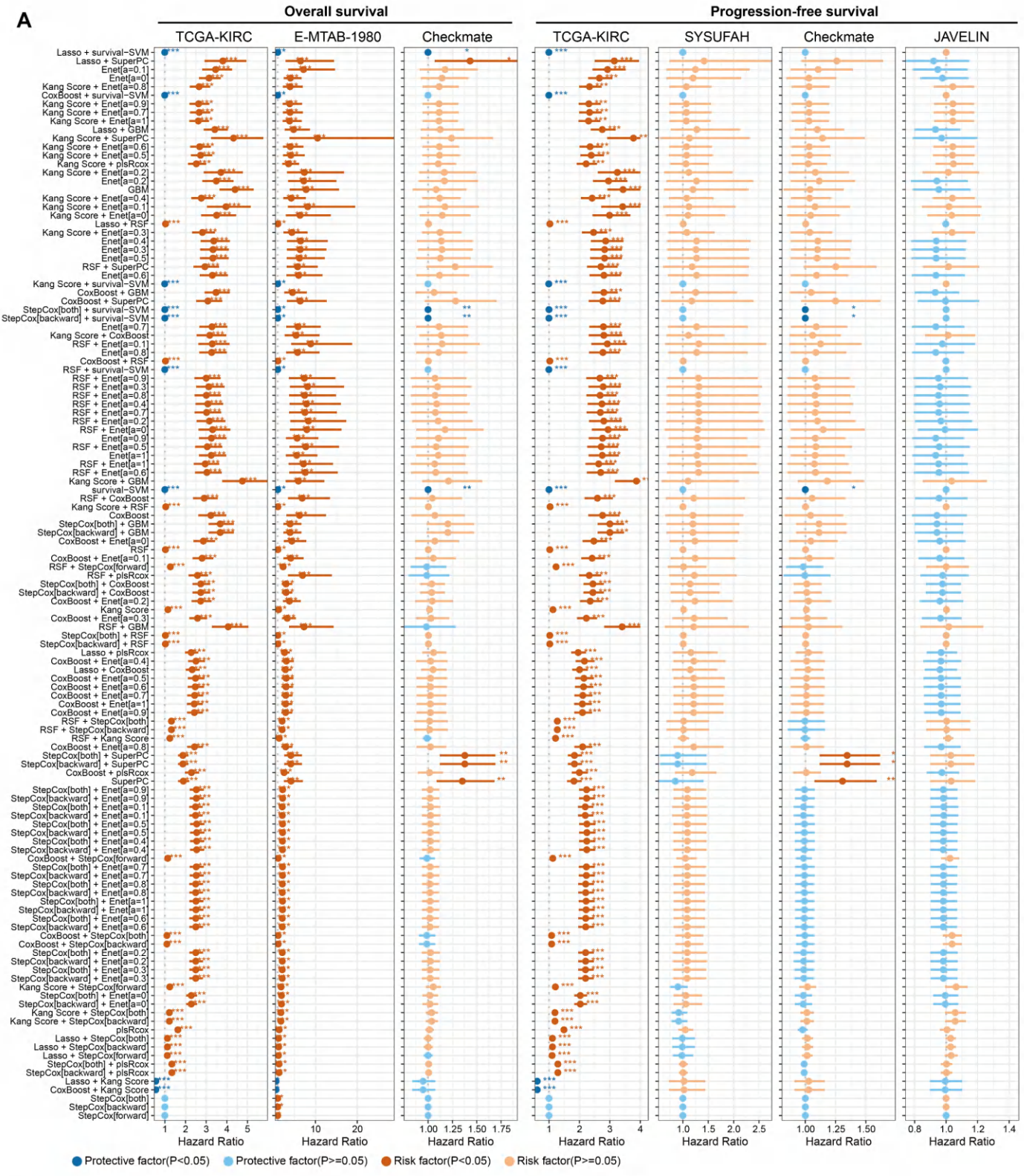
A
Overall survival
Progression-free survival
TCGA-KIRC
E-MTAB-1980
Checkmate
TCGA-KIRC
SYSUFAH
Checkmate
JAVELIN
Hazard Ratio
Protective factor(P<0.05)
Protective factor(P>=0.05)
Risk factor(P<0.05)
Risk factor(P>=0.05)
B
10-Fold Cross-Validation Predictions
Predicted Values
True Values
Fold 1
Fold 2
Fold 3
Fold 4
Fold 5
Fold 6
Fold 7
Fold 8
Fold 9
Fold 10
C
Mean R² = 0.847
Validation R²
Fold #

Figure S24. Assessment of prognostic model performance through forest plot and 10-fold cross-validation.

(A) Forest plot of hazard ratios for 126 prognostic models across multiple validation cohorts. The prognostic performance of each model is visualized by its HR (with 95% confidence intervals) for overall survival (OS) in the TCGA-KIRC, EMTAB-1980, CheckMate cohorts and progression-free survival (PFS) in the TCGA, SYSUFAH, CheckMate, JAVELIN cohorts. Each horizontal line represents the HR and confidence interval for a single model within a specific cohort and endpoint. The color of each marker indicates the effect direction and statistical significance: red (HR > 1, $P < 0.05$), light red (HR > 1, $P \geq 0.05$), blue (HR < 1, $P < 0.05$), light blue (HR < 1, $P \geq 0.05$). The vertical line (line of no effect) is set at HR = 1. Statistical significance was defined as a two-sided $P < 0.05$. Abbreviations: HR, hazard ratio; TCGA, The Cancer Genome Atlas. (B) Parity plot from 10-fold cross-validation of the optimal model, comparing the actual versus predicted prognostic values for each fold. Markers represent individual folds, and the solid diagonal line denotes the ideal 1:1 relationship. The close alignment of data points to the diagonal indicates consistent model performance across different data subsets. (C) Coefficient of determination (R^2) for each of the 10 cross-validation folds. The average R^2 value is 0.847, indicating that the model explains 84.7% of the variance and demonstrates robust predictive capability.

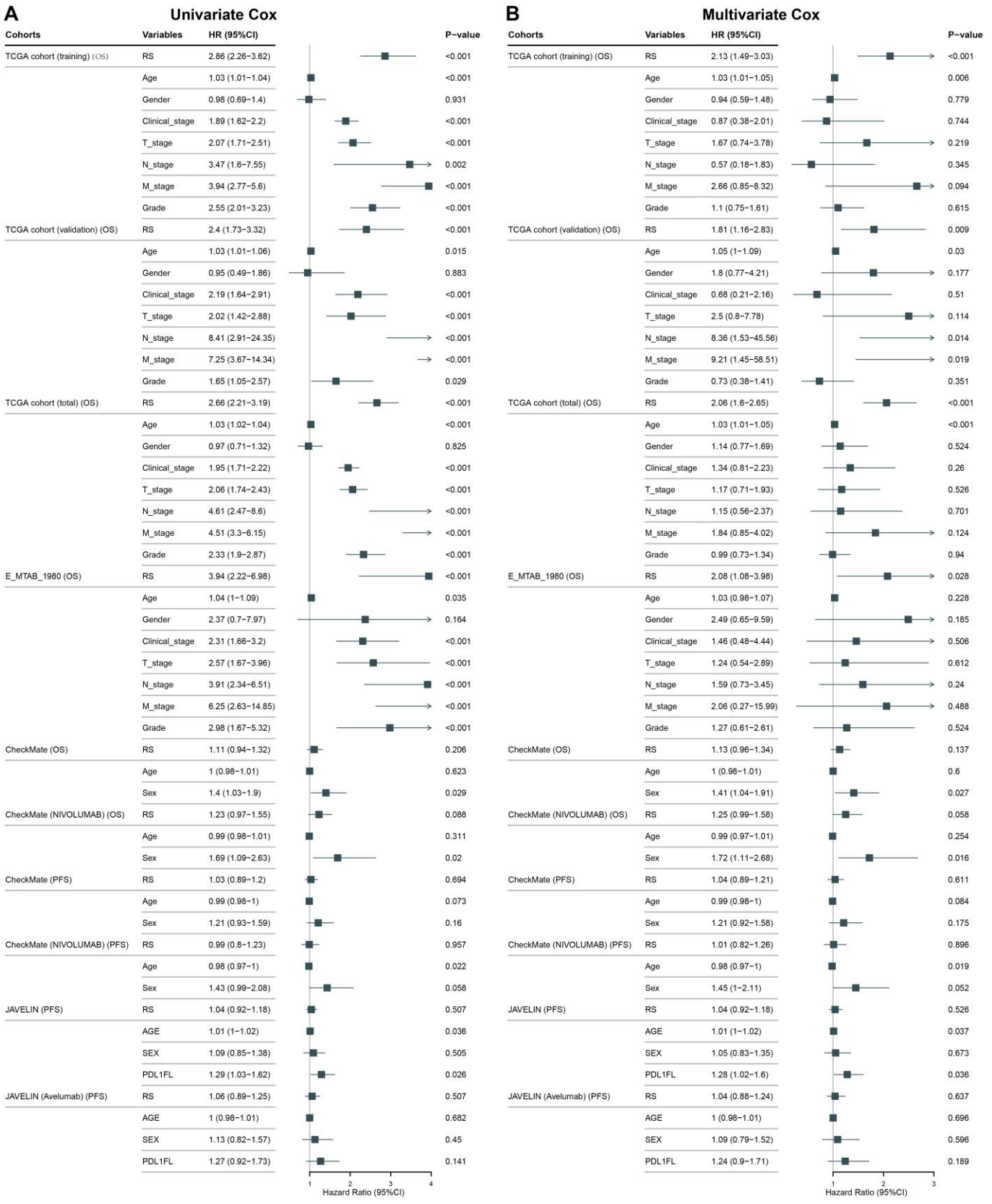

Figure S25 Forest plots of univariable and multivariable Cox regression analyses for the prognostic model across multiple cohorts.

(A-B) The prognostic value of the risk score (RS) derived from the model and key clinical variables was assessed in the TCGA, E-MTAB-1980, CheckMate (OS: overall survival), CheckMate (PFS: progression-free survival), and JAVELIN cohorts. For each cohort, panel (A) shows the univariable analysis results, and panel

(B) shows the multivariable analysis results. Hazard ratios (HRs) with 95% confidence intervals (CIs) are displayed both graphically (squares and horizontal lines) and numerically. The vertical grey line represents the null effect (HR = 1). A HR > 1 indicates a worse prognosis (risk factor), while an HR < 1 indicates a better prognosis (protective factor). Analyses were performed using the survival package in R. The specific statistical methods and sample sizes for each cohort are provided in the Methods section. Abbreviations: CI, confidence interval; HR, hazard ratio; OS, overall survival; PFS, progression-free survival.

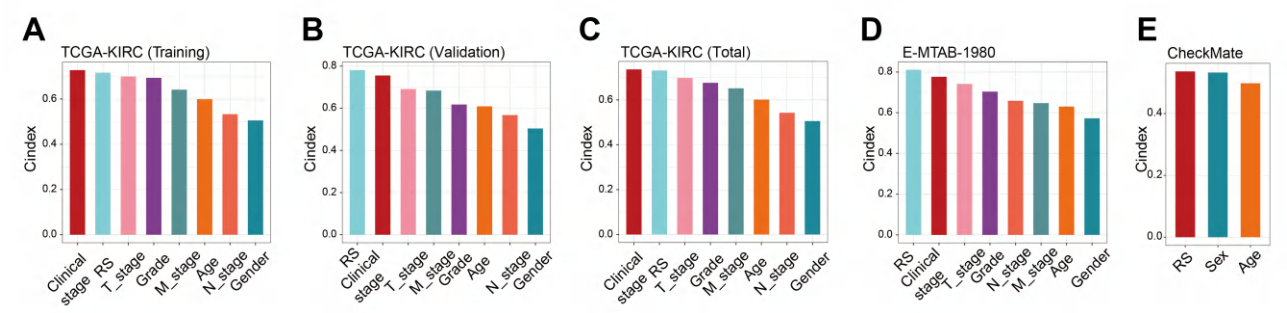

Figure S26 Validation and evaluation of ISM-EMTRS prognostic potentials.

(A-E) Histograms show the comparisons between performance of ISM-EMT- RS and other clinical variables in predicting prognosis.

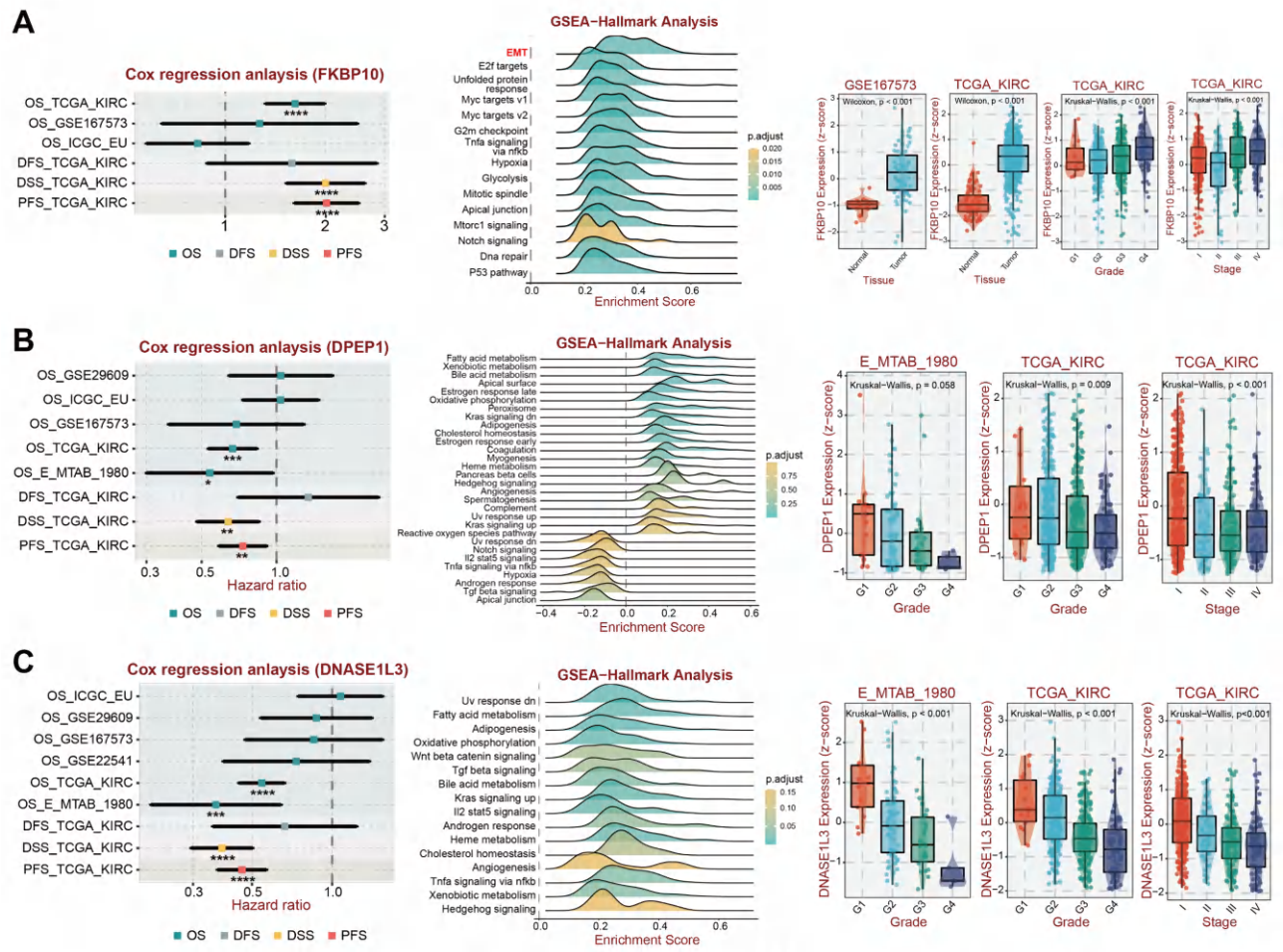

Figure S27 Validation of the role of FKBP10, DPEP1 and DNASE1L3 in ccRCC across 6 cohorts.

(A-C) (Left) Cox regression analysis revealed significant associations between the expressions of FKBP10, DPEP1, and DNASE1L3 with clinical outcomes such as Overall Survival (OS), Disease-Free Survival (DFS), Disease-Specific Survival (DSS), and Progression-Free Survival (PFS) across datasets like GSE29609 (n = 39), ICGC_EU (n = 91), GSE167573 (n = 63), E-MTAB-1980 (n = 101), GSE22541 (n = 68) and TCGA_KIRC (n = 533). (Middle) GSEA-Hallmark analysis identified key pathways enriched in correlation with these genes, including epithelial-mesenchymal transition, fatty acid metabolism and oxidative phosphorylation, and. (Right) Boxplots showed increase expression of FKBP10 and decreased expression of DNASE1L3, DPEP1 from early to advanced clinical stages or pathological grade. Significance was assessed using the Kruskal-Wallis test (multi-group comparisons) and Wilcoxon test (pairwise comparisons). All statistical tests were two-sided, $P < 0.05$.

Figure S28 Association of FKBP10, DPEP1, and DNASE1L3 expression with survival outcomes in immunotherapy cohorts.

(A-C) Kaplan-Meier curves illustrate progression-free survival (PFS) and overall survival (OS) for patients across multiple cohorts treated with immune checkpoint inhibitors. Patients were stratified into high- and low-expression groups based on the optimal cut-off value for each gene (FKBP10, DPEP1, DNASE1L3). The log-rank test was used to compare survival differences between groups.

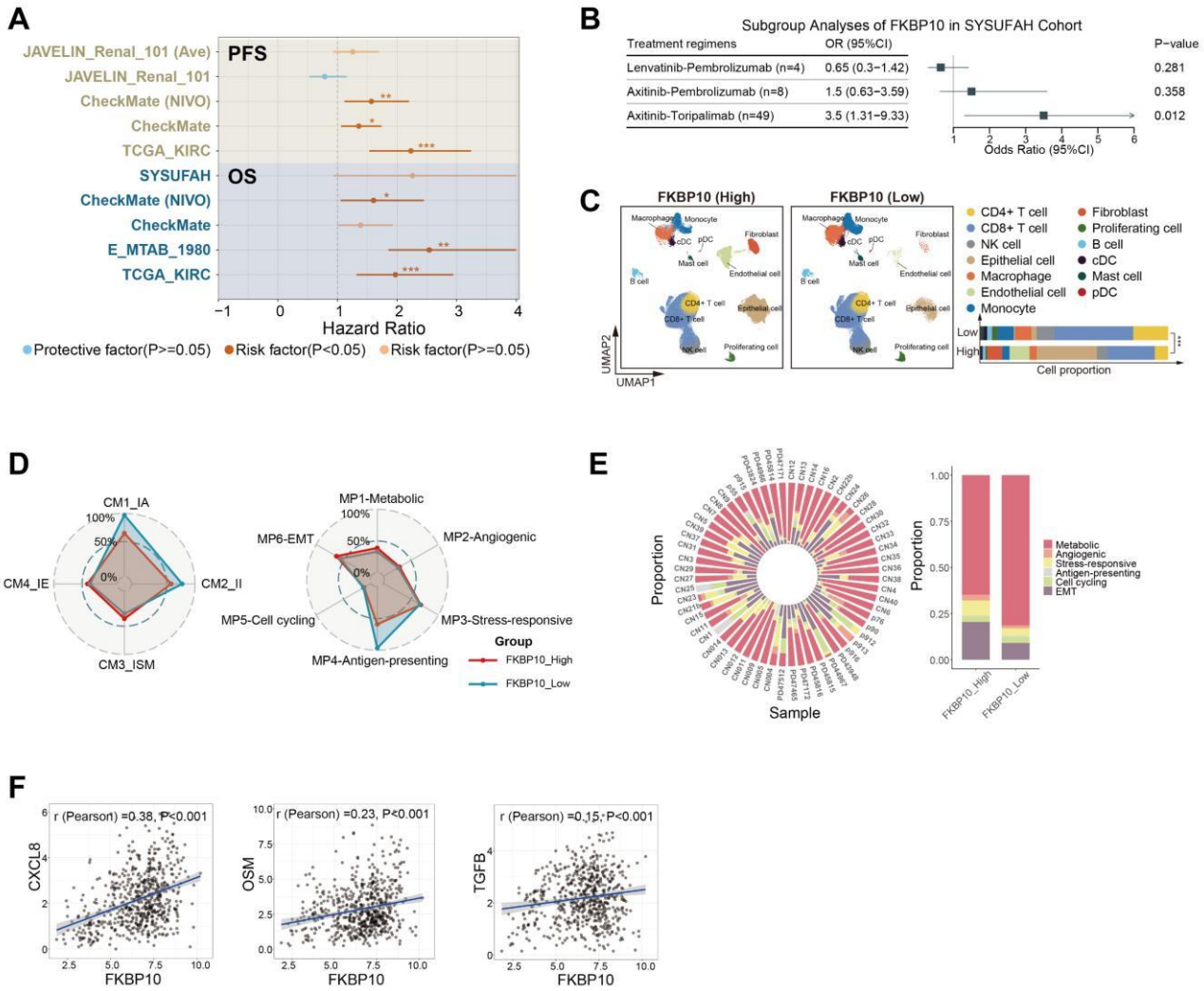

Figure S29 FKBP10 is an independent prognostic factor and remodels the tumor immune microenvironment in ccRCC.

(A) Multivariable Cox regression forest plot demonstrating that high expression of FKBP10 is an independent risk factor in ccRCC patients across the TCGA-KIRC, E-MTAB-1980, CheckMate, and JAVELIN cohorts. Analyses were adjusted for age, gender, clinical stage, pathological stage, and PD-L1 status. (B) Subgroup analysis of an independent validation cohort (SYSUFAH, n = 61) receiving different immunotherapy regimens. FKBP10 was a significant risk factor in the Axitinib plus Toripalimab treatment group (n = 49). No significant association (P > 0.05) was observed in the Lenvatinib plus Pembrolizumab (n = 4) or Axitinib plus Pembrolizumab (n = 8) groups, likely due to limited sample size. (C) UMAP visualization of tumor-infiltrating immune cells (External validation in Bi, Li, and Obradovic datasets, cells = 429,854) with FKBP10-high/-low grouping. Bar plot (right) showed the specific cell proportion of FKBP10-high/-low groups (χ^2 test, P < 0.001). (D-E) Analysis of TIME subtypes and malignant cell states in the independent external validation cohort (n = 62). (D) The proportion of antitumor TIME subtypes (CM1-IA and CM2-II) was significantly reduced, while the immunosuppressive CM3-ISM subtype was significantly increased in FKBP10-High tumors. (E) The proportion of tumor cells in the low-malignancy MP1-Metabolic state was decreased, whereas the EMT state was significantly increased in the FKBP10-High group (Chi-square test, P < 0.05 for all comparisons). (F)

Correlation analysis between FKBP10 expression and cytokine levels (CXCL8, TGFB, OSM). FKBP10 expression showed the strongest positive correlation with CXCL8 among the cytokines tested.

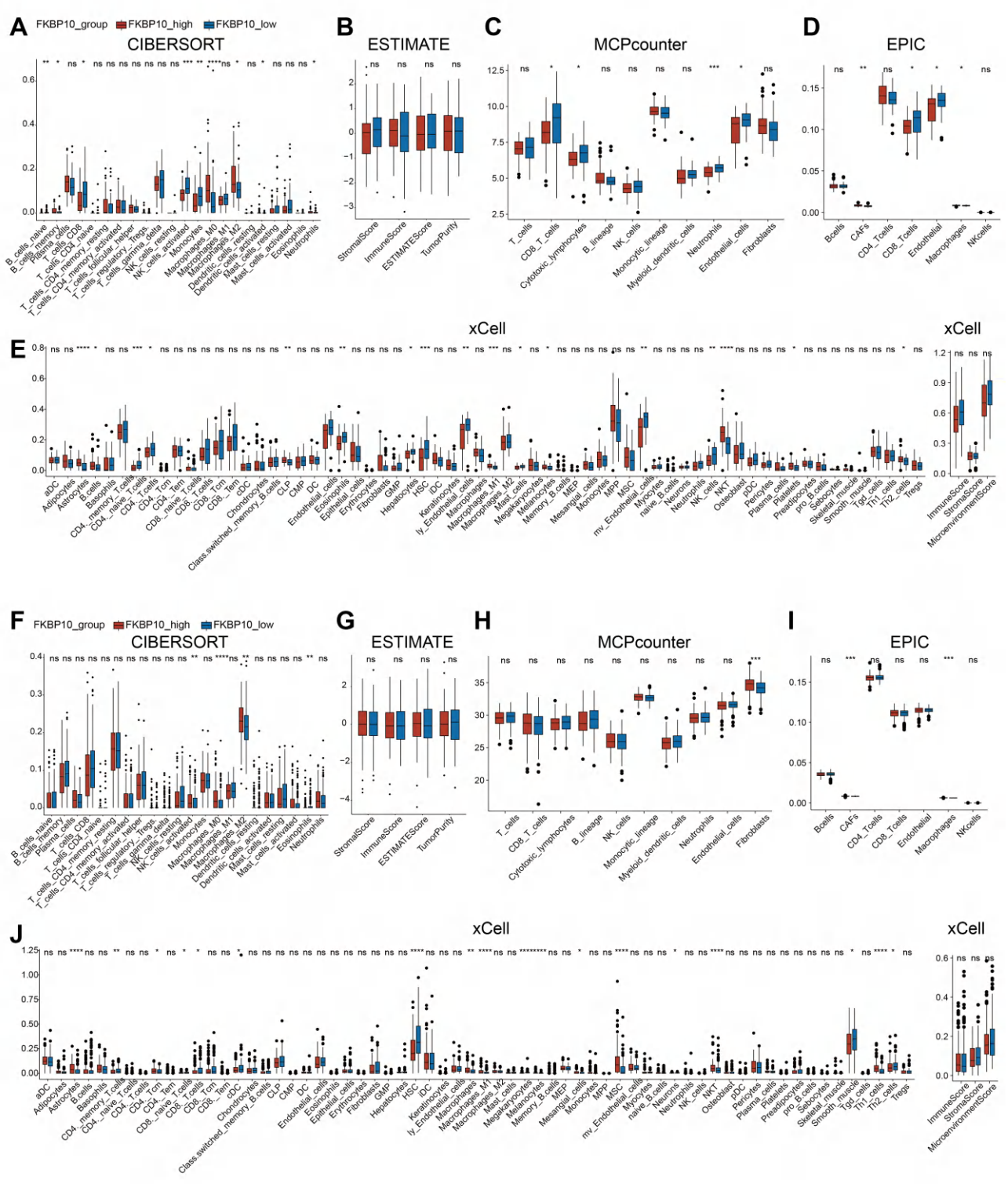

Figure S30 Analysis of immune cell infiltration stratified by FKBP10 expression levels in E-MTAB-1980 and Checkmate cohorts.

(A-E) The tumor immune microenvironment was evaluated using multiple algorithms (CIBERSORT, ESTIMATE, MCPcounter, EPIC, xCell) in E-MTAB-1980. Patients within the cohort were stratified into high and low FKBP10 expression groups. In the E-MTAB-1980 cohort, high FKBP10 expression was associated

with a significant decrease in T cells and an increase in macrophages (particularly M2 macrophages) and cancer-associated fibroblasts (CAFs). (F-J) The tumor immune microenvironment was evaluated using multiple algorithms in Checkmate cohort. In the Checkmate cohort, high FKBP10 expression was associated with a significant decrease in T cells and an increase in M2 macrophages, as well as CAFs. Data are presented as mean ± SD. Statistical significance was determined by the Wilcoxon rank-sum test (*$P < 0.05$, **$P < 0.01$,***$P < 0.001$).

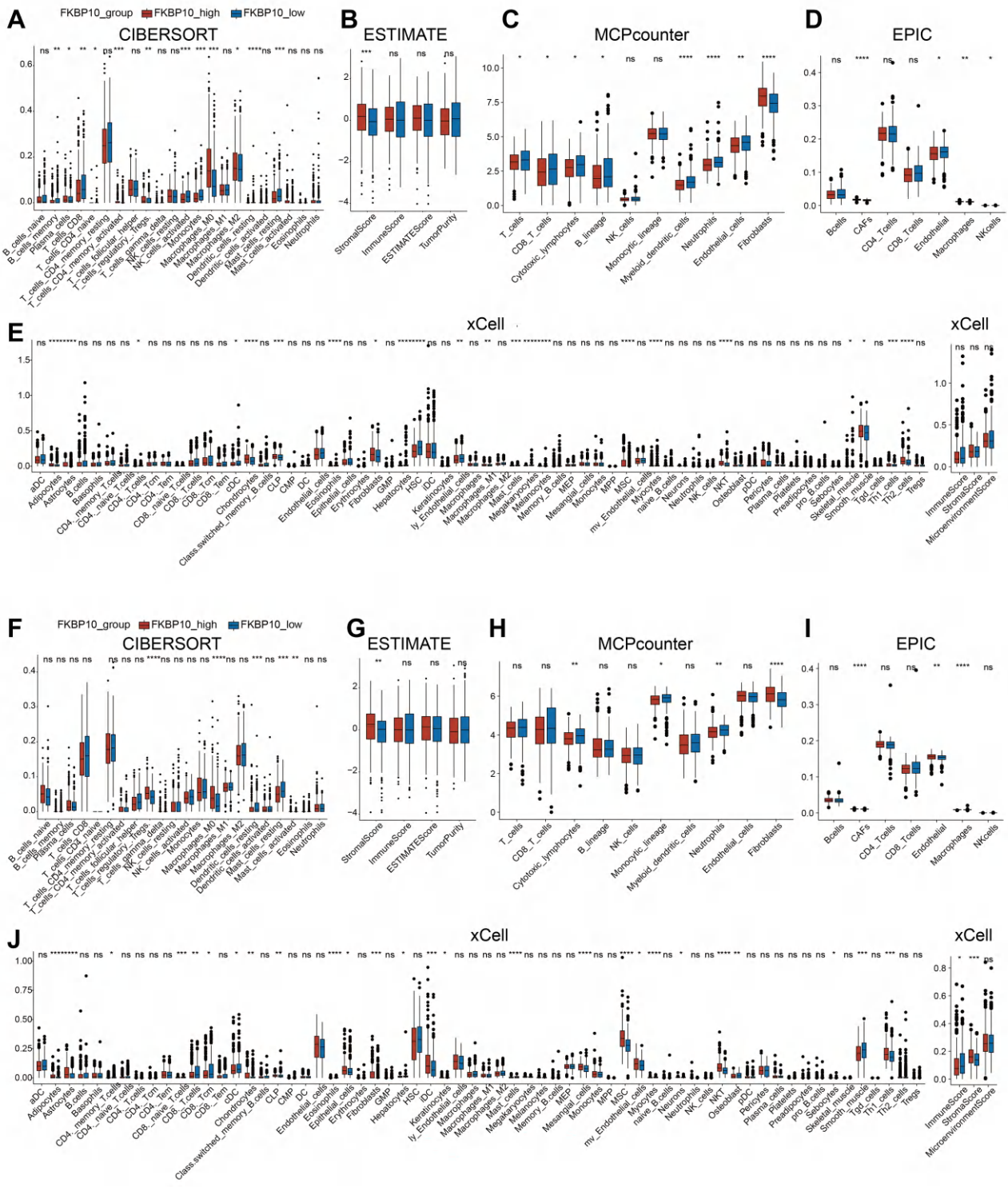

Figure S31 Analysis of immune cell infiltration stratified by FKBP10 expression levels in TCGA-KIRC

and JAVELIN cohorts.

(A-E) The tumor immune microenvironment was evaluated using multiple algorithms in TCGA-KIRC cohort. In the TCGA-KIRC cohort, the high FKBP10 group similarly showed reduced T cells, increased M2 macrophages and CAFs, and a significantly elevated stromal score. (F-J) The tumor immune microenvironment was evaluated using multiple algorithms in JAVELIN cohort. In the JAVELIN cohort, the high FKBP10 group exhibited T cell reduction, increased CAFs, a significantly decreased immune score, and a significantly increased stromal score. Data are presented as mean ± SD. Statistical significance was determined by the Wilcoxon rank-sum test (*$P < 0.05$, **$P < 0.01$,***$P < 0.001$).

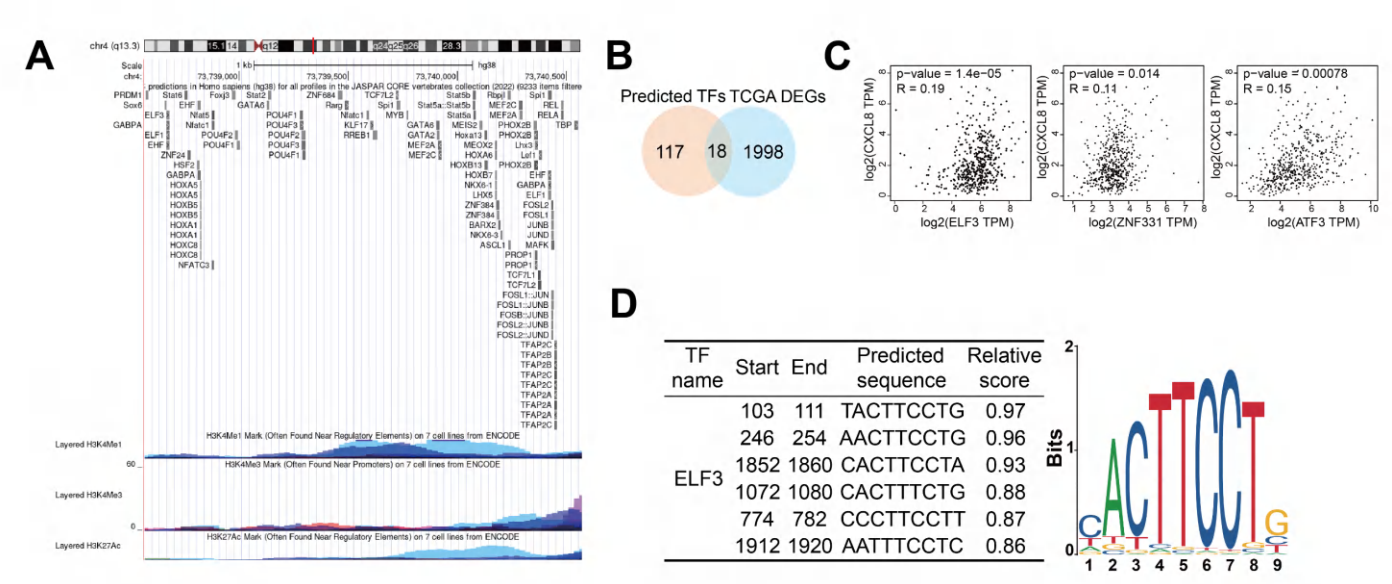

Figure S32 Analysis of transcription factor binding and prioritization of a key regulator at the CXCL8 locus.

(A) Analysis of ENCODE ChIP-seq data using MACS2 ($q < 0.01$) identifies 135 transcription factors (TFs). These TFs demonstrate coordinated occupancy at chromatin domains marked by active promoters (H3K4me3+/H3K27ac+) and putative enhancers (H3K4me1+) within the CXCL8 locus, spanning -2000 bp to +100 bp surrounding the transcription start site (TSS). (B) Venn intersection (n = 18 genes) between TCGA differentially expressed genes ($|log2FC| > 1$, FDR < 0.05) and predicted TFs. (C) Among these 18 genes, ELF3, ZNF331 and ATF3 demonstrate significant co-expression with CXCL8 ($P < 0.001$). (D) JASPAR analysis prioritizes ELF3 as the dominant regulator, showing both high binding potential (relative score > 0.85) and conserved motif at the CXCL8 promoter (right panel).

Reference

1. Zhang Y, Narayanan SP, Mannan R, Raskind G, Wang X, Vats P, et al. Single-cell analyses of renal cell cancers reveal insights into tumor microenvironment, cell of origin, and therapy response. Proc Natl Acad Sci U S A. 2021; 118.

2. Stewart BJ, Ferdinand JR, Young MD, Mitchell TJ, Loudon KW, Riding AM, et al. Spatiotemporal

immune zonation of the human kidney. Science. 2019; 365: 1461-6.

3. Coorens THH, Treger TD, Al-Saadi R, Moore L, Tran MGB, Mitchell TJ, et al. Embryonal precursors of Wilms tumor. Science. 2019; 366: 1247-51.

4. Melé M, Ferreira PG, Reverter F, DeLuca DS, Monlong J, Sammeth M, et al. Human genomics. The human transcriptome across tissues and individuals. Science. 2015; 348: 660-5.

5. McGinnis CS, Murrow LM, Gartner ZJ. DoubletFinder: Doublet Detection in Single-Cell RNA Sequencing Data Using Artificial Nearest Neighbors. Cell Syst. 2019; 8: 329-37.e4.

6. Zheng L, Qin S, Si W, Wang A, Xing B, Gao R, et al. Pan-cancer single-cell landscape of tumor-infiltrating T cells. Science. 2021; 374: abe6474.

7. Gulati GS, Sikandar SS, Wesche DJ, Manjunath A, Bharadwaj A, Berger MJ, et al. Single-cell transcriptional diversity is a hallmark of developmental potential. Science. 2020; 367: 405-11.

8. Yoshihara K, Shahmoradgoli M, Martínez E, Vegesna R, Kim H, Torres-Garcia W, et al. Inferring tumour purity and stromal and immune cell admixture from expression data. Nat Commun. 2013; 4: 2612.

9. Newman AM, Liu CL, Green MR, Gentles AJ, Feng W, Xu Y, et al. Robust enumeration of cell subsets from tissue expression profiles. Nat Methods. 2015; 12: 453-7.

10. Becht E, Giraldo NA, Lacroix L, Buttard B, Elarouci N, Petitprez F, et al. Estimating the population abundance of tissue-infiltrating immune and stromal cell populations using gene expression. Genome Biol. 2016; 17: 218.

11. Racle J, de Jonge K, Baumgaertner P, Speiser DE, Gfeller D. Simultaneous enumeration of cancer and immune cell types from bulk tumor gene expression data. Elife. 2017; 6.

12. Aran D, Hu Z, Butte AJ. xCell: digitally portraying the tissue cellular heterogeneity landscape. Genome Biol. 2017; 18: 220.